Summer 2004

The Effect of Submarine Canyon Width and Stratification on Coastal Circulation and Across Shelf Exchange

Kyung-Hoon Hyun
Old Dominion University

THE EFFECT OF SUBMARINE CANYON WIDTH AND STRATIFICATION ON COASTAL CIRCULATION AND ACROSS SHELF EXCHANGE

by

Kyung-Hoon Hyun
B.S. February 1991, Cheju National University, Korea
M.S. February 1997, Cheju National University, Korea

A Dissertation Submitted to the Faculty of
Old Dominion University in Partial Fulfillment of the
Requirement for the Degree of

DOCTOR OF PHILOSOPHY

OCEANOGRAPHY

OLD DOMINION UNIVERSITY
August 2004

Approved by:

John M. Klinck (Director)

Susan E. Allen

Chester E. Grosch

Arnoldo Valle-Levinson

ABSTRACT

THE EFFECT OF SUBMARINE CANYON WIDTH AND STRATIFICATION ON COASTAL CIRCULATION AND ACROSS SHELF EXCHANGE

Kyung Hoon Hyun
Old Dominion University, 2004
Director: Dr. John M. Klinck

A 3-D ocean circulation model is used to investigate the effect of the width of a submarine canyon and stratification on adjacent coastal circulation and across shelf exchange. Upwelling winds for 20 d drive circulation over six canyons of varying widths (8-60 km), two escarpments to represent infinitely wide canyons, and a generic shelf-slope without a canyon. Also six stratifications whose first internal Rossby radii (a) range over 2-18 km were applied to two canyons (20 and 40 km) to see the effect of stratification. All simulations adjust to the canyon after 5 days spinup and reach an approximate steady state after two weeks. Cyclonic circulation, continuous onshore transport and upwelling occur within the canyons. All canyons can be classified as narrow, intermediate or wide by the ratio of the internal deformation radius to the canyon width. A canyon with a width of about $2a$, which is the size of cyclone over wide canyon, separates wide from narrow canyons. Alongshore transport upstream of canyon and onshore transport within the canyon has a relationship of power function which has different parameters before and after the adjustment. The geometric effect of a narrow canyon is very strong based on the onshore transport per unit width and tracer moving speed within the canyon, even though wider canyons have larger onshore transport. Canyon drag decreases as the canyon narrows and stratification increases, which produces large alongshore transport for strong stratification and large onshore transport for weak stratification.

ACKNOWLEDGMENTS

During the writing of this thesis, I received considerable help from persons whom I would like to thank. First of all, I would like to thank my supervisor Dr. John Klinck for all his help and advice during the writing of this thesis. Secondly, I would like to thank to my committee members, Drs. Arnoldo Valle-Levinson, Chet Grosch at CCPO and Dr. Susan Allen from University of British Columbia for their many useful comments. I would like to thank Dr. Richard Zimmerman for his support. I would like to express special thanks to Mr. Mike Dinniman for helping me use ROMS. I also would like to thank all CCPO students for being good friends with helpful suggestions. I would like to thank my lifelong mentor Prof. Ig-Chan Pang in Cheju National University for his help and advice.

I feel a deep sense of gratitude for my mother who supported me through college and taught me the importance of family with my late father. I am grateful for my sister and three brothers for reminding me the value of brotherhood and hope to see them soon. My parents-in-law, a sister-in-law and three brothers-in-law always provided support. I would like to offer them many thanks. Finally, I am very grateful for my wife KyungRan, for her love and patience during the time I worked on this research. I will remember this time as one of the happiest experiences in life watching the growth of my lovely sons, Jinho and Minho.

TABLE OF CONTENTS

LIST OF TABLES

LIST OF FIGURES

CHAPTER I

INTRODUCTION

Submarine canyons cutting into the continental shelf are known to have a strong effect on the fluid dynamics in the shelf because of their steep and depressed topography (Klinck 1988; 1989; 1996; Allen 1996) . It has been reported that across shelf transport is enhanced greatly over steep sided, narrow submarine canyons (Freeland and Denman 1982; Klinck 1988; Hickey 1997), indicating that the presence of a submarine canyon is very important for addressing across shelf volume exchange. Hickey (1995) noted the importance of a submarine canyon in internal wave generation and modification, enhanced mixing, modification of coastal trapped waves and regional currents and water properties.

In most continental shelf seas, the strongest persistent gradients in water properties exist in the across shelf direction because the shelf region is located between land and oceanic influences and the across shelf flow is often inhibited by the continental slope, which is generally very steep and acts as a wall inhibiting the direct flow crossing isobaths between the continental shelf and the open sea. Flow over the continental slope generally follows isobaths. It has been known that the volume exchange across the shelf break is small (Huthnance 1995) and is limited to regions over relatively gentle slopes (Hydes et al. 2001; Burrows et al. 1999). This along-shelf dynamics is modified where a topographic change cutting into the shelf-slope such as a submarine canyon exists.

There are many topographic changes such as hills and depressions over the shelf-slope region. A submarine canyon cutting into the continental shelf is a typical topographic change along most ocean margins. The geometry of submarine canyons is defined by several factors such as width, length, depth, steepness and shapes, which

This dissertation follows the style of *Journal of Geophysical Research.*

Table 1. Scales of various submarine canyons on continental shelves in which current meter observations are available. Width (W) and length (L) are in kilometers. Depths (m) of the canyon rim (h_s) and the deepest part (h_c) of canyon are given. The slope was calculated from the aspect ratio (h_c-h_s)/0.5W.

Canyon	W	L	h_s-h_c	Slope	Reference
Astoria	7	20	150-600	0.13	Hickey (1997)
Baltimore	8	13	200-1200	0.25	Hunkins (1988)
Barrow	30	250	60-300	0.02	Aagaard and Roach (1990) Signorini et al. (1997)
Biobío	10	30	150-750	0.12	Sobarzo et al. (2001)
Blanes	12	35	200- 900	0.12	Granata et al. (1999) Ardhuin et al. (1999)
Cap-Ferret	30		200-2500	0.15	Durrieu de Madron et al. (1999a)
Carson	10	15	100-1000	0.18	Kinsella et al. (1987)
Foix	4		90-1000	0.46	Puig et al. (2000)
Hudson	7	12	150-600	0.13	Hotchkiss and Wunsch (1982) Hsueh (1980)
Juan de Fuca	7		180-800	0.18	Freeland and Denman (1982)
Lydonia	10	20	150-1500	0.27	Noble and Butman (1989)
La Jolla and Scripps	0.4	1.4	60-300	1.20	Shepard et al.(1979)
Palamós	35	30	200-2000	0.10	Alvarez et al.(1996)
Quinault	30	30	200-1800	0.21	Hickey et al.(1986)

tend to be relatively consistent for canyons scattered around the world. This general consistency is due to the most common formation mechanism of erosion by water or ice during low stands of sea level. Table 1 shows scales of various canyons in the world ocean where current measurement were performed. Along the Pacific coast of North America, roughly 20% of the shelf edge is interrupted by canyons (Hickey 1995). There exist many submarine canyons in the Chilean continental shelf off South America and many canyons in the Mediterranean Sea. Along the east coast of the United States, 14 canyons exist from the Georges Bank to Cape Hatteras.

Submarine canyons are known for their strong effect on the circulation in the shelf and slope. For example, a submarine canyon cutting into the shelf can enhance

upwelling derived across shelf transport on the order of 10 times over other shelf-slope areas (Allen 1996). Klinck (1996) also showed that across shelf transport was enhanced about 10 times over the canyon than the adjacent area and that vertical velocity of 44 m day^{-1} was calculated for strongly stratified upwelling flow. Vertical velocity was calculated as fast as 50 m day^{-1} in Astoria Canyon (Hickey 1997). For a flat bottom shelf sea, Ekman pumping velocity was calculated as 5 m day^{-1} for a strong wind stress of 0.1 N m^{-2} in a two layer model (Charney 1955). Thus, it can be said that the presence of a submarine canyon enhances across shelf and vertical transports on the order of 10 times stronger than outside shelf-slope region.

Volume exchange over submarine canyon regions can roughly be calculated and compared to those over the outside shelf-slope. Based on Hickey's (1995) scaling of Pacific coast of North America and on the assumption of 10 times enhancement of across shelf transport over a canyon, about 80% of volume exchange between the shelf and the open seas occurs over the canyons while 20% occurs elsewhere. Thus the fluid dynamics in and around submarine canyons is the key to understanding the volume exchange between the shelf and open seas.

Thus this research will focus on the topographic effects of submarine canyons on the exchange between the continental shelf and open seas. Previous research on canyon dynamics will be introduced in the next section.

I.1 BACKGROUND

Observational Studies

In spite of the significance of submarine canyons, physical dynamics in and near the canyon has not been investigated as vigorously with field and numerical studies compared to other areas in the ocean. Measurement of current and water properties in submarine canyons is very difficult because of steep slopes and intense fishing activities. The first current measurements in submarine canyons were made by Stetson

(1936) in the Georges Bank canyons and were followed by Shepard and Emery (1941) in submarine canyons off the California coast. Their main focus was the geological aspects of submarine canyons such as comparison of canyon shapes and the origin of canyons. Also Shepard et al. (1979) made current measurements over many canyons off east and west coasts of the United States to understand sediment transport.

Hsueh (1980) measured the deep flow in the Hudson Shelf Valley in the New York Bight with current-meters and concluded that up-valley flow can be expected in coincidence with eastward winds. Hotchkiss and Wunsch (1982) investigated internal waves in Hudson Canyon by hydrographic and current measurements and noted that internal wave energy was intensified at the head and near the floor of the canyon. Observations by Freeland and Denman (1982) showed that intense upwelling of dense, nutrient-rich and low dissolved-oxygen waters occurred over a spur of Juan de Fuca Canyon. They reported that water parcels from a depth of 400 m can be raised to the shelf and that the enhanced upwelling is due to an onshore pressure gradient that the Coriolis force does not balance within the canyon. Church et al. (1984) reported that canyons are privileged places for the exchange of water between the coastal zone and the open ocean from a study over Middle Atlantic Bight canyons.

Hickey et al. (1986) found suspended particle movement in Quinault Canyon off the Washington coast by current measurement. They found a significant correlation between along-shelf and along-canyon axis flows. In a second study, Hickey (1989) made current measurements in two canyons, Astoria and Quinault Canyons, to determine the role of canyons in the transfer of sediment from the shelf to the deep sea. She reported that the effect of canyons depends on both stratification and canyon width. A cyclonic eddy was induced below 50 m by the canyon topography in the narrow Astoria Canyon during equatorward flow while for the wider Quinault Canyon, flow at the shelf edge follows the large-scale canyon topography. Hickey (1997) used current and CTD measurements to describe the response of steep sided, narrow Astoria

Canyon to time variable wind forcing. A cyclonic circulation was found at depths 40-100 m above the canyon during weak incident flow. Vertical velocity within the canyon was estimated to be 50 m day^{-1} upward during upwelling and 90 m day^{-1} downward during wind relaxation following upwelling events.

Kinsella et al. (1987) used observations and a modeling study of the flow over Carson Canyon off Newfoundland to show that a baroclinic current at the shelf break interacts with canyon topography. Hunkins (1988) found mean down-canyon flow in the head of Baltimore Canyon, but up-canyon flow of 24 m day^{-1} occurred at 800 m farther seaward. Noble and Butman (1989) found subtidal flow of 9-26 m day^{-1} over the shelf and slope in Lydonia Canyon. Ocean-shelf exchange over Barrow Canyon in Arctic Ocean was studied by Aagaard and Roach (1990) through two years current measurement. They found cold and fresh waters advected downcanyon by the mean flow alternating with upcanyon flow of warm and saline waters upwelled onto the shelf.

Currents and hydrology over Cap-Ferret Canyon (Durrieu de Madron et al. 1999b) off west coast of France and Grand-Rhône Canyon (Durrieu de Madron 1999a) off south coast of France was investigated to see the shelf-slope exchange of particulate matter and showed that the exchange occurred mainly in the canyon head and enhanced by cross-slope current oscillations. Granata et al. (1999) reported that canyon topography enhanced horizontal and downward transport of particles in an anticyclonic flow region over Blanes Canyon off the northwestern Mediterranean Sea. Puig et al. (2000) investigated current and particle flux over Foix Canyon off east coast of Spain and reported that deep currents are strongly influenced by the bottom topography and have periods of the inertial motion and 6-10 days of atmospheric forcing passage. Sobarzo et al. (2001) investigated upwelling flow dynamics in the Biobío Canyon off Chile with current and hydrographic measurements and determined an ascent rate of 20 m day^{-1} in the canyon.

Theoretical Studies

Hickey (1995) mentioned that most modelers have given little attention to canyons due in part to the widely held idea that theories developed for a hill (which are comparatively numerous) can be applied directly to a depression; but that it is not the case because boundary layers are free to communicate at all depths within a depression. There were few studies on submarine canyon dynamics using models until late 1980's. Peffley and O'Brien (1976) showed in two-layer model that the cold water pool off Oregon was due to bottom topography rather than coastline shape.

Klinck (1988, 1989) first used analytical models for studying canyon dynamics. He showed in his homogeneous and stratified two-level analytical models that only a narrow canyon whose width is less than half of the internal radius of deformation enhances coastal upwelling, while the flow over a wide canyon follows isobaths. Klinck (1996) tested the stratification effect on circulation near a narrow submarine canyon using the 3-dimensional numerical model (SCRUM, S-Coordinate Rutgers University Model, see Hedström 1997) with periodic across shelf boundary conditions. He reported that dense water was pumped onto the shelf from the narrow canyon, even for strong stratification. She and Klinck (2000) simulated the flow near submarine canyon driven by constant winds using periodic boundaries and showed that in a narrow canyon a cyclone can be caused by the cyclonic turning and the stretching of planetary vorticity by vertical motion. Dinniman and Klinck (2002) tested the influence of across shelf boundaries on circulation near a narrow canyon by the comparison of open versus periodic boundary conditions using ROMS (Rutgers/UCLA Regional Ocean Model System).

Allen (1996) showed the enhancement of wind-driven upwelling over a finite length canyon and reproduced comparable circulation patterns in Astoria and Tully Canyons. She found that the nonlinearity advects the flow pattern to the downstream side of the canyon while strong cyclonic vorticity is generated over a canyon for linear

flow case. Chen and Allen (1996) suggested a parameter to measure the strength of canyon geometric effect called the canyon number. Allen (2000) compared two canyons, Astoria and Juan de Fuca Canyons, to examine the topographic effect on circulation. She concluded that geometry has a strong effect on the flow with very deep upwelling over Juan de Fuca Canyon, which is big and long, but with moderate episodic upwelling over Astoria Canyon which is small and narrow.

Chapman and Gawarkiewicz (1995) used SPEM (S-coordinate Primitive Equation Model) to examine the offshore transport of dense shelf water by the negative buoyancy forcing. They reported that a canyon is the important route for transporting dense shelf water away from Arctic coastal polynyas toward the deep ocean. Jiang and Garwood (1998) considered topographic steering and stratification over 7 different topographies (2 canyons, 2 ridges, 2 seamounts and a slope) using the Blumberg and Mellor (1987) model to describe deep water behavior dynamics near the Denmark Strait overflow. Ardhuin et al. (1999) simulated the circulation in Blanes Canyon in western Mediterranean and reported vertical exchange was enhanced in the canyon 4-6 times larger than outside the canyon. Also, steering of dense water over a canyon was displayed by analytical model (Wåhlin 2001). Yuan (2002) studied the intrusion of open ocean water across the head of DeSoto Canyon in the Gulf of Mexico using Bryan-Cox model and reported that offshore wind driven currents induce strong cross-isobath flow at the canyon head in the bottom Ekman layer.

I.2 RESEARCH QUESTIONS

This study will investigate the effect of canyon width and stratification on coastal circulation and across shelf exchange over a submarine canyon. This study is motivated by the following questions. Is there a specific width which distinguishes narrow and wide canyons? Do only narrow canyons enhance the canyon upwelling and across shelf exchange? How about the fluid dynamics over wide canyons? Can stratification

affect these results? Thus, this study focuses on the following research questions:

1. How does the canyon width affect transport, circulation, upwelling and across shelf exchange over a submarine canyon?

2. How does the stratification affect transport, circulation, upwelling and across shelf exchange over a submarine canyon?

3. What characteristics classify canyon sizes, such as narrow and wide?

4. What is the source and route of deep water for across shelf exchange?

As described in the previous section, the fluid dynamics within the canyon is controlled by the canyon width and stratification (Klinck 1996; Hickey 1997; Allen 2000). If only narrow canyons whose widths are less the internal deformation radius has a strong enhancement of upwelling, increased across shelf exchange, the ratio of width to the radius can characterize the fluid dynamics within the canyon. In this study, this hypothesis is examined using a numerical model simulation with various canyon widths and stratifications. The details of a three-dimensional ocean circulation model will be described in Chapter II. Model domains, forcing and initial stratification will be presented with model parameters and boundary conditions. Results are presented in Chapter III-IV. The effect of canyon width is presented in Chapter III. Transport, circulation and upwelling over nine cases (6 canyons, 2 escarpments and a general shelf-slope) with a stratification will be compared and described with respect to the effect of canyon width. In Chapter IV, the effect of stratification is presented. Transport, circulation and upwelling over two canyons with 6 stratifications are described with respect to the effect of stratification. Discussion and conclusions will follow in Chapter V and VI.

CHAPTER II

METHOD

II.1 MODEL

The Regional Ocean Model System (ROMS) was used in this study. ROMS is a free surface primitive equation 3-dimensional ocean circulation model (Haidvogel and Beckmann 1998; Shchepetkin and McWilliams 2000; Ezer et al. 2002), derived from the σ-coordinate Rutgers University Model (SCRUM, see Hedström 1997). The primitive equation in Cartesian coordinates is expressed as

$$u_t + \vec{u} \cdot \nabla u - fv = -\phi_x + F^x + D^x \quad (1)$$

$$v_t + \vec{u} \cdot \nabla v + fu = -\phi_y + F^y + D^y \quad (2)$$

$$T_t + \vec{u} \cdot \nabla T = F^T + D^T \quad (3)$$

$$S_t + \vec{u} \cdot \nabla S = F^S + D^S \quad (4)$$

$$\rho = \rho(T, S, P) \quad (5)$$

$$\phi_z = -\rho g / \rho_0 \quad (6)$$

$$u_x + v_y + w_z = 0. \quad (7)$$

Subscripts indicate partial derivatives. The definitions and initial values of model parameters are listed in Table 2. Horizontal curvilinear and vertical terrain following σ-coordinates are used. Grid schemes are horizontally (Arakawa C-grid) and vertically staggered (Arakawa and Lamb 1977).

Baroclinic and barotropic horizontal currents and water properties (T and S) are basic variables calculated in the model. Horizontal mixing was proportional to the Laplacian of basic variables. The vertical mixing is calculated by the KPP scheme (Large et al. 1994). The flux of heat and salt at model boundaries were set to zero. Quadratic bottom stress, with a coefficient of 3.0×10^{-3} was applied as a body force

Table 2. Domain scales, time steps and various parameters and coefficients used in the model.

Parameters	Used values
Domain (km)	120 × 400
Grid (km)	dx=dy=1
Duration (day)	20
Time step (sec)	120 (internal), 4 (external)
Wind stress (m^2s^2)	τ=0.05 after 2d
Initial stratification	Figure 3
Coriolis parameter (s^{-1})	1.05×10^{-4}
Gravitational acceleration (m s^{-2})	9.8
Deepest level for surface bodyforce	14
Shallowest level for bottom bodyforce	1
Horizontal Mixing Coefficient (m^2s^{-1})	5 (T, S), 0 (u, v)
Vertical Mixing Coefficient (m^2s^{-1})	10^{-5} (T, S), 5×10^{-5} (w)
Quadratic bottom drag coefficient	3×10^{-3}

over the two bottom layers.

II.2 DOMAINS

Canyons on the northwest US coast provide the basic shape of canyon in this study because of considerable previous work in this area. Also, extensive measurements are available for Astoria Canyon (Hickey 1997) which is a typical example of these canyons. Canyons are characterized by width, length and steepness. Width (W) of canyon is based on the width along the shelf break depth. Canyon length (L) is determined by the intrusion distance from the shelf break to the head of canyon. Steepness of canyon is given as the aspect ratio (%) of the fractional depth of canyon (h_f), which is the depth difference between the shelf break and the deepest canyon depth (h_c), to the length of canyon.

Various canyons with different widths are constructed (Figure 1) based on the geometry of Astoria Canyon, which has a width of 10 km and a length of 15 km.

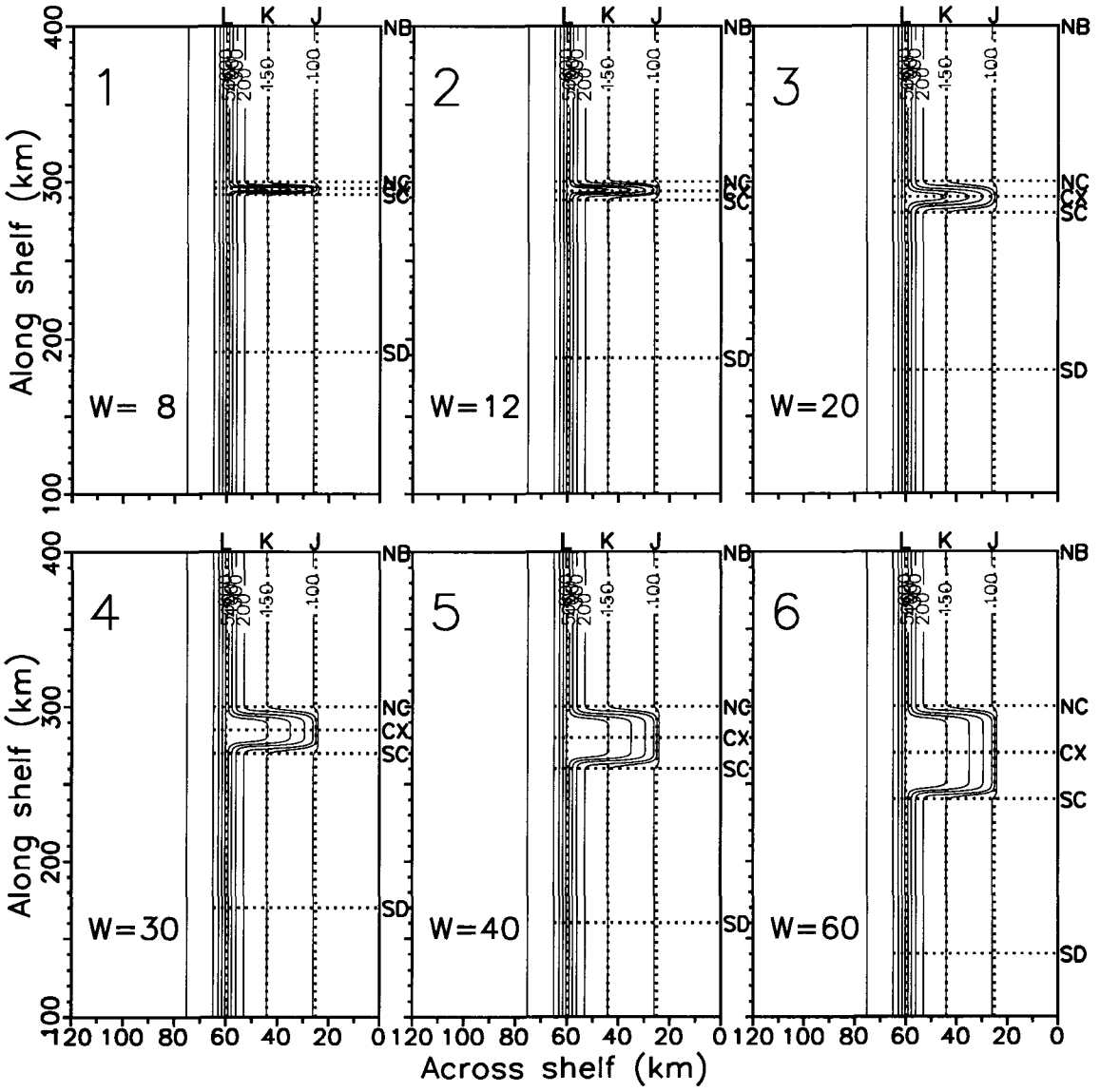

Figure 1. Model bathymetry. Locations of alongshore sections NB-SD, across shelf sections J-L and the width of canyon are given for nine bottom topographies (6 canyons, 2 escarpments, 1 general shelf-slope). Section SE (not shown in this figure) is 100 km downstream from Section SD.

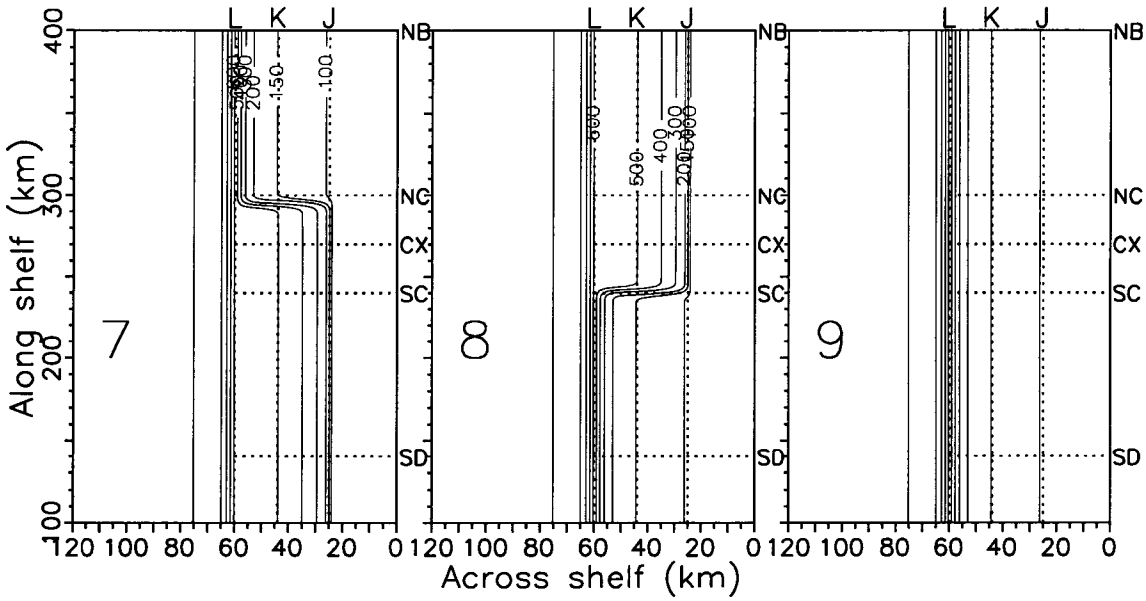

Figure 1. (continued)

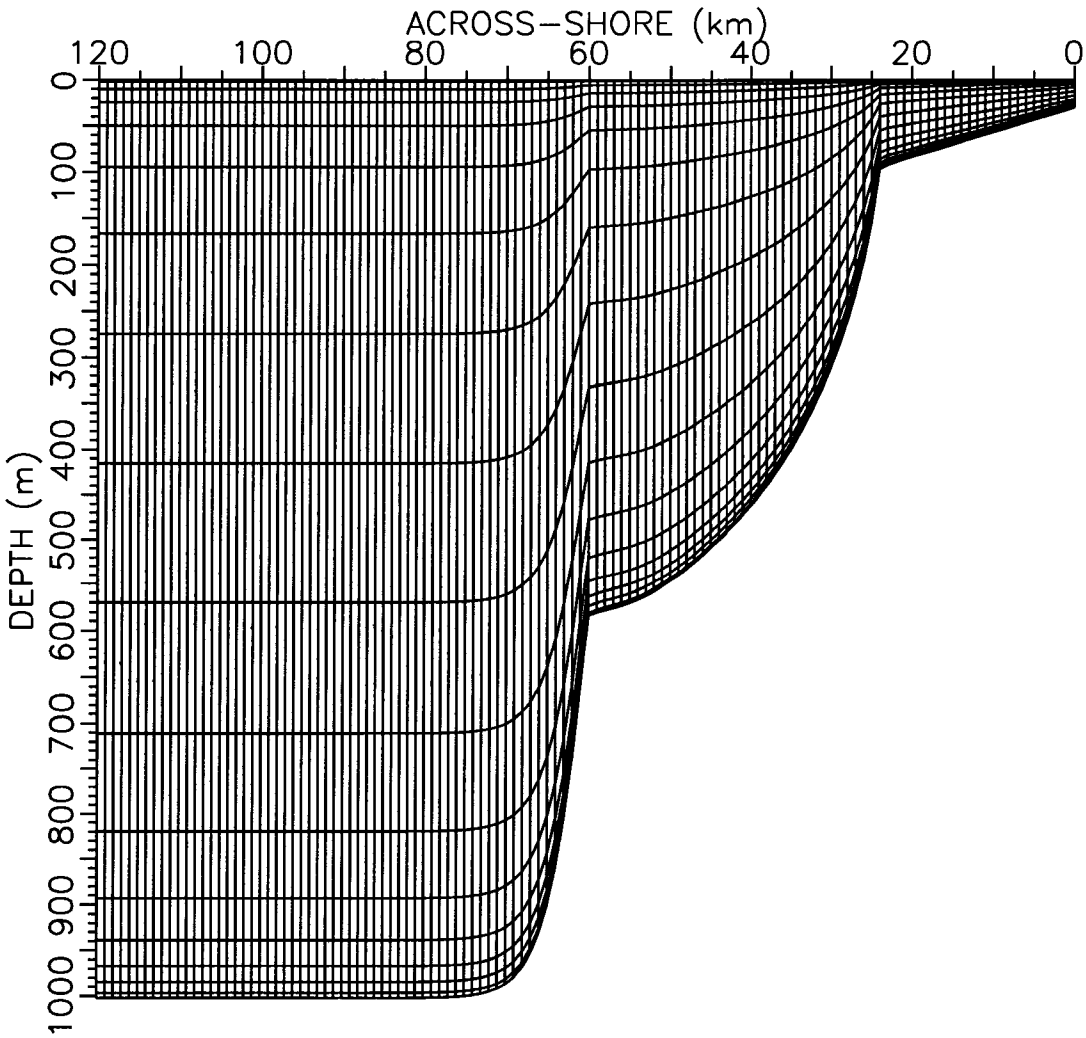

Figure 2. Numerical grid system along the canyon axis, showing every horizontal and vertical grid box. The density point is at the center of each box with vertical velocity on the upper and lower edges and horizontal velocity on the left and right edges.

Ratio of the width of canyon to the internal Rossby radius (stratification number S=a/W) calculated from the initial stratification described in the next section is given in Table 3 to compare the dynamical width. For all cases, the shallowest depth is 30 m at the coast, 150 m at the shelf break and 1000 m depth in the abyssal plain.

C1 to C6 are six canyons with the same length (20 km) and depth (600 m) but with differing widths (Figure 1). C1 represents the narrowest canyon (8 km) in this study. C2 also represents a narrow and steep canyon whose scales are similar to Astoria Canyon. The width of these two cases is less than the first internal deformation radius (a) which was calculated as 13 km from the basic stratification (details in the next section). The fractional depth (h_f) is 450 m from the shelf break to the deepest part of the canyon. The slope is about 2% (h_f/L) in the across shelf direction and 11% (h_f/0.5W for C1) in the alongshore direction. Widths ranges 12 km to 60 km in C2 to C6, indicating narrow, intermediate and wide canyons. In order to investigate the interactive strength of canyon edges, two escarpments are considered (C7 and C8). Escarpments represent infinitely wide canyon since one edge is missing. C9 is a shelf-slope without a canyon for comparison with canyon cases.

Alongshore sections NB-SD and across shelf section J-L (Figure 1). These sections will be used for transport calculations. Sections NB and NC indicate sections along the northern boundary and the northern edge of canyon (y=300 km). Section CX is along the axis of canyon. Section SC is the section at the southern edge of canyon. Section SD is 100 km downstream of the southern edge of canyon (SC). Section SE is 100 km downstream from Section SD. Across shelf sections J, K and L are along the head of canyon, the middle of canyon and the offshore end of canyon in the alongshore direction, respectively.

Each domain is 400 km alongshore and 120 km across shelf distances with 1 km grid interval and 16 levels (Figure 2). The alongshore distance is much longer than

Table 3. Model cases by the canyon width (W, km) and the first internal Rossby radius (a, km). The stratification number (S=a/W) is shown in the parenthesis.

	a=18	16	13	10	6	2
W=8			C1 (1.62)	D1 (1.25)		
12			C2 (1.08)	D2 (0.83)		
20	A3 (0.90)	B3 (0.80)	C3 (0.65)	D3 (0.50)	E3 (0.30)	F3 (0.10)
30			C4 (0.43)	D4 (0.33)		
40	A5 (0.45)	B5 (0.40)	C5 (0.32)	D5 (0.25)	E5 (0.15)	F5 (0.05)
60			C6 (0.22)	D6 (0.17)		
upstream			C7	D7		
downstream			C8	D8		
no canyon			C9	D9		

used in previous canyon model studies (Klinck 1996; She and Klinck 2000; Dinniman and Klinck 2002) in order to minimize errors near the southern open boundary, especially for wide canyons (40-60 km). Previous canyon models used a horizontal grid size of 0.5 km. In general finer grid resolution produces better results. However, before this study, cases with grid sizes of 0.5 km and 1 km were shown to have comparable results, so the larger grid interval is used in this study. Steep topography and strong stratification can cause truncation errors in terrain following coordinate models (Haney 1991). Allen et al. (2003) reported truncation errors in SCRUM due to the abrupt change of curvature of bottom topography by comparing with laboratory experiments. Case 1 is the narrowest case which involves the some truncation error (30%). However it is very difficult to make a steep sided narrow canyon without abrupt change of bottom curvature. Case 1 was included to compare other cases even though it has relatively large truncation errors.

Table 4. Coefficients for temperature, salinity used as the initial stratification, and density profiles calculated from T, S. The internal Rossby radius (a, km) was obtained from the speed (c) of the first normal mode.

	T_1	T_2	S_1	S_2	ρ_1	ρ_2	ρ_3	remarks
a=18	0.78	23.8	34.49	-6.07	27.58	-9.04	-0.11	strong stratification
16	1.41	18.3	34.47	-4.87	27.53	-6.77	-0.11	increased stratification
13	2.05	12.8	34.44	-3.67	27.57	-4.69	-0.11	basic stratification
10	2.68	7.3	34.41	-2.47	27.42	-2.82	-0.11	reduced stratification
6	3.31	1.8	34.38	-1.27	27.36	-1.18	-0.11	weak stratification
2	3.43	0.8	34.36	-0.07	27.33	-0.13	-0.09	nearly homogeneous

II.3 BOUNDARY CONDITIONS

The eastern (coastal) boundary is land and has a free slip condition. The other three sides of the model domain require open boundary conditions. The offshore (west) boundary is not critical because it has little influence on the wind-driven coastal dynamics and the no-gradient open boundary condition for all variables works well. The north and south across shelf open boundaries are more important and the choices are less clear. Dinniman and Klinck (2002) tested the influence of various boundary conditions on circulation near a narrow canyon using ROMS. The best results were obtained with the implicit Flather radiation scheme (Flather 1976) for the "free" part of the normal component of barotropic flow and the modified Orlanski radiation conditions (Camerlengo and O'Brien 1980) for a baroclinic flow, the free surface and tracers at northern and southern boundaries. Separating "free" and "forced" components of the depth averaged flow was suggested by Røed and Smedstad (1984). The "forced" solution does not require an open boundary condition since it uses a linear subset of the governing equations with no normal derivatives. The "free" mode is computed by subtracting the forced mode from the total solution.

II.4 STRATIFICATION AND FORCING

Six stratifications including a nearly homogeneous case were created (Figure 3) to use as initial stratification. The basic stratification was taken from a CTD profile observed on 10 June, 1995, near Astoria Canyon (46° 22.4′ N 124° 49.0′ W) (heavy solid curves). Dashed curves fit the data to the equation

$$T = T_1 + T_2 e^{T_3\sqrt{z}}, \tag{8}$$

$$S = S_1 + S_2 e^{S_3\sqrt{z}}, \tag{9}$$

$$\rho = \rho_1 + \rho_2 e^{\rho_3\sqrt{z}}, \tag{10}$$

where z is the depth in meters. Each coefficient for the six stratifications are listed in Table 4 except T_3=-0.068 and S_3=-0.12 for all cases. Each curve is shown in Figure 3 with each equation. The internal Rossby radius (a) was calculated as 18, 16, 13, 10, 6 and 2 km for six stratifications from a dynamic normal mode analysis (Section 6.13, Gill 1982). The first two stratifications represent strong stratification. The third stratification is a typical case during an upwelling event in the west coast off Oregon and Washington. The fourth case represents reduced stratification. The fifth case represents weak stratification. The final case represents a nearly homogeneous water column. Coriolis parameter f (=1.05 $\times$ 10^{-4}) at 46° 15′N was used to calculate a.

Upwelling favorable winds are applied to drive coastal upwelling flow over various canyons. Note that northerly wind is upwelling favorable along the eastern boundaries in the northern hemisphere. Wind stress (τ_y) is ramped from zero to its maximum of 0.05 N m^{-2} (about 7 m s^{-1}) over two days and then held constant. This choice corresponds to a moderate wind (Hickey 1997). There is no spatial variability in the wind field. All simulations are run for 20 days by which time the flow is approximately steady.

Circulation by upwelling wind stress was generated over six canyons, two escarpments and a generic shelf-slope topography for 20 days. It takes about 20 cpu hours for 20 days of simulations using a 10-processor shared memory computer. Six stratifications are applied to two canyons (W=20, 40 km) to see the effect of stratification. All cases are listed in Table 3. The model state was saved every day. Neutrally buoyant tracers were released at 2 d in a horizontal grid with 2 km spacing every 50 m of depth in and around the canyon and escarpments. Tracer trajectories are calculated as $d(x, y, z)/dt = (u, v, w)$ and recorded every 6 hours for 18 days.

The model solution for each case is analyzed from figures of horizontal flow vectors, vertical sections of across shore flow speed, locations of isopycnals over time and vertically integrated volume transport in both along and across shelf directions. Integrated volume transport (U,V) is calculated as $U = \int_0^{L_y} \bar{u}hdx$, $V = \int_0^{L_x} \bar{v}hdy$ where $(\bar{u}, \bar{v})$ is vertically averaged flow, (L_x, L_y) the length of each section and $h(x, y)$ is the total depth of water.

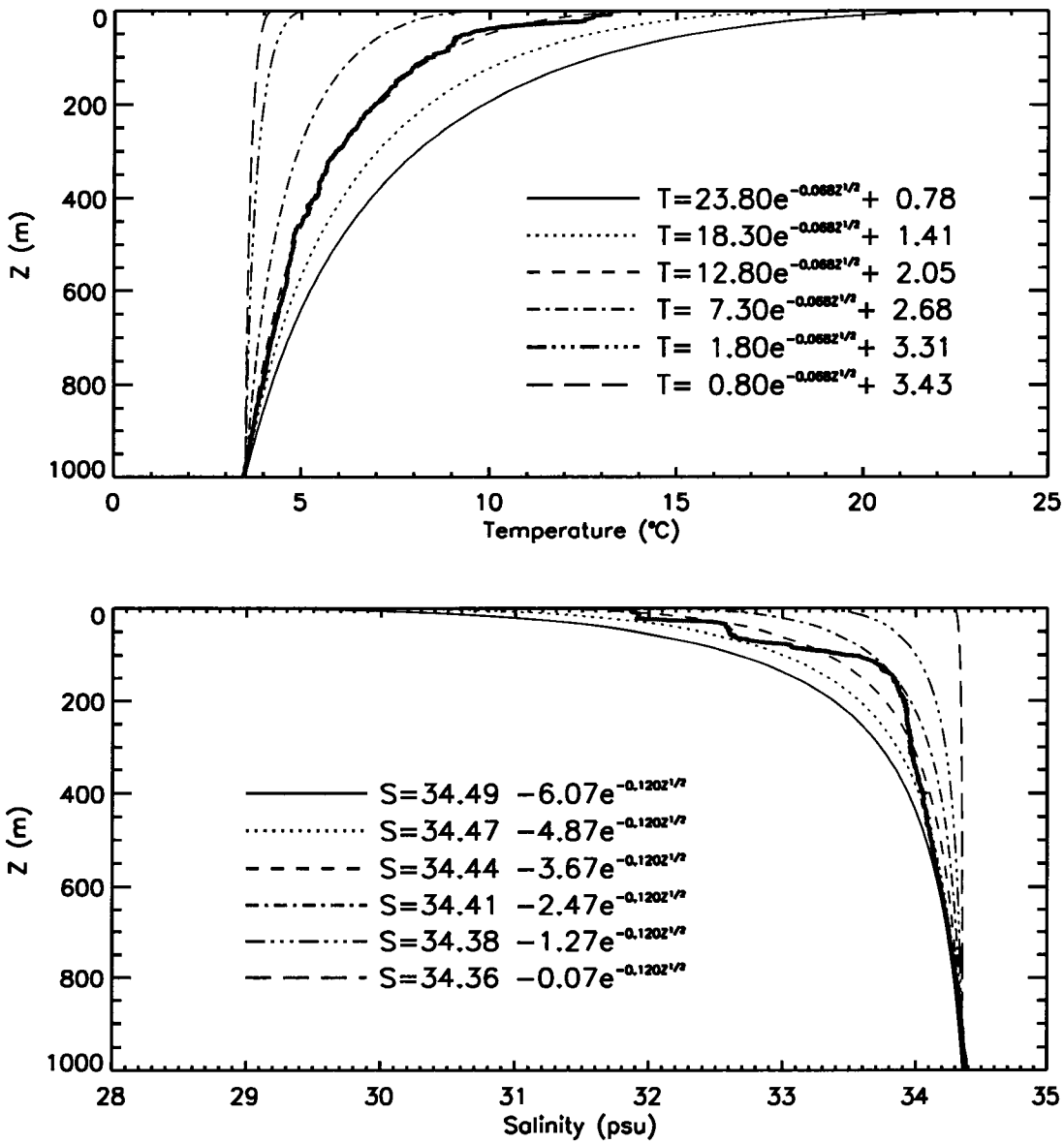

Figure 3. Temperature, salinity and density profiles used for initial stratification to the model. Data were observed near Astoria Canyon on 10 May 1996 (heavy solid curve). Six stratifications were created from the basic T and S profiles.

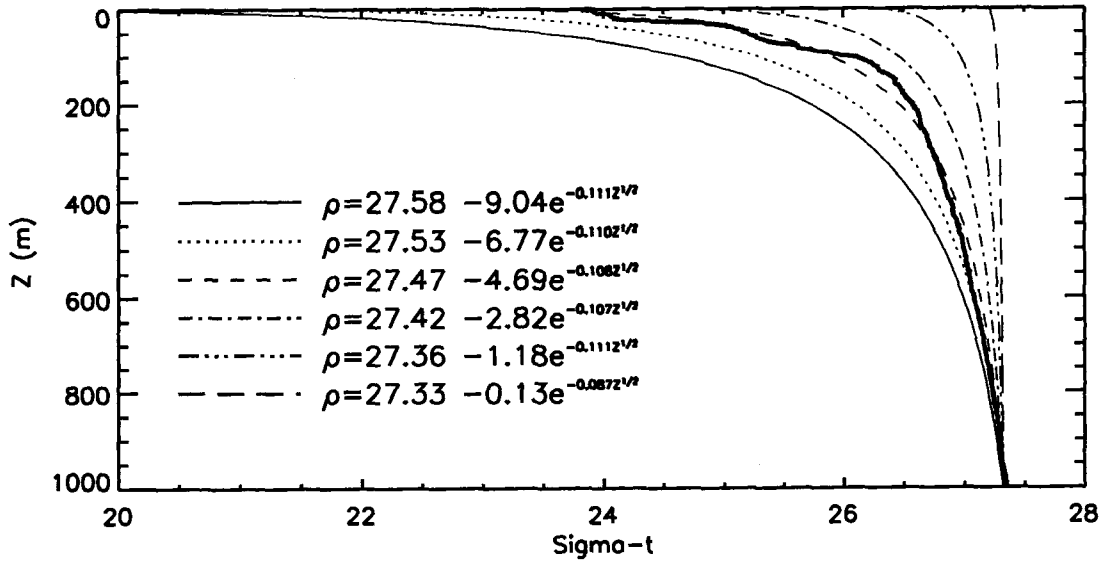

Figure 3. (continued)

CHAPTER III

EFFECT OF CANYON WIDTH

III.1 QUASI-STEADY STATE

The gross time behavior of the model solution is seen in the vertically and laterally integrated alongshore volume transport over time for cases C1-C9 (Figure 4) and cases D1-D9 in Figure 5 for the six sections NB-SE. Alongshore transport was integrated from the shelf break (Section K) to the coast at each section. The transport is approximately steady after 2 weeks.

A hyperbolic function

$$V = \frac{V_m t}{K_d + t}, \tag{11}$$

is fit to the time varying transport for each case (Tables 5 and 6). The quality of fit is good (r^2 is greater than 0.95 for most cases) except Section CX within the canyon where along-shelf dynamics are modified. V_m and K_d range over 1.6-1.8 Sv and 11.5-13.0 d, respectively, for the general shelf-slope (C9), a narrower range than the canyon cases.

For all cases, alongshore transport increases with time until 15 d after which it reaches an approximate asymptote which indicates the end of the fast adjustment. Some cases show further changes due to oscillations or continued baroclinic adjustment from canyon upwelling. At this point, surface wind forcing is largely in balance with the bottom drag.

Transports at Sections NB and NC are similar for all cases except C7 and C8 (two escarpment cases). Downstream sections SD and SE also show the similar transport for all cases except C7. The large transport in sections NB, NC and CX for C8 are due to the integration to Section K which is well offshore of the shelf break and includes a considerable portion of the offshore, downwind flow. Similarly, sections SD and SE

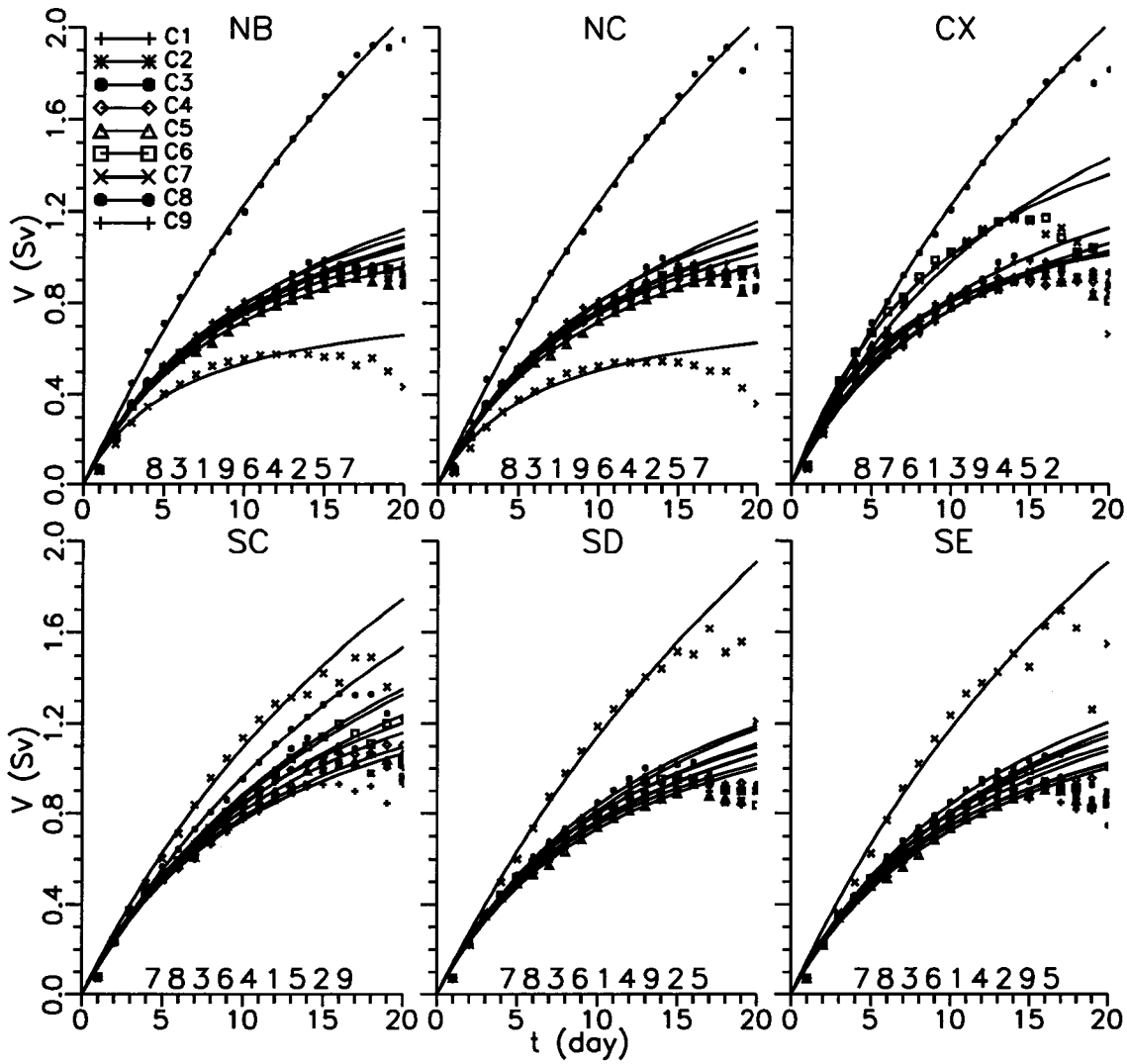

Figure 4. Vertically integrated alongshore transport V (Sv) over the shelf (integrated from the coast to Section K) as a function of time along sections NB-SE. Each model case (C1-C9) is shown by a different line style. Positive transport is downwind (southward). A function $V=V_m t/(K_d+t)$ is related alongshore transport V to time t in days. Parameters V_m and K_d are given on Table 5. Numbers at the bottom indicate cases by the order of transport magnitude at 15 d estimated by fitted curves.

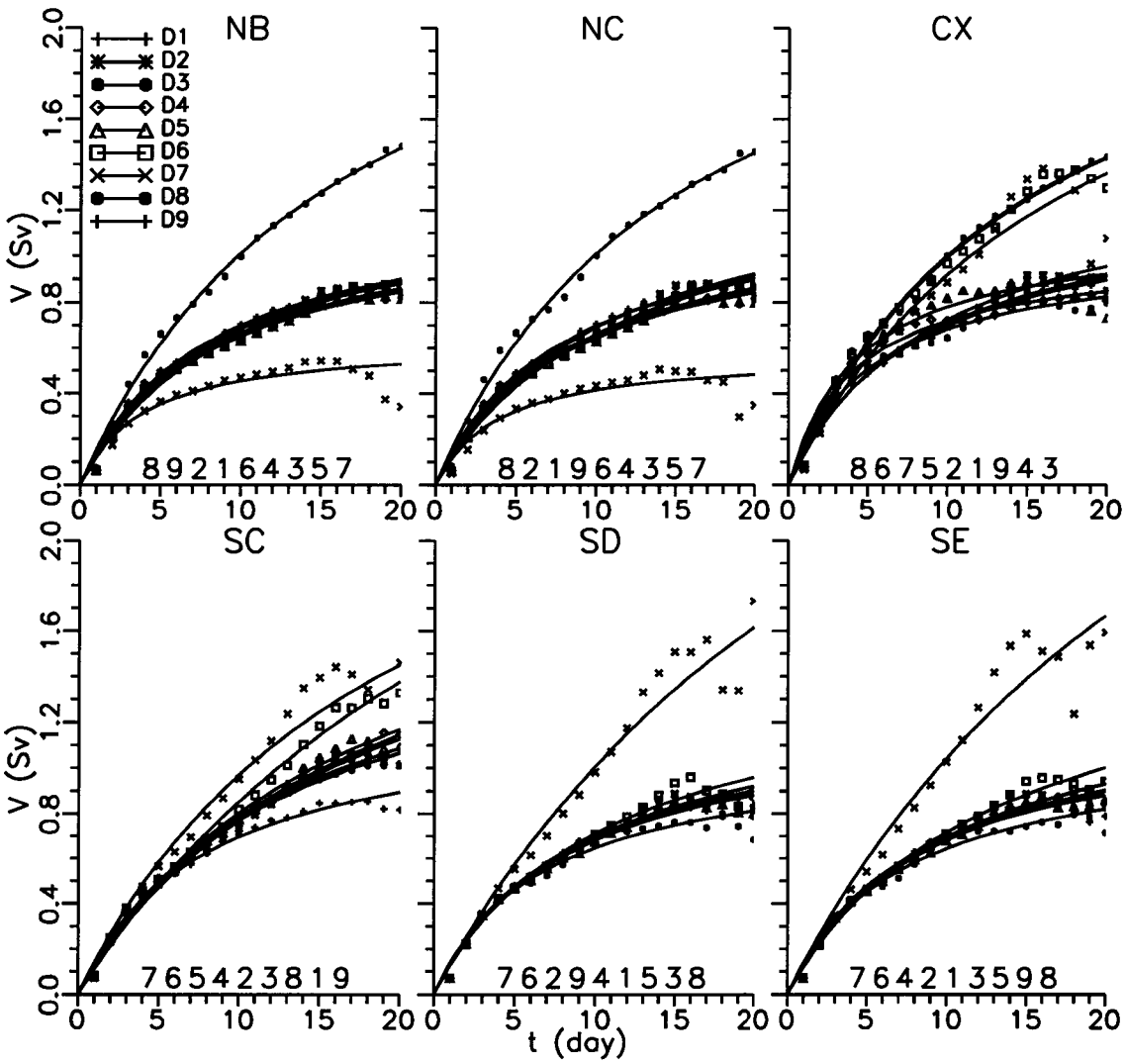

Figure 5. Same as Figure 4 except cases D1-D9. A function $V=V_m t/(K_d+t)$ is related alongshore transport V to time t in days. Parameters V_m and K_d are given on Table 6. Numbers at the bottom indicate cases by the order of transport magnitude at 15 d estimated by fitted curves.

Table 5. Parameters V_m and K_d of fitted curves to alongshore transport versus time for cases C1-C9 in Figure 4.

	Section	C1	C2	C3	C4	C5	C6	C7	C8	C9
V_m	NB	1.72	1.49	1.93	1.66	1.43	1.64	0.86	6.12	1.67
	NC	1.83	1.57	2.08	1.70	1.49	1.71	0.82	5.81	1.67
	CX	1.80	1.54	1.79	1.41	1.34	2.09	2.64	5.72	1.70
	SC	2.09	1.82	2.90	2.38	2.03	2.85	4.34	3.77	1.73
	SD	1.74	1.59	2.13	1.72	1.58	1.83	5.75	2.07	1.75
	SE	1.77	1.62	2.09	1.81	1.62	1.99	5.01	2.13	1.62
K_d	NB	11.55	9.84	14.32	11.76	9.85	11.48	5.95	39.68	11.51
	NC	12.67	10.86	15.96	12.32	10.66	12.38	6.26	36.88	11.71
	CX	11.95	9.97	11.81	7.58	6.55	10.71	16.91	36.59	12.01
	SC	14.69	13.11	22.73	18.39	14.96	22.89	29.62	29.06	12.45
	SD	11.70	11.12	16.30	12.38	11.65	12.99	40.36	14.75	12.93
	SE	12.17	11.75	15.94	13.54	12.41	14.90	32.63	15.37	11.74

Table 6. Parameters V_m and K_d of fitted curves to alongshore transport versus time for cases D1-D9 in Figure 5.

	Section	D1	D2	D3	D4	D5	D6	D7	D8	D9
V_m	NB	1.24	1.31	1.20	1.22	1.20	1.36	0.63	2.71	1.26
	NC	1.34	1.38	1.20	1.23	1.21	1.44	0.58	2.59	1.26
	CX	1.28	1.40	1.04	1.03	1.12	2.55	2.64	2.52	1.25
	SC	1.73	2.12	1.79	2.13	2.14	3.58	2.87	1.72	1.25
	SD	1.24	1.36	1.25	1.30	1.28	1.48	4.08	1.09	1.28
	SE	1.31	1.39	1.33	1.42	1.33	1.66	4.16	1.13	1.23
K_d	NB	8.06	9.07	8.01	8.24	8.31	10.50	3.98	16.82	8.01
	NC	9.18	10.03	8.06	8.65	8.65	11.81	3.97	15.62	8.00
	CX	8.20	9.41	5.25	4.31	4.39	15.76	18.80	15.20	7.98
	SC	12.49	17.53	13.03	17.12	16.68	31.94	19.62	12.30	8.03
	SD	8.02	9.46	8.34	8.79	8.82	10.76	30.53	6.81	8.48
	SE	8.93	10.03	9.44	10.40	9.59	13.22	30.01	7.53	7.88

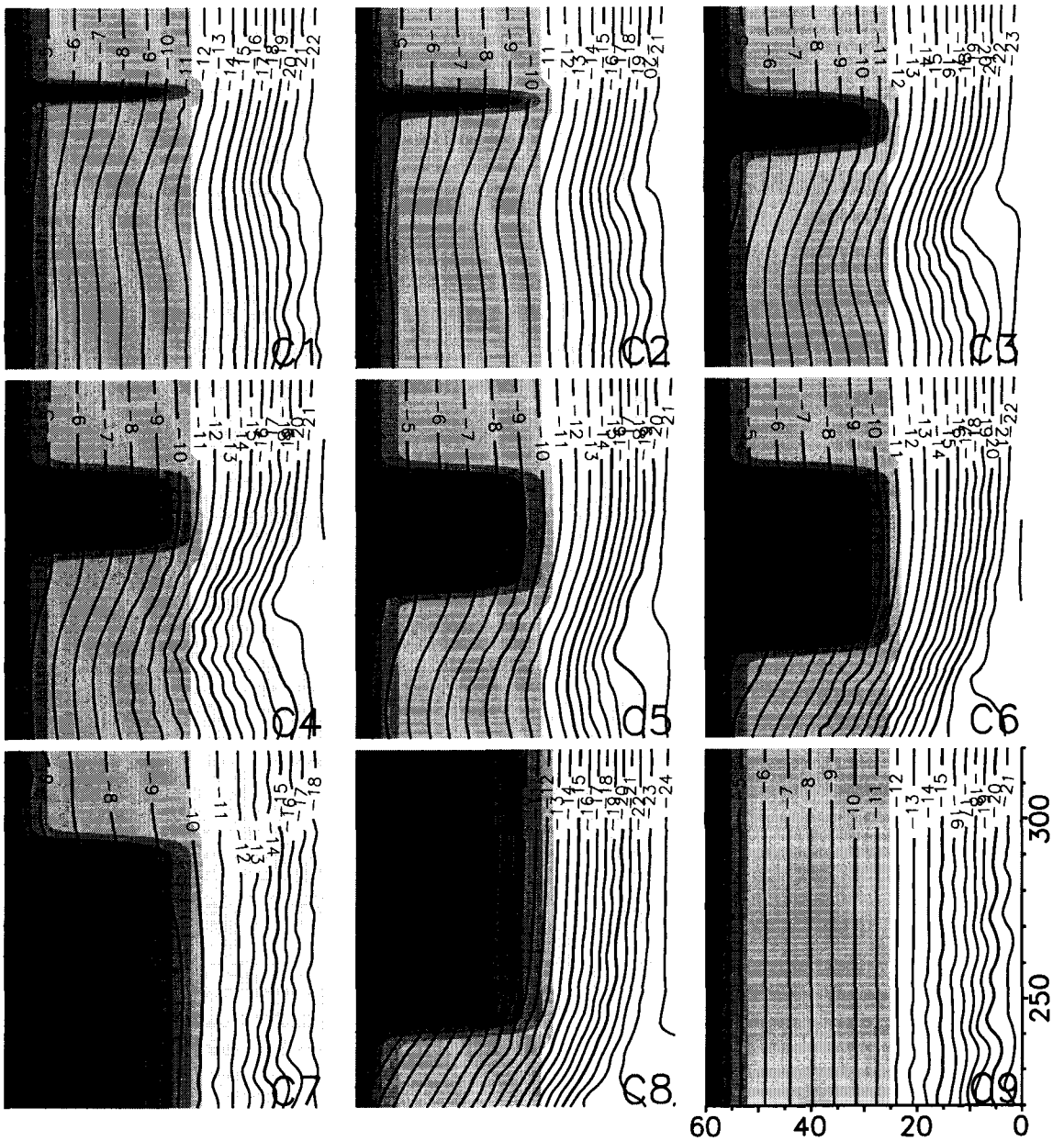

Figure 6. The free surface elevation (cm) at 15 d for nine cases with a=13 km. Bathymetry is shaded with an interval of 100 m. A subarea of 60 by 90 km is shown.

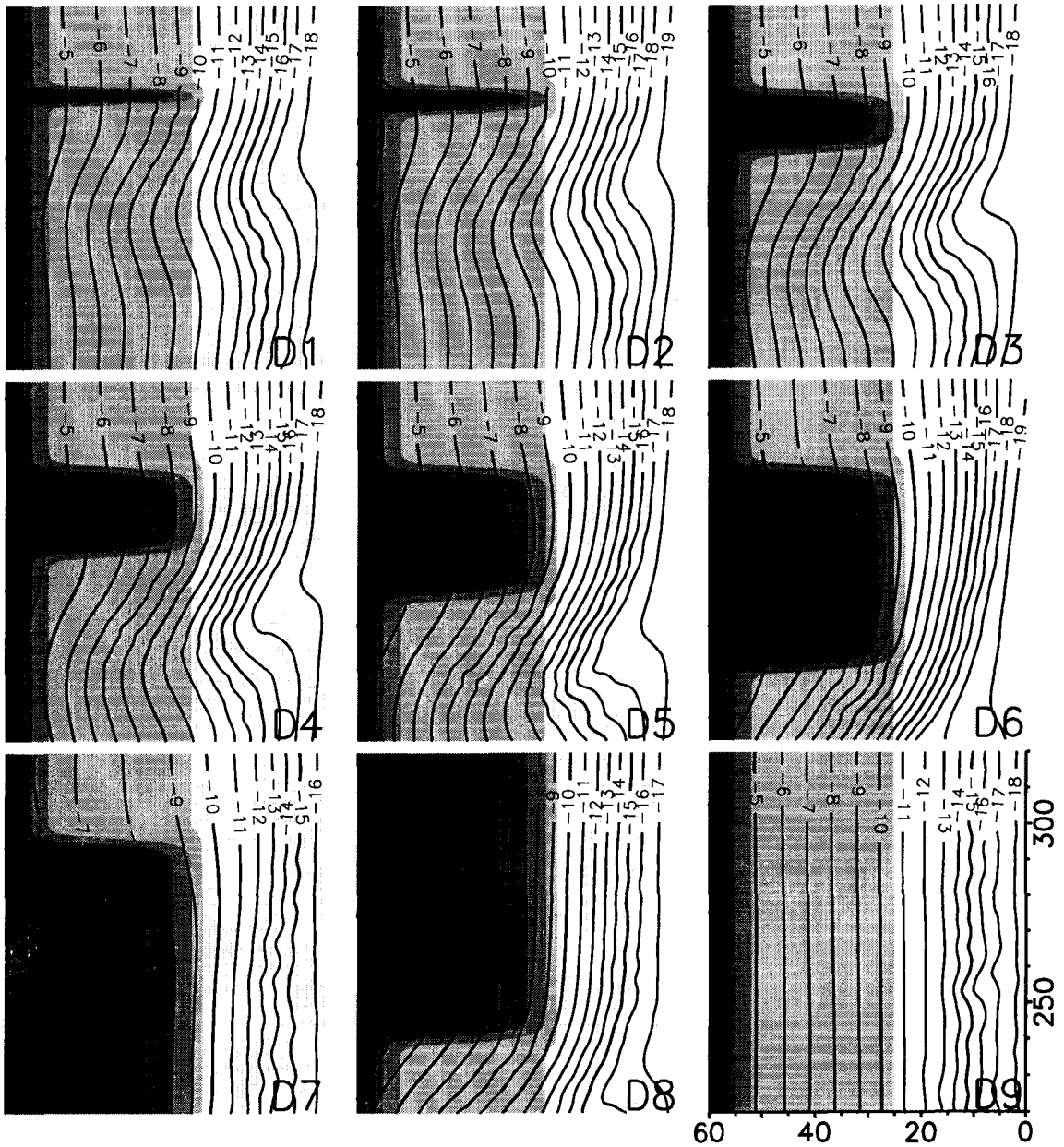

Figure 7. The free surface elevation (cm) at 15 d for nine cases with a=10 km. Bathymetry is shaded with an interval of 100 m. A subarea of 60 by 90 km is shown.

for C7 have a large transport due to the narrowing of the shelf in the southern part of the domain.

These results indicate that alongshore transport far upstream and downstream from the canyon (> 100 km) are not strongly disturbed by the canyon topography. Thus most of the onshore volume transport caused by the canyon returns offshore within 100 km of the downstream canyon wall (for this choice of stratification). The upstream escarpment (C7) has a much smaller transport at Sections NB and NC due to the drag effect created by the baroclinic pressure gradient between the shallow upstream shelf and the deep infinitely wide canyon. Section SC, which is the southern edge of canyon, displays the effect of canyon presence. All cases have larger alongshore transport than C9 indicating that canyon enhances alongshore transport crossing the downstream edge of canyon by pulling water onshore though the canyon.

The free surface elevation is consistent with a geostrophic balance of the alongshore flow over the general shelf-slope (C9 in Figure 6 and D9 in Figure 7). Upwelling induces changes in the mean sea level due to both offshore volume flux and the steric adjustment produced by changes in the density of the nearshore water column. Gill and Clarke (1974) demonstrated that when stratification is present, coastal upwelling results in a lower sea level height at the coast. A rising of the thermocline coupled with a lowering of the sea surface will tend to produce additional shrinking of the mixed layer depth toward the coast.

The free surface falls near the coast by about 20 cm after two weeks of spinup for a fixed stratification a=13 km (Figure 6). Canyon cases show that the free surface falls more than that of the case without a canyon (C9). Escarpment cases (C7 and C8) show that downstream wall enhances strongly the free surface tilting, indicating that the downstream wall causes the additional tilt. The upstream escarpment has (C7 in Figure 6) upwind alongshore pressure gradient between the upstream shelf and the deep infinitely wide canyon. The downstream escarpment (C8 in Figure 6) also

has downwind alongshore pressure gradient between both sides of the downstream wall. These upwind and downwind free surface slopes produce the drag effect of canyon ("canyon drag", see Discussion for details). Over wide canyons (C5 and C6), the water piles up in the middle of canyon with two upwind and downwind slopes. Over narrower canyons (C1, C2 and C3), the free surface tile does not change over the canyon but the overall tile is downwind between the two sides of canyon. The downwind free surface slope also appears over wide canyons, i.e. the free surface is high upstream of canyon and low downstream of canyon. Onshore flow can be induced within the canyon by this tilt (geostrophic balance). The free surface is higher in the middle of wide canyons than on either side, which can induce the anti-cyclonic circulation following the canyon rim.

III.2 CIRCULATION

Hickey (1997) observed a cyclonic circulation within a narrow Astoria Canyon under upwelling wind. Klinck (1996) and She and Klinck (2001) generated a cyclonic circulation within the canyon using a numerical model with a periodic across shelf boundary conditions. Thus study uses radiation conditions, the effect of which is seen in horizontal circulation within canyons with varying width.

The near-surface flow is downwind above the canyon rim and is not strongly modified by the canyon topography (figure not shown). The surface flow is southwest (due to Ekman turning) with speeds up to 0.6 m s^{-1} at 15 d. The near shore upwelling jet is confined to within 20 km of the coast and is nearly the same upstream of the canyon (section NB) for all canyon cases (C1-C7 and C9) except the downstream escarpment (figure not shown).

The horizontal velocity at 200 m (just below the shelf break) at 15 d over a 40×70 km subarea containing the canyon shows the strong effect of the canyon topography (Figure 8) on alongshore flow. Only the cases with a=13 km are shown in this figure

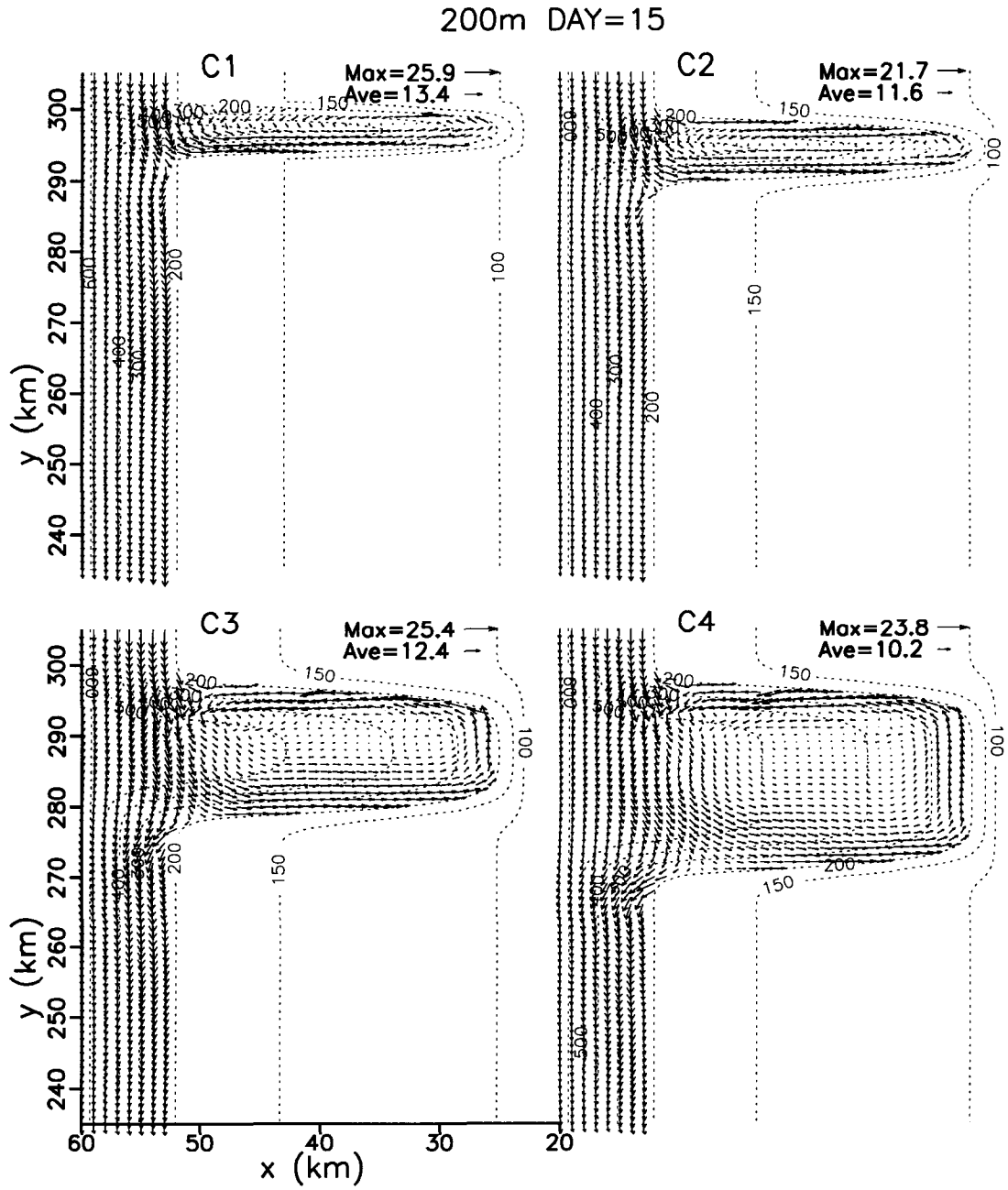

Figure 8. Horizontal flow at 200 m for day 15 for C1-8 in a 40 by 70 km subarea around the canyon. Every vector across shore and every vector alongshore are displayed. The mean and maximum speed are shown on each figure. The vector scale is consistent among these figures.

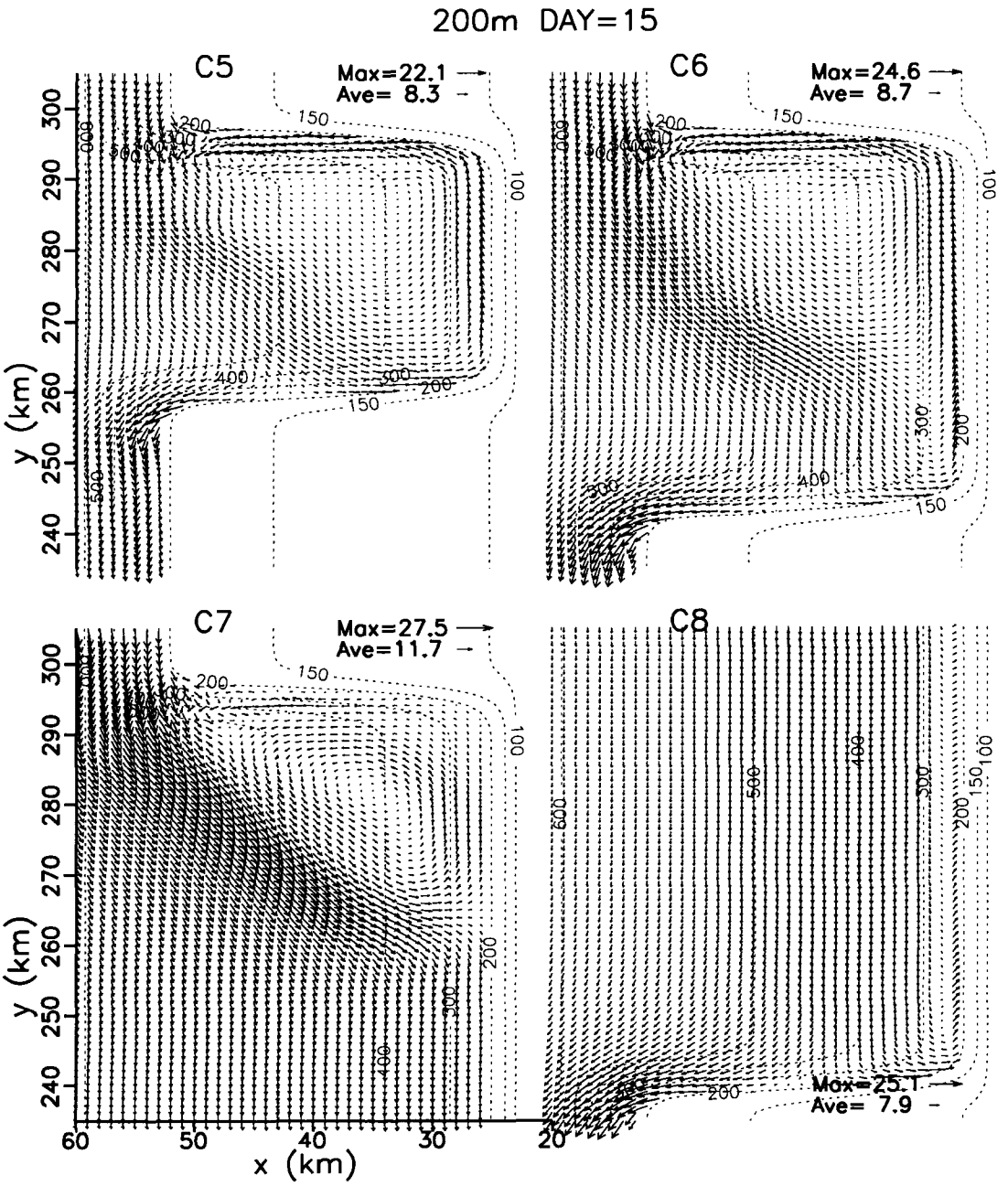

Figure 8. (continued)

because the cases with a=10 km have a quite similar flow pattern as that of a=13 km except the width of canyon cyclone is a little bit smaller. Flow over the continental slope is southward (downwind). The mean flow speed reduces in the canyon as the canyon widens, with the narrowest canyon being an exception. The maximum flow in the subdomain follows about the same pattern.

Circulation within the canyon can be separated into two patterns with time. At the early spinup until 5 d, the flow is slow and follows isobaths over all canyons (figure not shown), being onshore at the upstream wall, downwind along the head of canyon and offshore at the downstream wall. After 5 d, the upstream slope jet strengthens and detaches from the upstream offshore corner, and generates a cyclonic circulation within the canyon. Cyclonic circulation occurs in all canyons. Onshore flow along the downstream wall is stronger than the offshore flow along the upstream wall, indicating that net onshore flow occurs within the canyon.

There are three general features of these solutions which are best seen in the widest canyon (C6, Figure 8): a cyclone on the upstream wall, the flow along the slope turning into the canyon and a dividing flow with a stagnation point on the downstream wall. These features are clearly seen in the escarpment cases, which have only a downstream or upstream wall; however, C6 is wide enough that the two canyon walls interact only weakly. The flow along the head of the canyon is upwind. As the canyon becomes narrower, the cyclone becomes more elliptical and smaller and the stagnation point moves offshore (the slope flow does not penetrate as far towards the coast before hitting the downstream wall). For the narrowest canyons, the stagnation point does not appear as the slope flow jumps across the mouth of the canyon; only the cyclone remains.

For the wider canyon cases (C3-C6 and C7), the center of cyclone is about 10 km south of the upstream wall and does not get larger as the width of canyon increases. The separated slope current flows around the cyclone, being constrained by

stratification and inertia as to how rapidly the flow can change direction.

It is possible to classify these canyons into three types: narrow, intermediate and wide. Narrow canyons have mainly onshore flow over the whole canyon (C1-C2). Some offshore flow exists at the upstream wall but it is much weaker than onshore flow, due to the compressed shape of cyclone. Intermediate canyons have almost symmetrical cyclones filling the canyon with onshore flow only slightly stronger than the offshore (C3-C4). Wide canyons have a cyclone attached to the upstream wall and a detached slope jet turning into the canyon, ultimately separating into onshore and offshore flows at the downstream canyon wall (C5-C6). The two escarpment cases show the two halves of the wide canyon circulation. The upstream escarpment (C7) has very weak offshore flow at the upstream wall and very weak upwind flow along the canyon head. Thus, offshore flow at the upstream wall and upwind flow along the head is strongly influenced by the presence of the downstream wall. Note that the offshore and upwind flows are strong for wider canyons but weak for narrower canyons (C1, C2). So, narrow canyons have little effect of the pattern on the downstream wall. As the width increases, the downstream wall effect increases. Ultimately, the effect decreases until it disappears for infinitely wide canyons.

A second view of the circulation is the across shelf flow (u) at 15 d on section K (Figure 9), which crosses the middle of the canyons. All cases have similar features, although with different strengths. There is a thin, offshore flow at the surface due to the wind stress in the surface Ekman layer. There is also a thin, onshore flow at the bottom downstream of the canyon due to the bottom Ekman layer. The disturbed flow near the canyon becomes weaker nearer to the surface.

All cases have offshore flow just downstream of the canyon due to the shelf water trying to follow isobaths and thus turning anti-cyclonically around the canyon. All cases also have a cyclone in the canyon that extends above the canyon by 50 m or more. The onshore limb of the cyclone tends to have higher speed and be wider

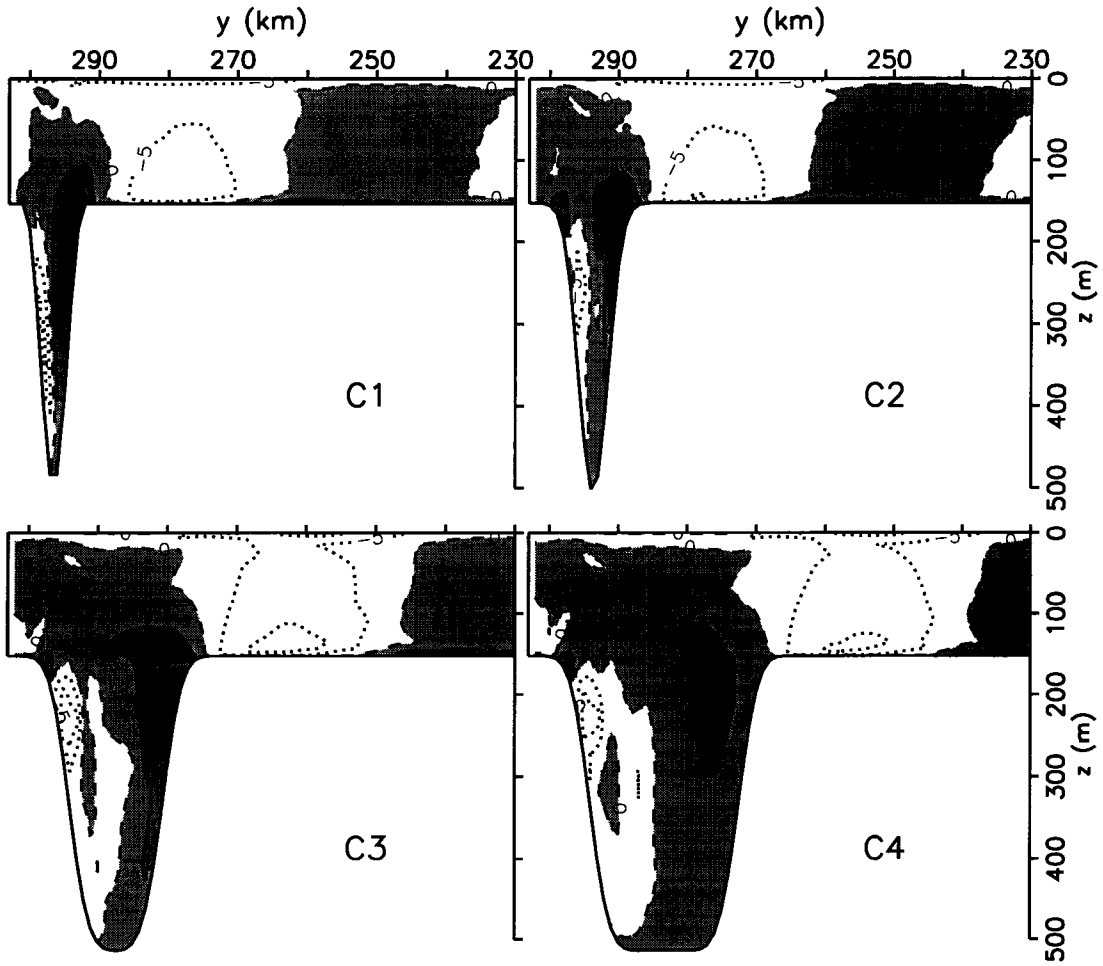

Figure 9. Across shelf flow speed at day 15 for Section K for cases C1-C8. Solid and dotted contours are onshore and offshore, respectively. The zero contour is dashed. Onshore transport are shaded. The view is from offshore looking towards the coast.

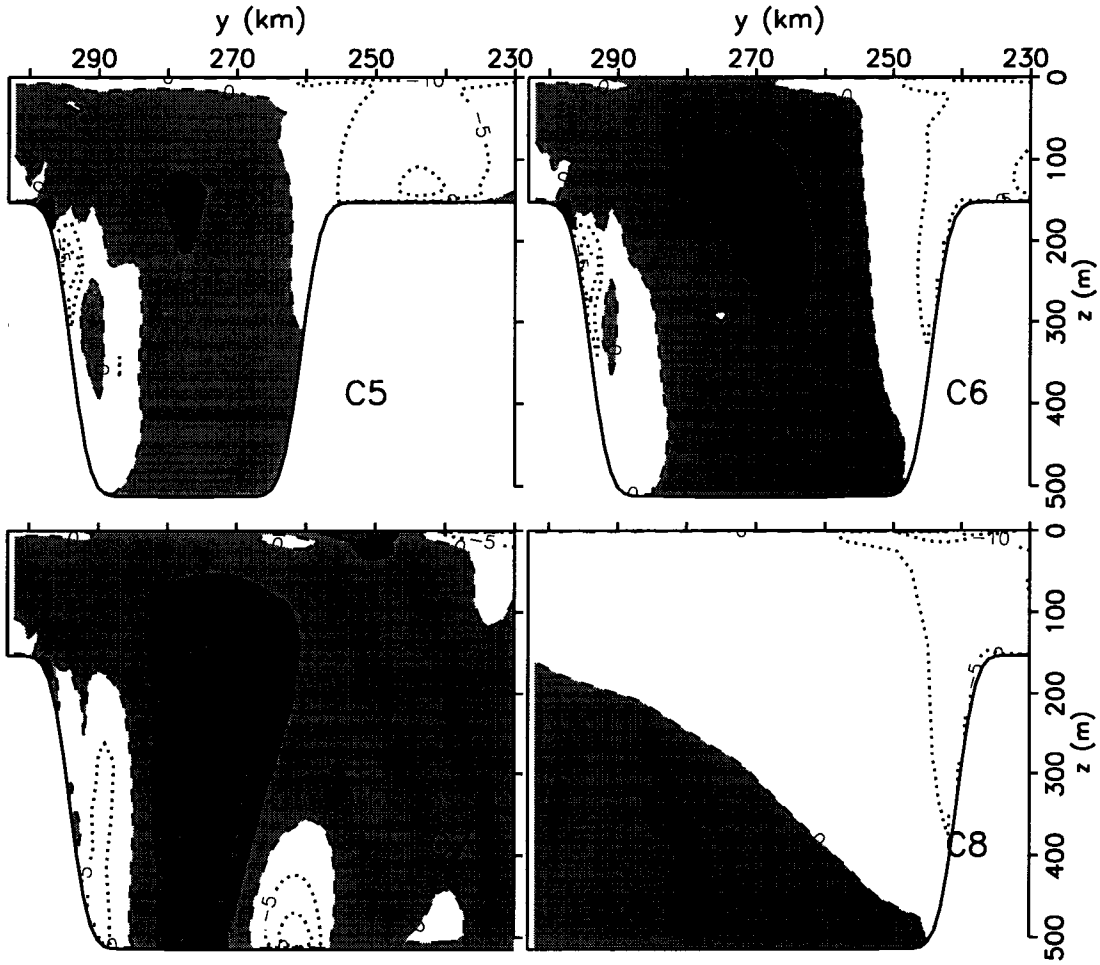

Figure 9. (continued)

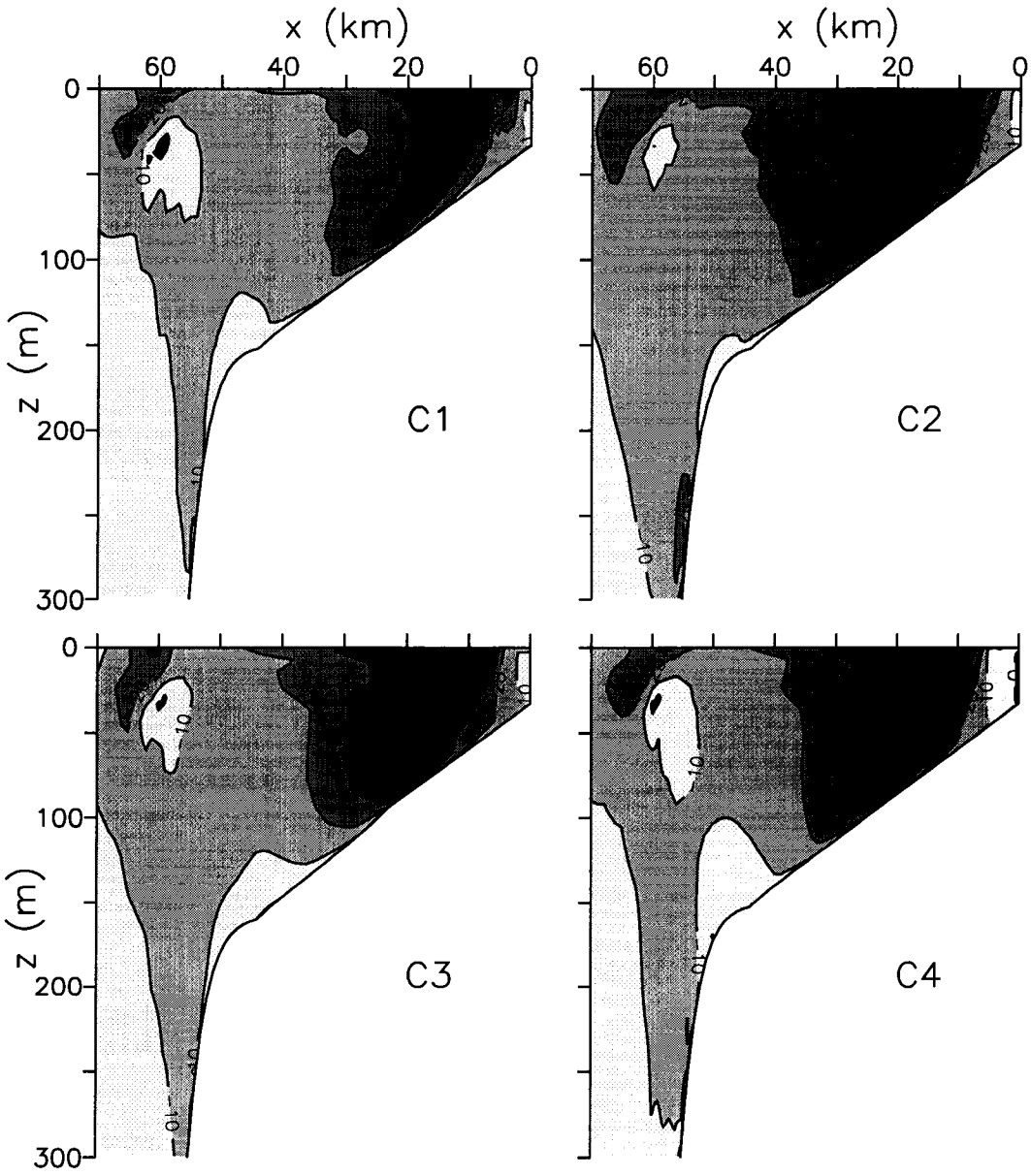

Figure 10. Across sectional view of alongshore flow (v, cm s^{-1}) at Section SC at 15 d for C1-C9 except C7. Contour interval is 10 cm s^{-1}.

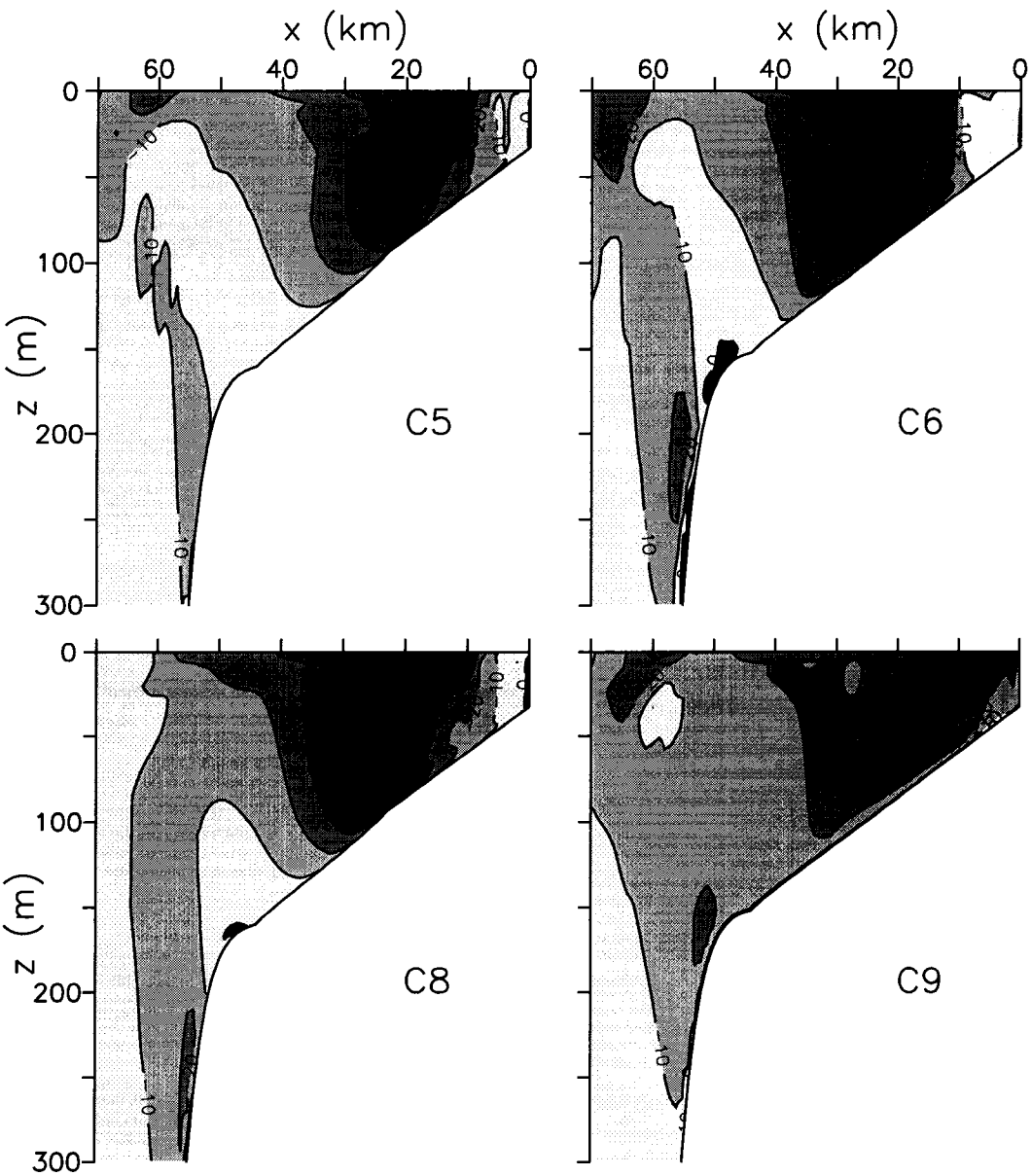

Figure 10. (continued)

indicating a net onshore flow. The offshore limb of the cyclone tends to be deeper so some of the onshore flow circles within the canyon and exits at a deeper depth. As the canyons become narrower, the offshore limb of the cyclone becomes weaker and deeper.

A final minor feature in all canyon cases appears on the upstream canyon edge where there is onshore flow. This is clearly distinct from the onshore flow due to the cyclone, and is due instead to the "falling in" phenomenon (Hickey 1997). Some water that moves along the continental shelf does not turn sharply enough to follow isobaths and is thus pushed into the canyon. These vortex lines near the bottom are stretched and develop cyclonic vorticity, which causes the flow to turn toward the coast. This flow feature occurs within about 5 km horizontally and 20 m vertically of the edge of the canyon.

Across shelf sectional view of alongshore flow at the downstream edge shows the canyon effect (Figure 10). The upwelling jet is seen near the coast in all cases; C9 shows the typical view without the influence of a canyon. The core of upwelling jet is 10 km offshore at the surface, with a peak speed of 0.4 m s^{-1}. The speed of the upwelling jet in this model matches the observation of Barton et al. (1977) off Northwest Africa (Figure 10.14 in Gill (1982)). They showed that after three days of strong wind forcing (10 m s^{-1}), alongshore current located 20-30 km offshore reaches 0.4 m s^{-1}. The slope jet which has a speed of 0.2 m s^{-1} is seen near the shelf edge.

The presence of a canyon modifies these upwelling and slope jets. The core of the upwelling jet moves 10 to 20 km offshore as the canyon becomes wider. The maximum speed increases to 0.6 m s^{-1}. A slope jet is seen over wide canyons (C6 and C8) but not as strongly over narrower canyons. A strong alongshore flow occurs in the middle shelf at the bottom below the upwelling jet, with a maximum speed up to 0.5 m s^{-1} This lower layer jet is the slope jet modified by the canyon circulation. The strength of the lower layer jet increases as the width increases, indicating that

wider canyons have a stronger geometric effect than narrower canyons.

III.3 ISOPYCNAL MOTION

The time behavior of selected isopycnals shows the upwelling of dense water within the canyon and the effect of this upwelling on the adjacent shelf area (Figure 11).

The first consideration is the location along the canyon axis at daily intervals of a few isopycnals for selected cases (C2, C6, C7, and C9; Figure 11). All isopycnals were initially horizontal. C9 shows the coastal upwelling response with no submarine canyon. The surfacing of isopycnals within 10 km of the coast is the well known coastal upwelling. The bottom Ekman layer on the shelf lifts the 26.0 isopycnal. The deeper isopycnals along the slope rise by a few 10's of meters within 10 km of the slope. By contrast, the narrow and wide canyon cases (C2, C6) have strongly elevated isopycnals, rising by 50 to 100 m within the canyon. Sobarzo et al. (2001) estimated the ascent rate of about 20 m day^{-1} for isotherms 10.5-11.0 °C above the canyon rim of Biobío Canyon off Chile. The model result shows a little bit slower rise compared to Sobarzo et al. (2001). The narrow canyon isopycnals rise more than the wide canyon. The other canyon cases have similar results (figures not shown). Away from the upstream escarpment (C7) the isopycnals rise slightly more than the no topography case but the elevated isopycnals span a much wider distance (20-30 km).

The layer between isopycnals 26.0 and 26.5 shows the layer compression for C2 and C6, which produces anti-cyclonicity. Thus flow in this layer is expected to turn downstream onto the shelf. On the other hand, the layer between isopycnals 26.8 and 27.0 shows vortex stretching, which produces a cyclonic circulation below the canyon rim. This result matches Hickey's (1997) report that upwelling from the canyon results in layer compression at the top of the canyon and stretching throughout the rest of the canyon.

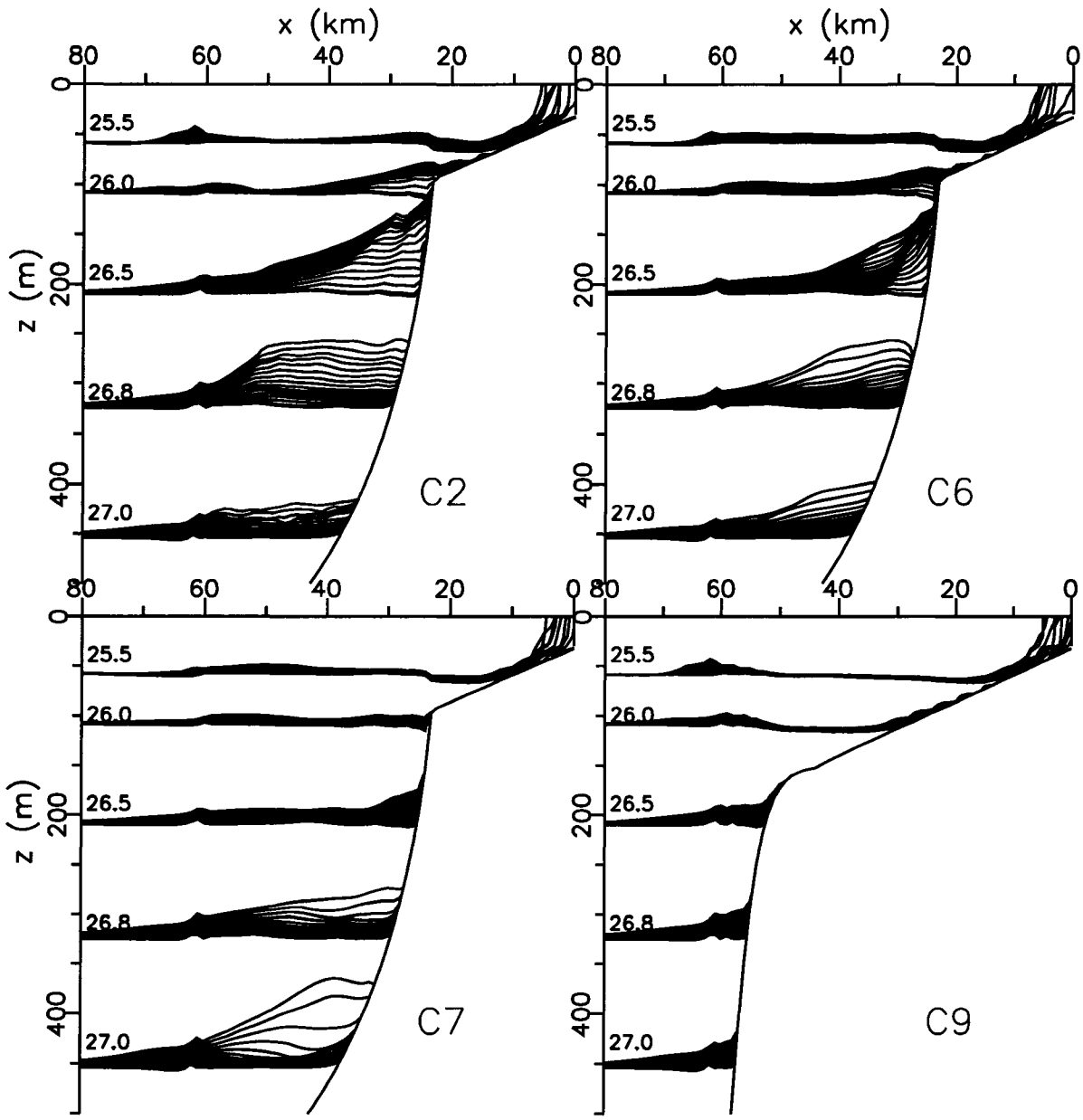

Figure 11. Location of selected isopycnals (ρ=25.0, 25.5, 26.0,26.5, 26.8, 27.0) at daily intervals for four cases (C2, C6, C7 and C9) along the canyon axis (Section CX) for the period of 0-15 d.

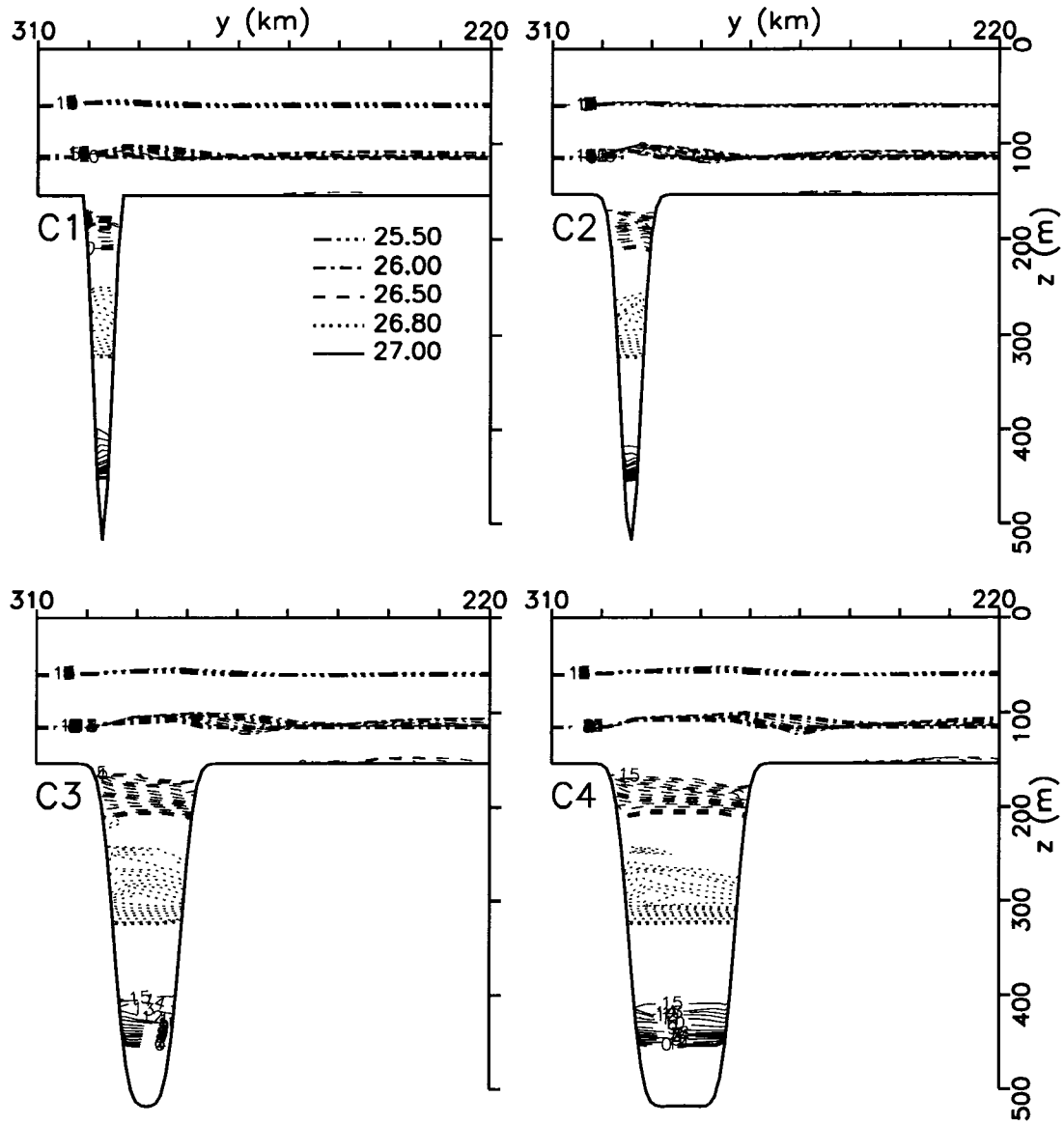

Figure 12. Location of isopycnals initially at 50, 100, 200, 350 and 500 m at daily intervals for eight cases C1-C8 along Section K for the period of 0-15 d. Initial isopycnals are level. Each isopycnal is shown in upper left.

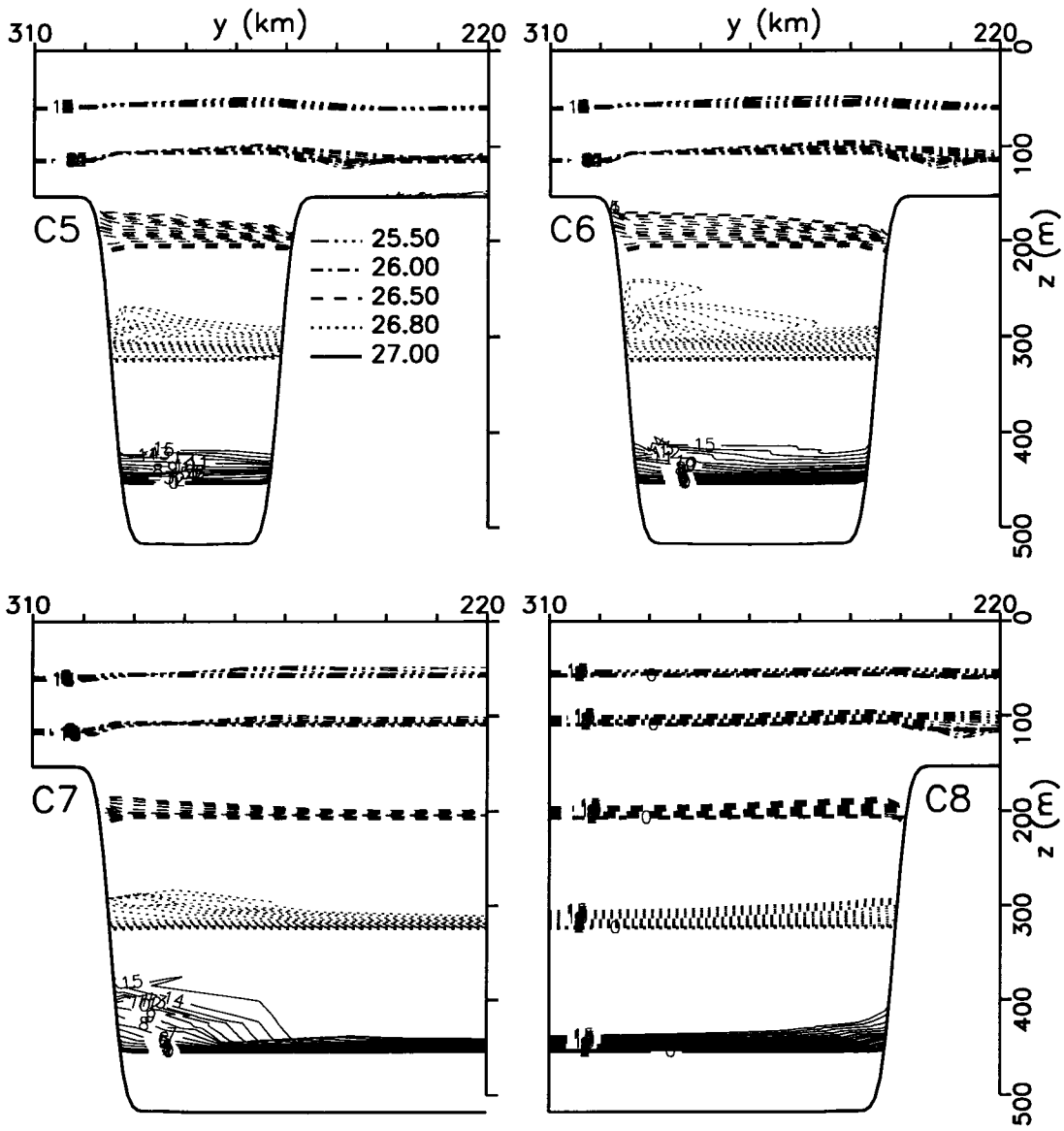

Figure 12. (continued)

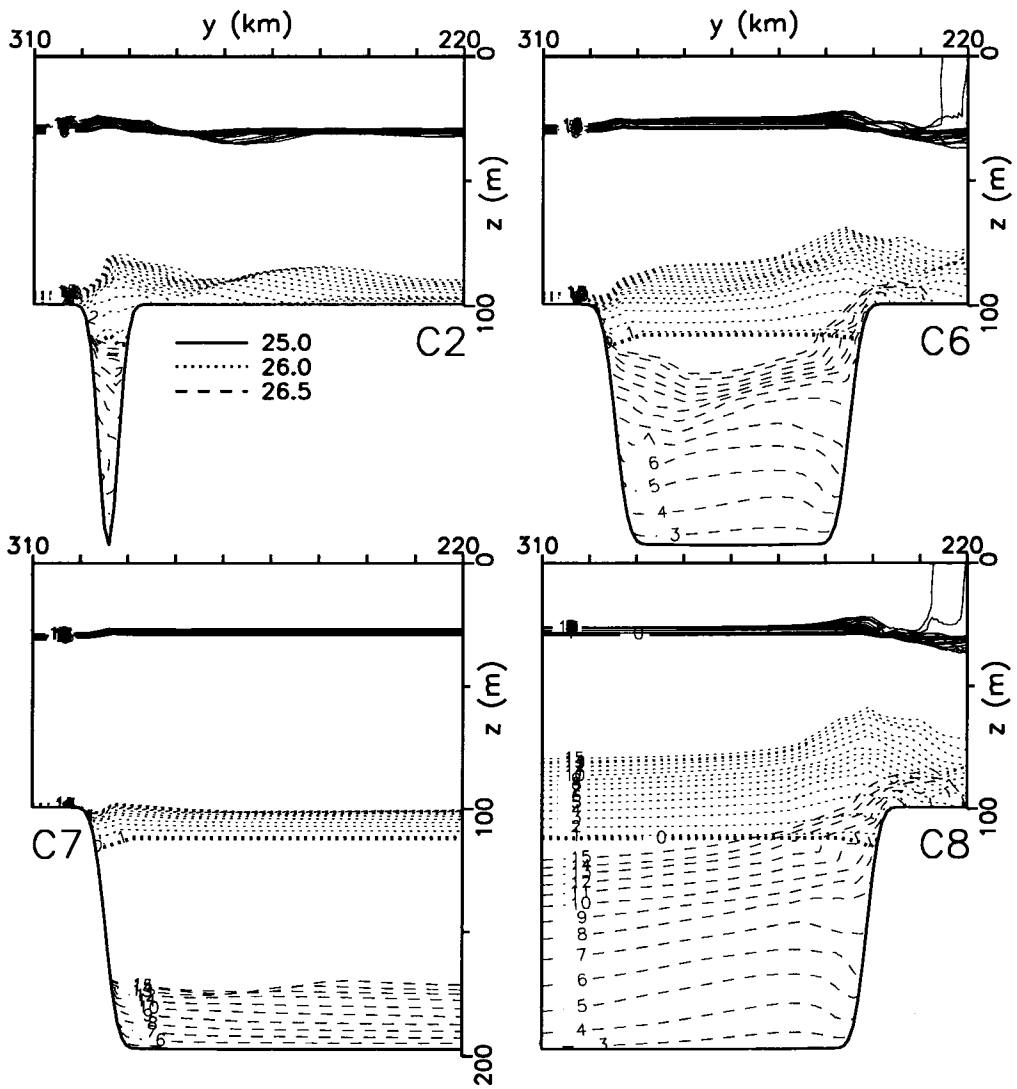

Figure 13. Location of selected isopycnals (ρ=25.0, 25.5, 26.0) at daily intervals for four cases (C2 and C6-C8) across the inner canyon (Section J). The numbers on the isopycnals are the time in days.

The alongshore view of the isopycnals (Figure 12) along section K illustrates the stretching and compression of the upper and lower layers within the canyon. The stretching vorticity was calculated as

$$(\frac{h_c}{h} - 1)f = RV, \tag{12}$$

where h is a layer thickness and h_c is a layer thickness after stretched or compressed to see the vortex stretching (Hickey 1997). For case C3, the original layer thickness of the upper layer (26.5-26.8) is about 110 m which was compressed to 80 m after 15 days. The stretching vorticity is about -0.3 f which drives anti-cyclonic circulation in the upper layer below the canyon rim. The thickness (130 m) of the lower layer (26.8-27.0) is stretched to 160 m, creating a cyclonic vorticity of 0.2 f, driving a cyclonic circulation in the lower layer. Other cases show similar results except that the stretching is active near the upstream wall of wider canyons.

Another alongshore section which illustrates the effect of canyon upwelling on the surrounding water properties is along a section through the head of the canyon (Section J in Figure 13). The narrow and wide cases along with the two escarpment cases (2, 6, 7 and 8) are displayed; the intermediate canyon cases have similar results (figures not shown).

In all cases, the upper isopycnal above the canyon shows only limited motion, except downstream of the canyon due to the offshore flow there. Also, the near steadiness of the solution after 15 d is evident in the relatively tight clustering of the isopycnals after this time. Finally, for all cases, there is a very weak motion of the isopycnals upstream of the canyon but a relatively dramatic upward motion over and downstream of the canyon. The upstream escarpment (C7) has the weakest isopycnal distortion near the head of the canyon. The canyon and downstream escarpment cases show a strong lifting of the isopycnals over the canyon by 10 to 50 m (similar to the results of Hickey 1997). The deep isopycnal in these cases shows a persistent lifting

with an eventual spilling of the dense water onto the shelf. Over the 20 d simulation, the isopycnal in the canyon head rises by 100 m and more. Finally, the middle isopycnal (26.0) remains elevated far downstream of the canyon while the deeper isopycnal hits the bottom about 10 km downstream of the canyon edge. In this case the dense water is being swept offshore along the canyon rim due to the shelf flow going around the canyon. Similarly in across shelf section, the layer between isopycnals 26.0 and 26.5 shows strong vortex compression for C2, C6 and C8. Strong anti-cyclonic flow toward the downstream is observed in this layer.

Also the baroclinic tile matches the circulation within the canyon described in the previous section. For example, offshore deepening of density surfaces within the canyon (C2 and C6 in Figure 11) and even in escarpment case (C7) induces the upwind flow along the head of canyon by the baroclinic geostrophic balance. The tilt of density surface over wide canyon (C6 in Figure 13), representing onshore flow near the downstream wall and offshore flow near the upstream wall (cyclonic circulation). This results indicate that the general dynamical balance is baroclinically geostrophic within wide canyons.

III.4 TRACER TRAJECTORY

Neutrally-buoyant tracers were released at 2 d into the simulations at several depths in an array upstream of the canyon for each of these cases (except the no-canyon case). The 99 tracers (11 lines of 9 particles) are released for all cases except C8 where 253 (23×11 strings) were released. The locations of the tracers were calculated while the model ran and were saved at every 6 hours. Trajectories of the tracers released at 250 m depth upstream of the canyon illustrate the path of water parcels in the upper canyon and show where water crosses onto the shelf (Figure 14).

In all cases, tracers travel downwind due to the wind driven flow on the upper continental slope. C4 (Figure 14) illustrates all of the patterns that are observed in

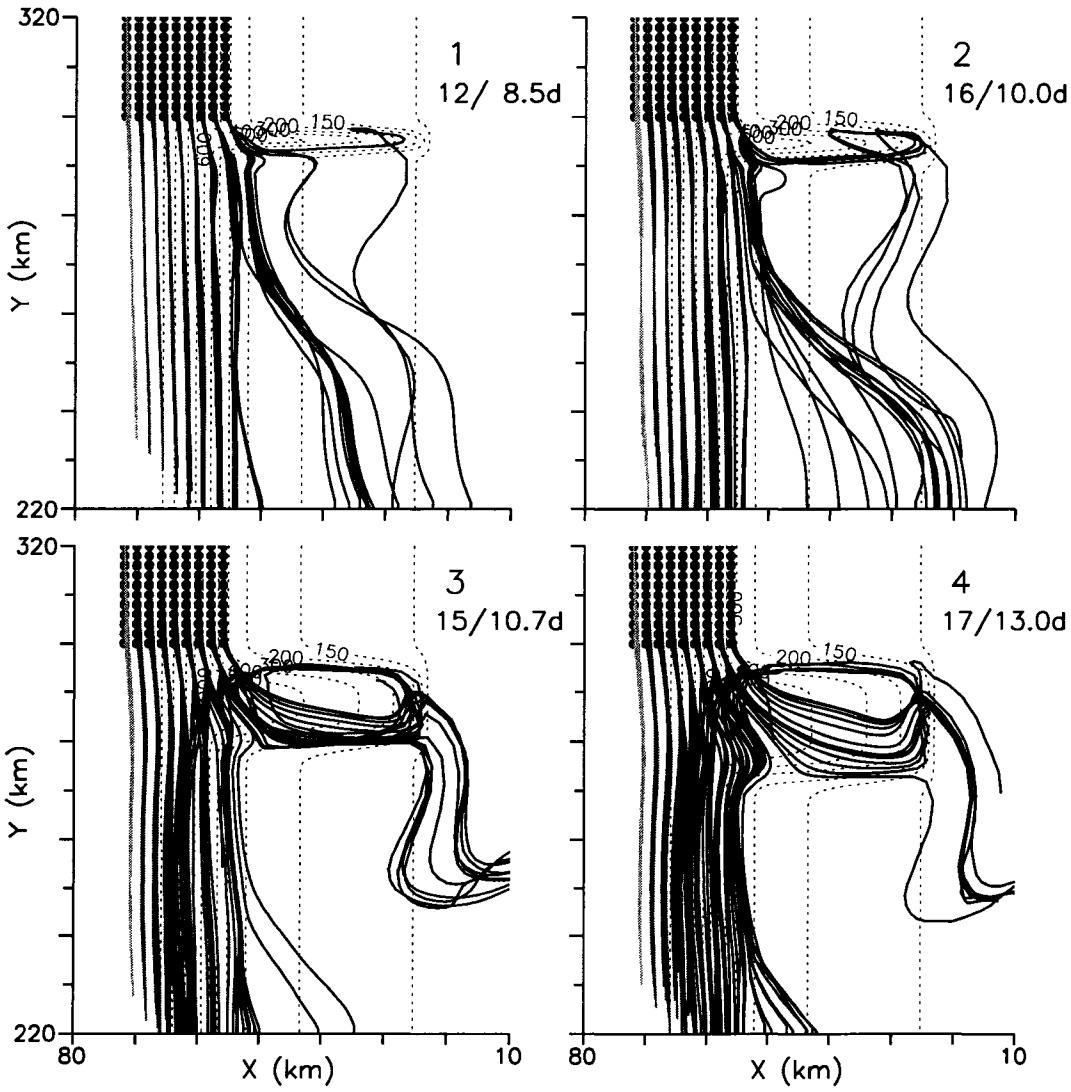

Figure 14. Tracer trajectories for C1-C8. Ninety nine tracers are released in a rectangular pattern spaced every two grid points at 250 m on day 2; C8 has 253 tracers. The gray scale of each trajectory shows the released locations offshore. The numbers on the upper right of each panel are the number of tracers that upwell onto the shelf break depth (150 m) and the average time taken until they reach the shelf break depth.

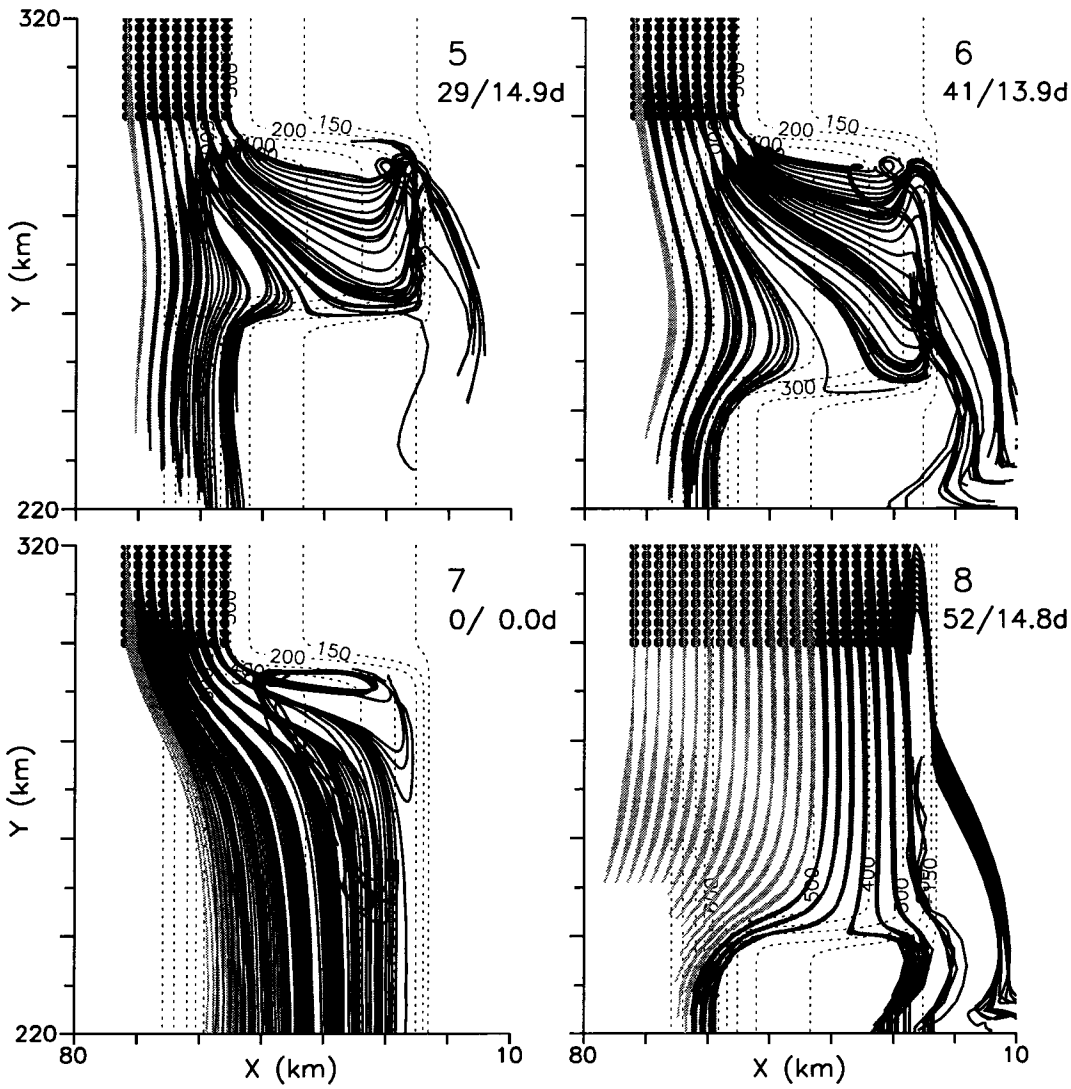

Figure 14. (continued)

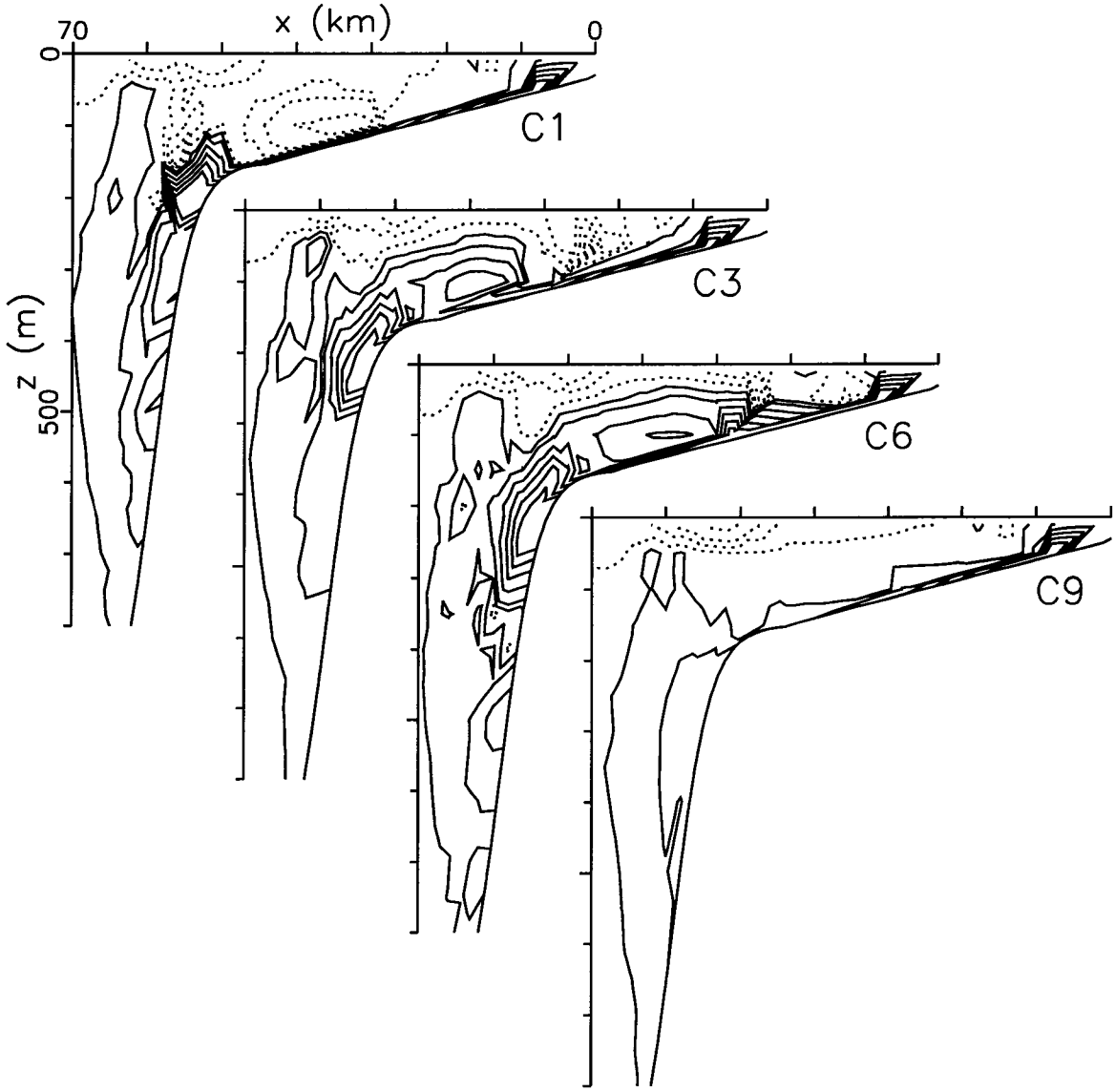

Figure 15. Upwelling distance (m) of tracers initially located at every 50 m vertically and every 2 km horizontally at y=302 km which is upstream edge of canyon for the period of 2-15 d. Contour intervals are -16, -12, -8, -4, -2, 0, 2, 4, 8, 12, 16, 20 m. Negative values including zero are dotted, indicating downwelling region. Four cases C1, C3, C6 and C9 are depicted.

these cases. A large number of the tracers either travel alongshore and avoid the canyon entirely, or dip into the outer part of the canyon and return to the alongshore flow downstream of the canyon. Tracers closest to the shelf enter the canyon and follow a cyclonic path in the upstream part of the canyon. Some of these tracers circle more than once and either exit the canyon into the alongshore flow on the upper slope or jump onto the shelf near the head of the canyon, typically at the downstream corner. Finally, some tracers get close enough to the bottom that the bottom Ekman layer pulls them onto the shelf. There is a preferred place, downstream of the canyon, where many tracers cross onto the shelf (Figure 14, C1-C4). Interestingly, the upstream escarpment (C7) has no tracers that cross onto the shelf. This result may be a statistical fluke based on the initial location and time of these tracers; however, many fewer tracers cross the shelf for the upstream escarpment than for any other case.

The total number of tracers that cross the shelf break increases as the canyon widens (Figure 14, C1-C6). The largest number occurs for the downstream escarpment while the smallest is for the upstream escarpment. It is important to note that many of the tracers that cross the shelf break do so downstream of the canyon and not within the canyon, so one must consider the direct upwelling within the canyon as well as the enhanced upwelling in the downstream canyon wake when analyzing the effect of canyons on cross shelf exchange.

The source region of deep water which is upwelled onto the downstream shelf was investigated by tracking upwelling and downwelling tracers which were initially dropped at the upstream edge of canyon. The upwelling distance of tracers was displayed (Figure 15). Most tracers over the slope upwell despite the canyon presence. But canyon cases shows strong upwelling than the case without canyon. Canyon cases has the strong upwelling source region ($>$ 20 m) near the shelf edge centered at 200 m. This result indicates that it is very hard for the deep slope water to reach the shelf from the depth below 400 m. The only possibility for the deep slope water to upwell

onto the shelf is the route through the canyon where upwelling is stronger than the outside. As the canyon narrows, the source region becomes deeper, indicating that a narrow canyon enhances upwelling of deep water.

III.5 ACROSS SHELF EXCHANGE

The temporal variation of vertically-integrated across shelf volume transport across Section K versus alongshore locations shows the effect of the canyon on across shelf exchange (Figure 16). For all cases, onshore transport increases within the canyon until 13-15 d after which the transport decreases or remains steady (with some oscillation) depending on the case. Downstream of the canyon, transport is alternatively offshore then onshore. The oscillation does not extend more than 80 km south of the downstream wall of canyon even for the widest canyon case (C6). This result indicates that the canyon disturbance does not extend further than 80 km downstream. Further downstream, some small disturbances continues after 13 d which may be caused partly by the numerical truncation errors of the southern open boundary.

Within the canyon before 5 d, onshore transport occurs at the upstream half of the canyon and offshore transport occurs at the downstream half for wide canyons; offshore flow appears to be outside the canyon for cases 1 and 2. For all cases, the initial flow follows isobaths, entering the canyon on the upstream half. After 5 d, onshore transport expands to the downstream half. However, some onshore transport remains in the upstream half of the canyon, increasing for 5 to 8 d (depending on the case) after which it declines. Offshore transport develops at the upstream half between 5-7 d (dotted contours between solid contours within the canyon), which shows the development of the cyclone within the canyon. Adjustment occurs earlier over narrower canyons compared to wider ones. Notice that the inertial adjustment is not present in the narrowest canyon (C1) until 10 d; there is onshore transport over the whole canyon until 10 d. As the flow speed develops, inertial effects cause the onshore

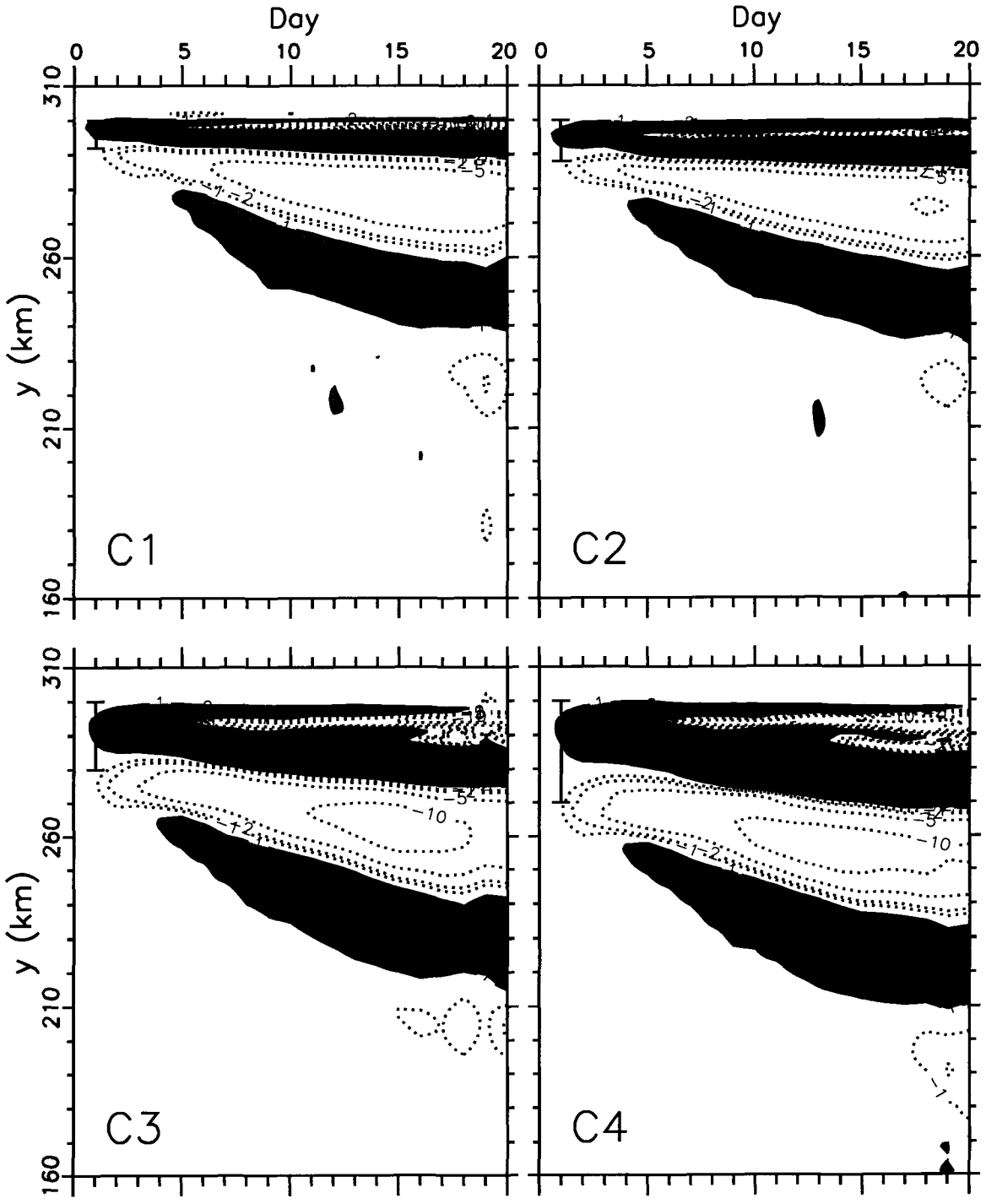

Figure 16. Temporal variation of across shelf transport (mSv) across section K by alongshore locations y=160-310 km. Solid line indicates onshore transport and dotted line does offshore transport. Contours are -20, -15, -10, -5, -2, -1, 1, 2, 5, 10, 15, 20 mSv. Canyon widths are marked by the bar on the figure.

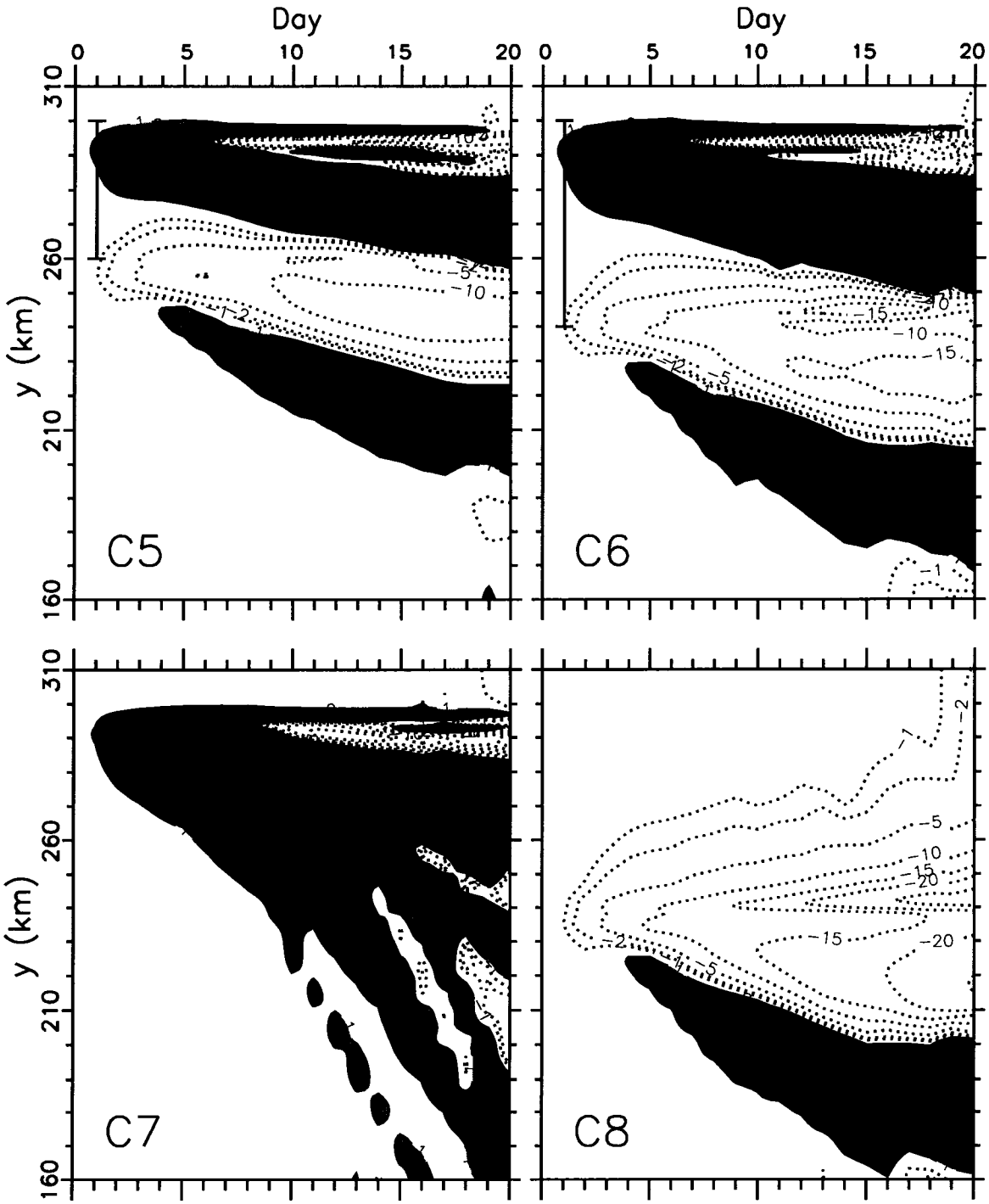

Figure 16. (continued)

flow to separate from the upstream corner and occur mostly in the downstream half of the canyon. This adjustment takes a week or two for the cases considered here. Offshore transport near the downstream edge of canyon continues until 15 d over wide canyons (C4-C6). This shows the offshore flow separated from onshore flow at the stagnation point at the downstream wall of wide canyons.

The total transport into the canyon increases with time until 15 d in all cases except the downstream escarpment (C8). There is continually increasing upwelling in all canyons and the inertial effects merely determine which side of the canyon feeds the upwelling. Net canyon transport clearly shows that wider canyons have larger onshore transport. The upstream escarpment (C7), however, has very weak transport, comparable to the no-canyon case. Downstream of the canyon there is continuous offshore transport. Most of the onshore flow over the canyon is compensated by offshore transport downstream of the canyon. Onshore and offshore transport involves different water, which is clear from the tracer trajectories (Figure 14). Much of the onshore flow involves water near the shelf break depth. The offshore flow occurs in the upper water column (figures not shown). Because of this vertical segregation of the across shelf exchange, there is a net flux of offshore, deeper water properties onto the shelf in exchange for onshore, shallower water properties. In effect, there is a net salt and density flux onto the shelf and a heat flux off the shelf. For most circumstances, there would also be a net nutrient flux onto the shelf.

Alongshore and across shelf transports are related by a power function

$$U = m_1 V^{n_1} \quad \text{before adjustment,} \tag{13}$$

$$U = m_2 V^{n_2} \quad \text{after adjustment,} \tag{14}$$

where parameters m_1, n_1 and m_2, n_2 are listed in Table 7 and Figures 17 and 18. The alongshore transport was obtained from the depth-averaged along shelf current crossing Section NC over the shelf (Section K to the coast). Across shelf transport (U) is the depth-integrated transport crossing the canyon between two walls along

Table 7. Coefficients of power function (Equation 13) between alongshore transport at Section NC and across shelf transport crossing the middle of canyon for all cases. Power curves are depicted on Figures 17 and 18 for topographic cases and Figures 31 and 32 for stratification cases. m_1 and n_1 are listed on the upper panel and m_2 and n_2 are listed on the lower panel.

Case	A	B	C	D	E	F
1			0.04, 0.6	0.06, 0.6		
2			0.03, 0.5	0.05, 0.5		
3	0.02, 0.2	0.03, 0.3	0.04, 0.4	0.06, 0.4	0.09, 0.5	0.19, 0.7
4			0.05, 0.4	0.07, 0.5		
5	0.03, 0.1	0.05, 0.4	0.23, 2.6	0.53, 2.7	0.12, 0.5	0.22, 0.6
6			0.07, 0.4	0.09, 0.4		
1			0.06, 1.7	0.15, 2.1		
2			0.09, 2.2	0.22, 2.5		
3	0.03, 1.3	0.06, 1.8	0.15, 2.4	0.30, 2.4	0.95, 2.7	2.60, 2.7
4			0.18, 2.4	0.41, 2.6		
5	0.06, 1.9	0.11, 1.7	0.23, 2.6	0.53, 2.7	1.24, 2.6	2.70, 2.5
6			0.30, 2.5	0.67, 2.9		

Section K. Daily values are depicted in Figures 17 and 18. The adjustment occurs approximately after 5 days of spinup under stratifications of a=13 and 10 km. Across shelf transport is onshore within the canyon and increases with time and alongshore transport. This onshore transport increases gradually with alongshore transport before adjustment until 5 d. After the adjustment, it increases rapidly with alongshore transport.

The U-V curves are broken at the time point where adjustment occurs because the canyon circulation is different before and after the adjustment. As described in Section III.2, the alongshore flow is not fully developed to detach from the upstream slope so that the overall canyon circulation follows isobaths (onshore at upstream slope and offshore at downstream slope) before the adjustment. After 5 d, the flow into the canyon is adjusted to the canyon topography and generates a cyclone within the canyon (onshore flow at the downstream and offshore at the upstream). The U-V curves responds the change of circulation within the canyon then have different

coefficient in power function. This curve shows that the effect of canyon width is less before than after adjustment because U values are widely distributed for a given V after adjustment. After 15 d which is in quasi-steady state, U-V points group around the tip of power curves, which indicates that the power curve is still valid at the steady state. Stratification has an effect on the timing of adjustment then the shape of power curves. It was turned out that the adjustment occurs earlier under weaker stratification. Details of stratification effect will be considered in the next chapter (Section IV-5).

Wide canyons have larger onshore transport than narrow canyons for a given alongshore transport despite before and after the adjustment. This result may be expected given the wider area for onshore flow. However, the smaller canyons (C1-C2) have a larger transport per unit width (U/W) than the larger cases. For example, for an alongshore transport of 0.9 Sv, which is near the quasi-steady solution for each case presented here, the across shore transport per width for the 6 cases, based on the power function fit is 6.3, 5.9, 5.8, 4.7, 4.4, 3.8 mSv/km, for C1-C6, respectively (Figure 17). The narrowest case has the largest onshore transport per unit width. The next two width cases have a little smaller values, followed by the wider cases being about 60-70 % of the narrowest case. For the cases with a=10 km, the across shelf transport per width is 11.7, 10.5, 8.8, 7.7, 7.3, 5.8 mSv/km for a given alongshore transport 0.8 Sv, based on the power function fit (Figure 18). Cases D1-D6 are quite similar to C1-C6. The narrowest case has the largest onshore transport per unit width, with the next two width case a little smaller, followed by the wider cases being about 50-65 % of the narrowest case. This result indicates that a canyon width of $2a$ is the separating case between narrow and wide canyons. For the case with a=13 km, the width about 26 km which is between C3 and C4 is the separating case. For a=10 km, the width of 20 km (D3) is the case separating narrow and wide canyons.

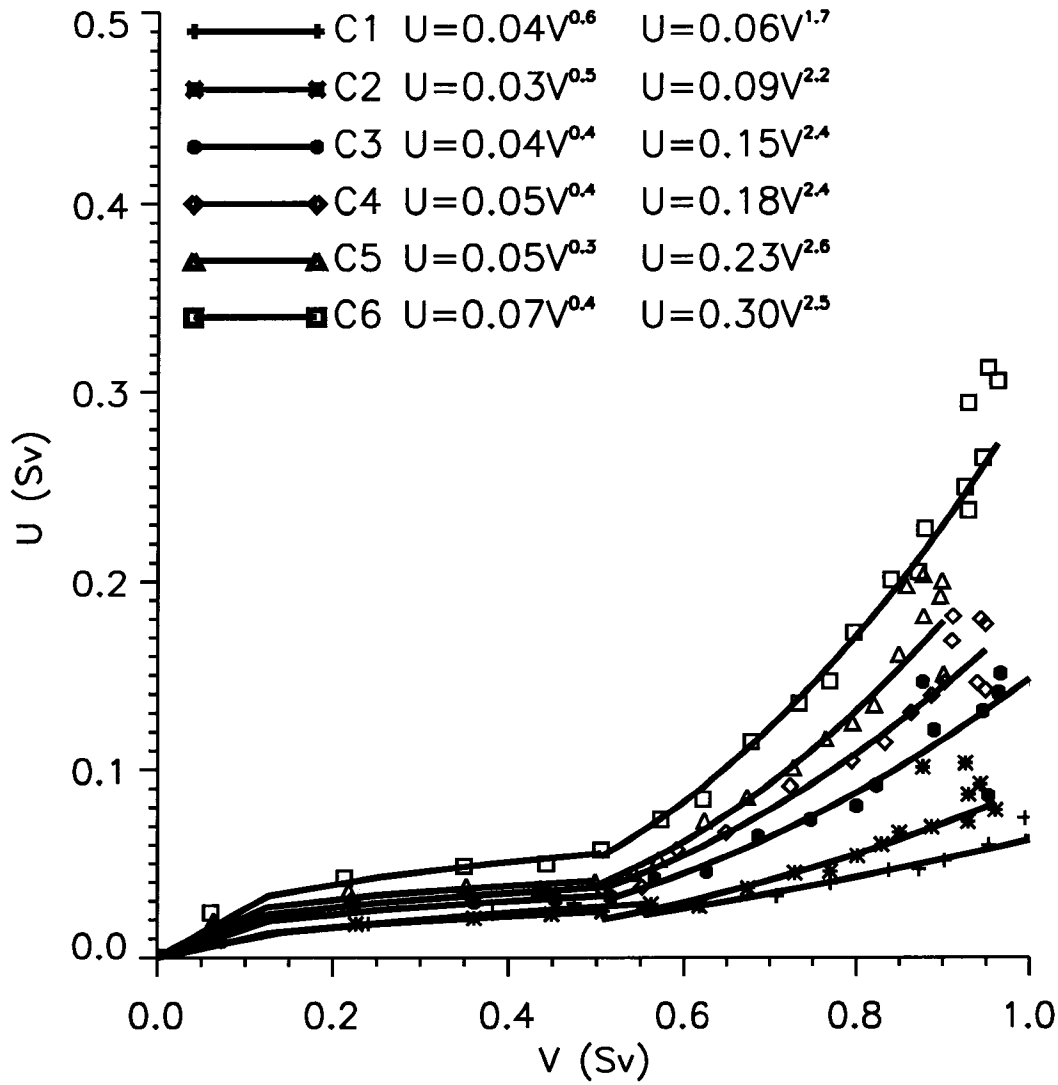

Figure 17. Relationship between across shelf transport (U) within the canyon and alongshore transport (V) crossing Section NC over the shelf (Section K to the coast) for each day of each case with a=13 km over 20 d. The different lines are a power function ($U=mV^n$) fit to each case. The parameters of each functional fit are included on the figure.

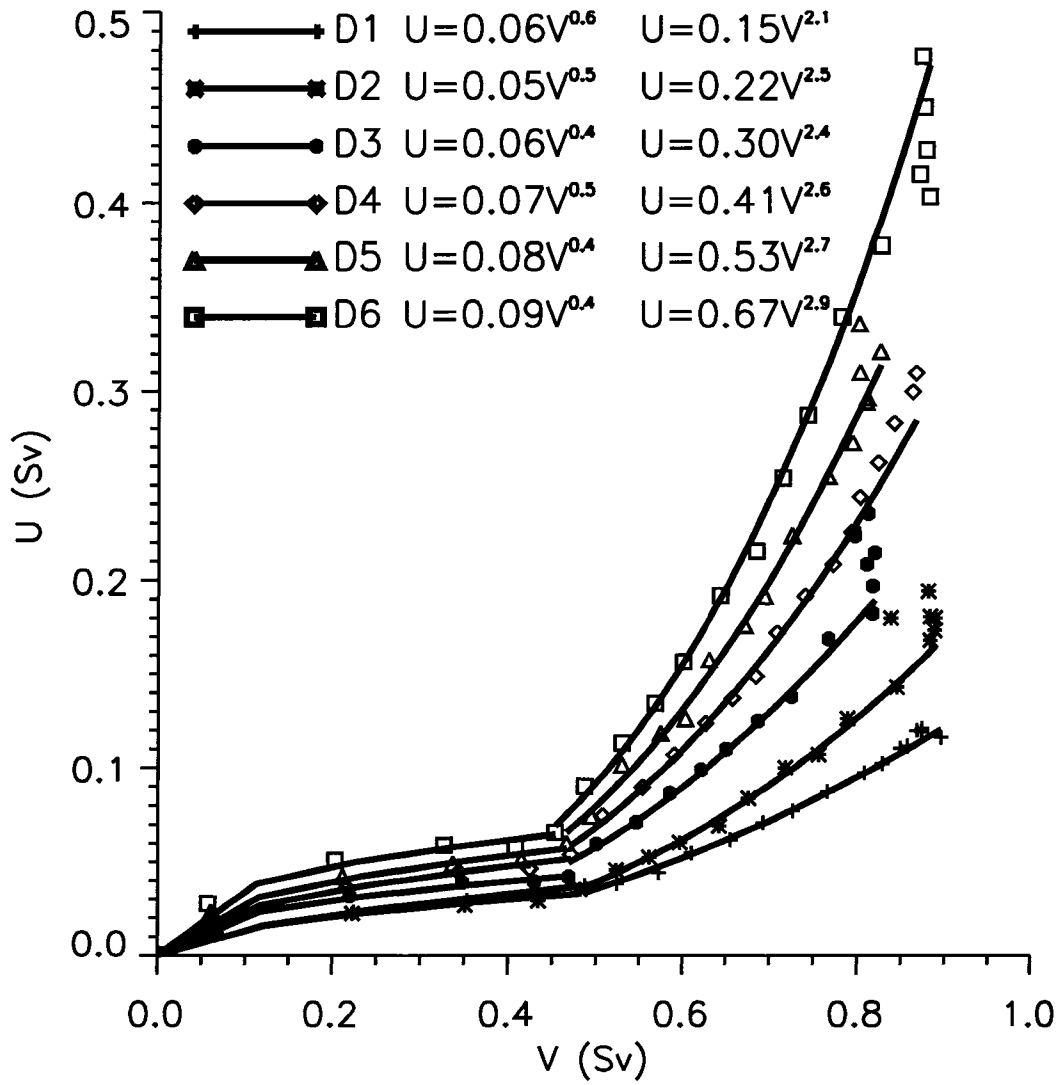

Figure 18. Same as Figure 17 except reduced stratification (a=10 km).

CHAPTER IV

EFFECT OF STRATIFICATION

This chapter describes the effect of stratification on canyon dynamics. Stratification increases the internal deformation radius and suppresses the vertical movement within the water column by increasing the stability. The ratio of the internal deformation radius to the canyon width (the stratification number) decreases as stratification increases, which can change the characteristics of canyon dynamics. Thus stratification is an important factor for canyon dynamics. According to Klinck (1996), a canyon can be separated into two types such as narrow and intermediate by different stratifications. In this chapter, the response of 20 km and 40 km canyons to six stratifications is described.

IV.1 QUASI-STEADY STATE

Alongshore transport over the shelf increases with time until 15 d under stronger stratifications (A3-D3) or 10-12 d under weaker stratifications (E3-F3) after which it reaches an approximate steady state (Figure 19). There occur further changes due to oscillations or continued baroclinic adjustment from canyon upwelling after 15 d. Quasi-steady state indicates that surface wind forcing is largely in balance with the bottom drag.

As in Chapter 3, Equation (11) was related alongshore transport (V) to time (t). Two parameters V_m and K_d are given in Table 8. This equation has a good fit to data. The quality of fit (r^2) is greater than 0.93 except the section along the canyon axis under weak stratification.

Upstream sections NB and NC show strong downwind transport under strong stratification. Stronger stratification cases (A3-C3) show twice the alongshore transport than the nearly homogeneous case F3 (0.5 Sv). Alongshore transport increases

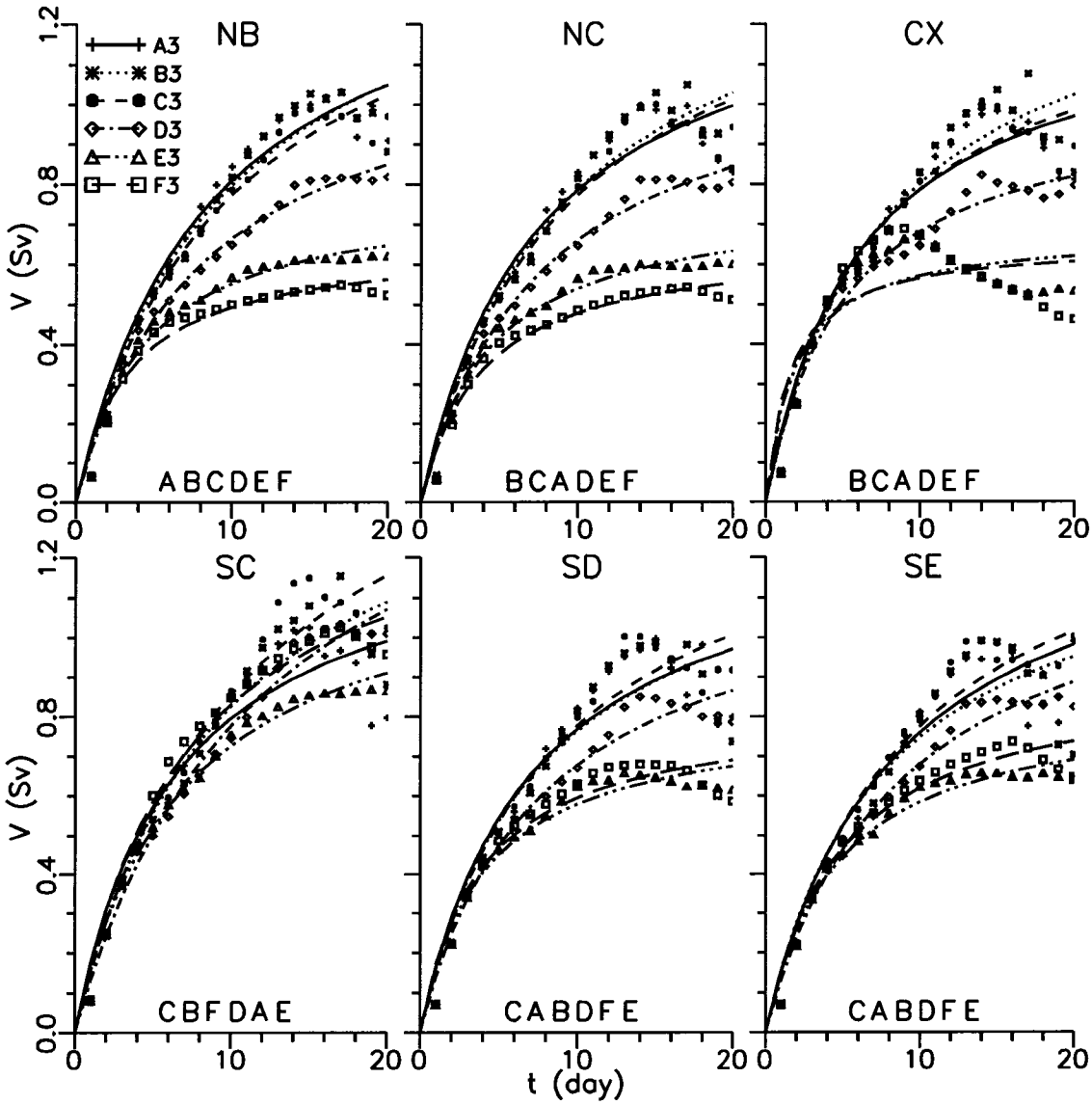

Figure 19. Vertically integrated alongshore transport (Sv) over the shelf (integrated from the coast to Section K) as a function of time (t, days) for 0-20 d along sections NB-SE for cases. Each model case (A3-F3) is shown by a different line style. Positive transport is downwind (southward) in this figure. A function $V=V_m t/(K_d+t)$ is related alongshore transport V to time t in days. Parameters V_m and K_d are given on Table 8.

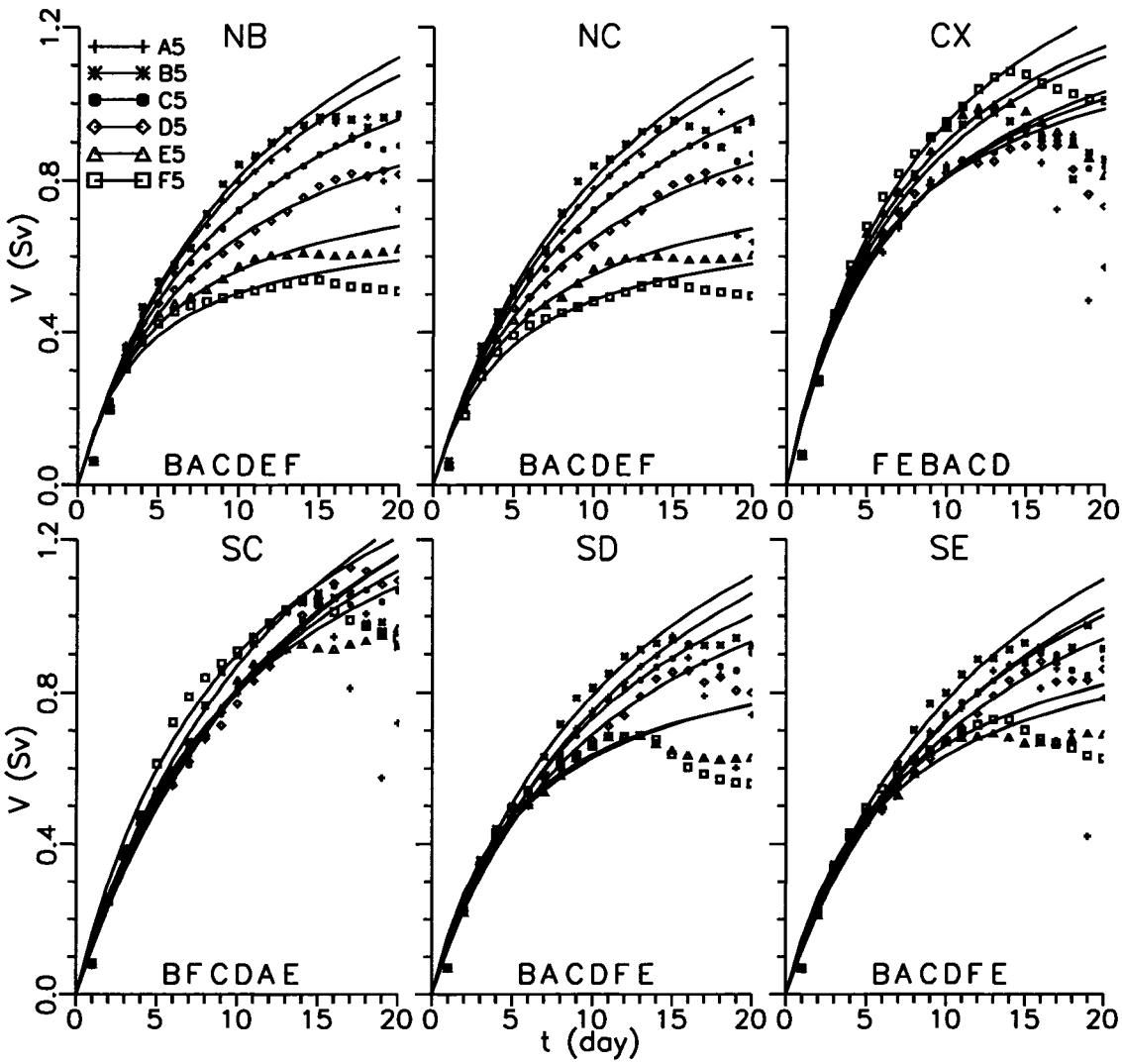

Figure 20. Same as Figure 19 except the 40 km canyon. Parameters V_m and K_d are given on Table 9.

Table 8. Parameters V_m and K_d of fitted curves to alongshore transport versus time for cases A3-F3 in Figure 19.

	Section	A3	B3	C3	D3	E3	F3
V_m	NB	1.49	1.54	1.51	1.18	0.78	0.66
	NC	1.36	1.48	1.47	1.17	0.76	0.66
	CX	1.27	1.42	1.31	1.03	0.68	0.65
	SC	1.31	1.60	1.77	1.72	1.22	1.43
	SD	1.32	1.33	1.43	1.20	0.81	0.82
	SE	1.39	1.31	1.47	1.28	0.85	0.91
K_d	NB	8.42	9.28	9.52	7.74	4.12	3.29
	NC	7.33	8.84	8.96	7.73	4.12	3.74
	CX	6.14	7.67	6.69	5.14	1.86	1.55
	SC	6.48	9.36	10.70	12.13	6.77	7.24
	SD	7.11	7.41	8.37	7.66	3.98	3.82
	SE	8.29	7.51	8.99	8.80	4.53	4.80

Table 9. Parameters V_m and K_d of fitted curves to alongshore transport versus time for cases A5-F5 in Figure 20.

	Section	A5	B5	C5	D5	E5	F5
V_m	NB	1.70	1.83	1.43	1.18	0.86	0.71
	NC	1.74	1.84	1.49	1.22	0.86	0.72
	CX	1.42	1.56	1.34	1.27	1.59	1.77
	SC	1.85	2.16	2.03	2.09	1.64	1.83
	SD	1.80	1.82	1.58	1.44	0.99	0.97
	SE	1.74	1.86	1.62	1.49	1.03	1.08
K_d	NB	11.67	12.60	9.85	8.09	5.20	4.07
	NC	12.55	12.85	10.66	8.88	5.65	4.88
	CX	7.45	7.84	6.55	5.78	7.64	8.59
	SC	13.01	14.82	14.96	16.15	10.49	10.27
	SD	14.01	12.97	11.65	10.90	5.81	5.22
	SE	14.10	13.89	12.41	11.70	6.32	6.33

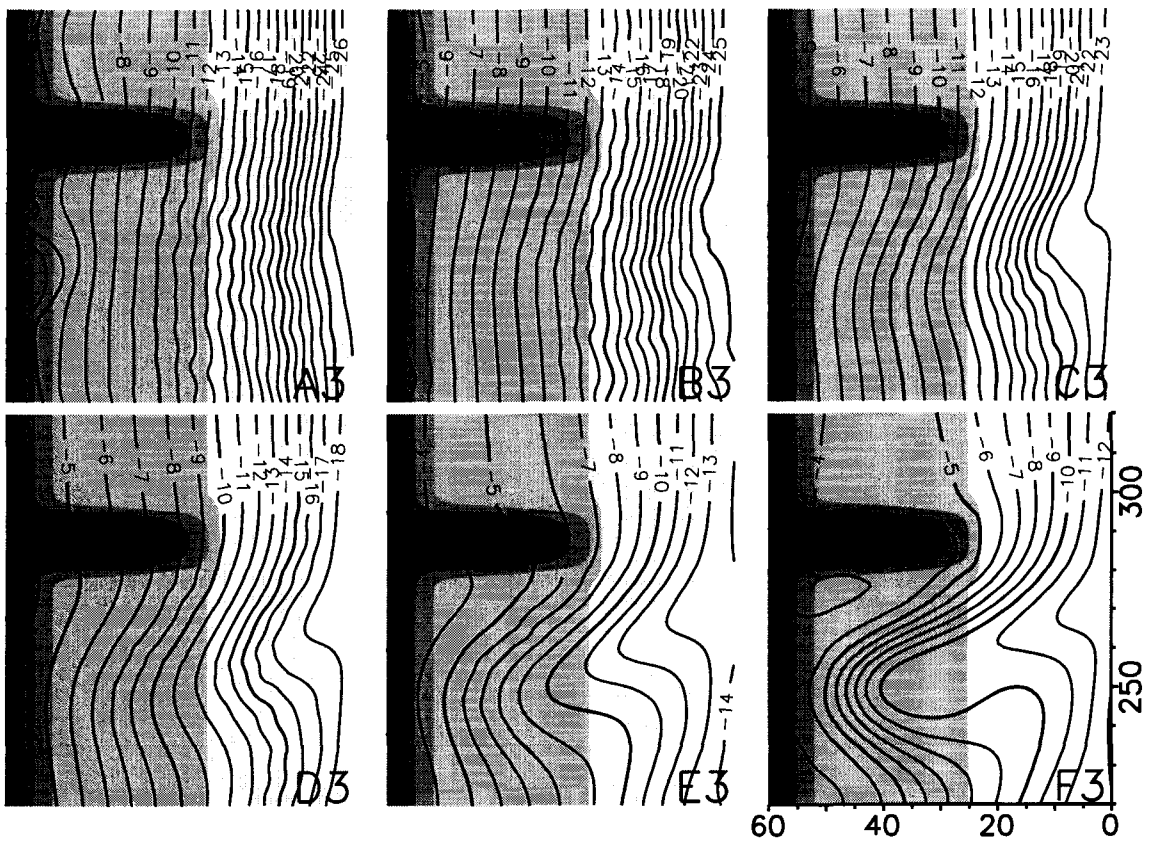

Figure 21. The free surface elevation (cm) at 15 d for six stratifications for the 20 km canyon. Bathymetry is shaded with an interval of 100 m. A subarea of 60 by 90 km is shown.

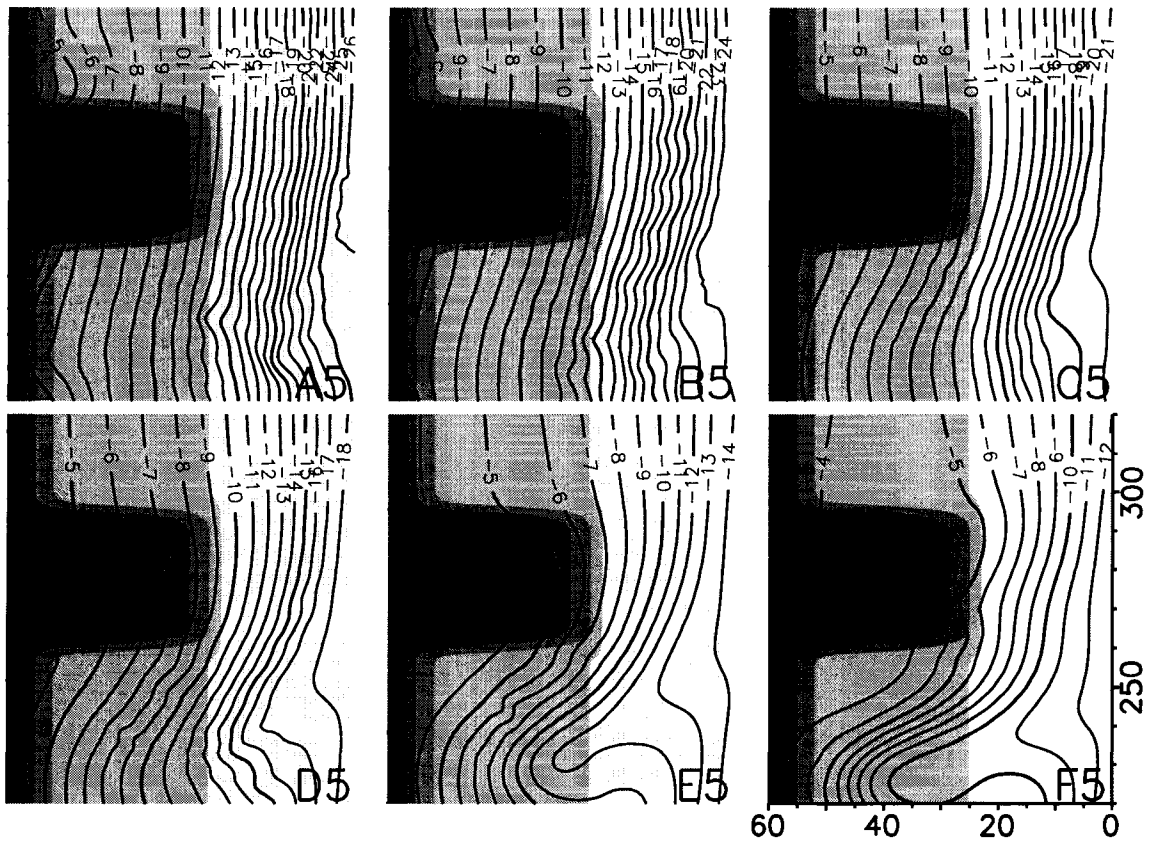

Figure 22. The free surface elevation (cm) at 15 d for six stratifications for the 40 km canyon. Bathymetry is shaded with an interval of 100 m. A subarea of 60 by 90 km is shown.

rapidly with time under strong stratification. This result indicates that weaker stratification reaches the quasi-steady earlier than stronger stratification. In other words, the bottom drag is stronger for weak stratification. The transport difference between strong and weak stratifications decreases at the downstream sections SC, SD and SE, indicating that the presence of canyon enhances the alongshore transport more for weak stratification.

The free surface slope is largest for strong stratification (A3 in Figure 21) and lowest for the nearly homogeneous case (F3). Steep surface slope for stronger stratifications (A3-C3) matches the larger alongshore transport described above. The free surface contour lines are alongshore and straight forward for A3-C3 but a meandering like a tongue occurred at the downstream shelf for weaker stratifications (D3-F3), indicating strong geometric effect of canyon for weaker stratification.

IV.2 CIRCULATION

The transport analysis shows that all simulations reach an approximate steady state at 15 d. This section analyzes the circulation in and around the canyon at quasi-steady state, with respect to the effect of stratification. Also the relationship between the stratification number and the characteristics of canyon circulation will be reviewed. The horizontal flow vectors at 200 m at 15 d for six stratification cases of the 20 km and 40 km canyons are compared (Figure 23).

The first four cases (A3-D3) show the cyclonic circulation occupying the whole canyon. The mean flow speed ranges 20-25 cm s^{-1}. There is a jet over the upstream slope turning into the canyon and separating into two branches at the downstream offshore corner of the canyon.

The turning flow is less clear under stronger stratification (A3 and B3) than weaker stratifications. One branch of the turning flow is connected to the onshore flow along the downstream wall, upwind flow along the head of canyon and offshore

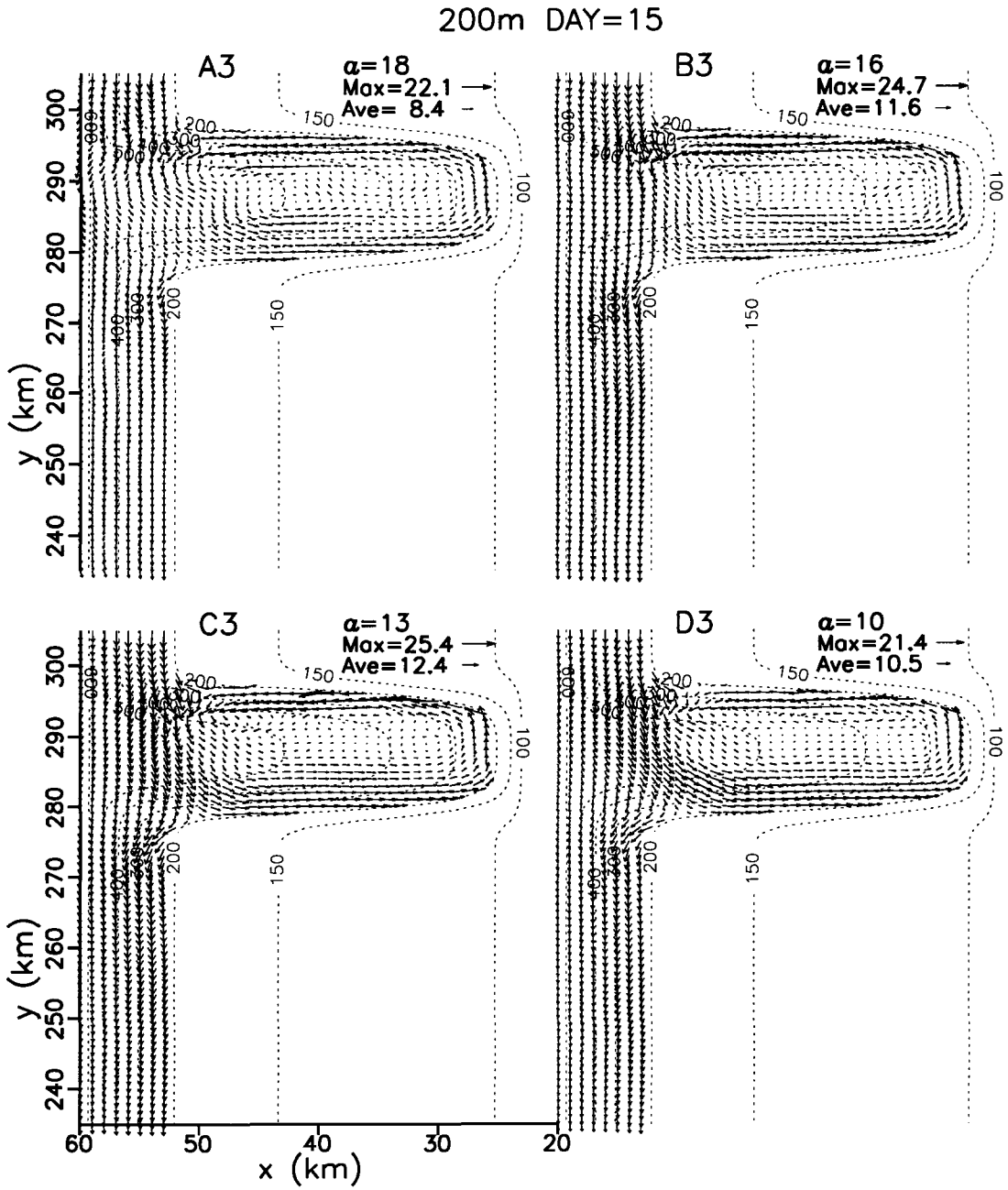

Figure 23. Horizontal flow at 200 m for day 15 in a 40 by 70 km subarea around the 20 km and 40 km canyons. Every vector across shore and alongshore are displayed. The internal deformation radius (a, km), the mean and maximum speed (cm s^{-1}) are shown on each figure. The vector scale is consistent among these figures.

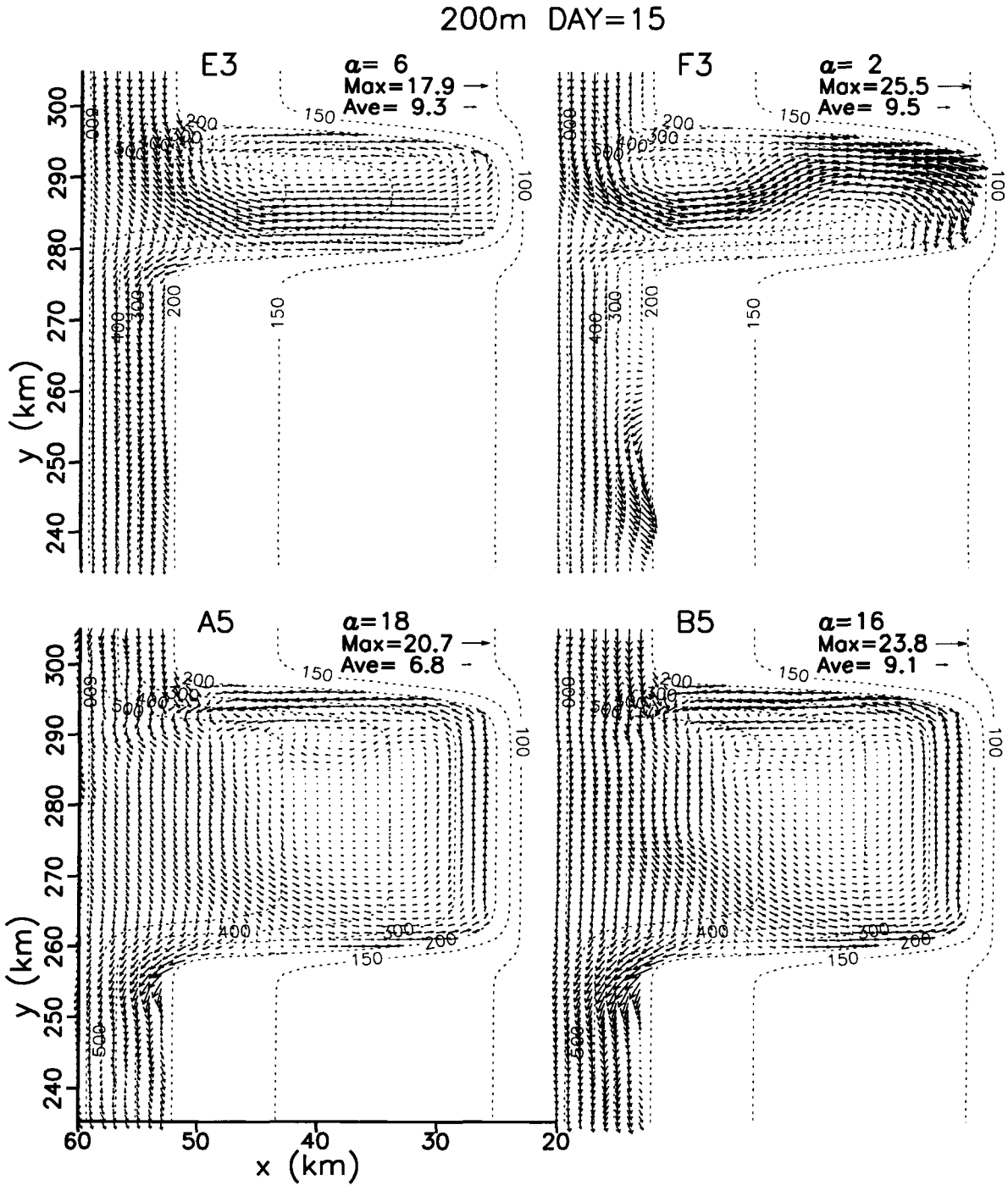

Figure 23. (continued)

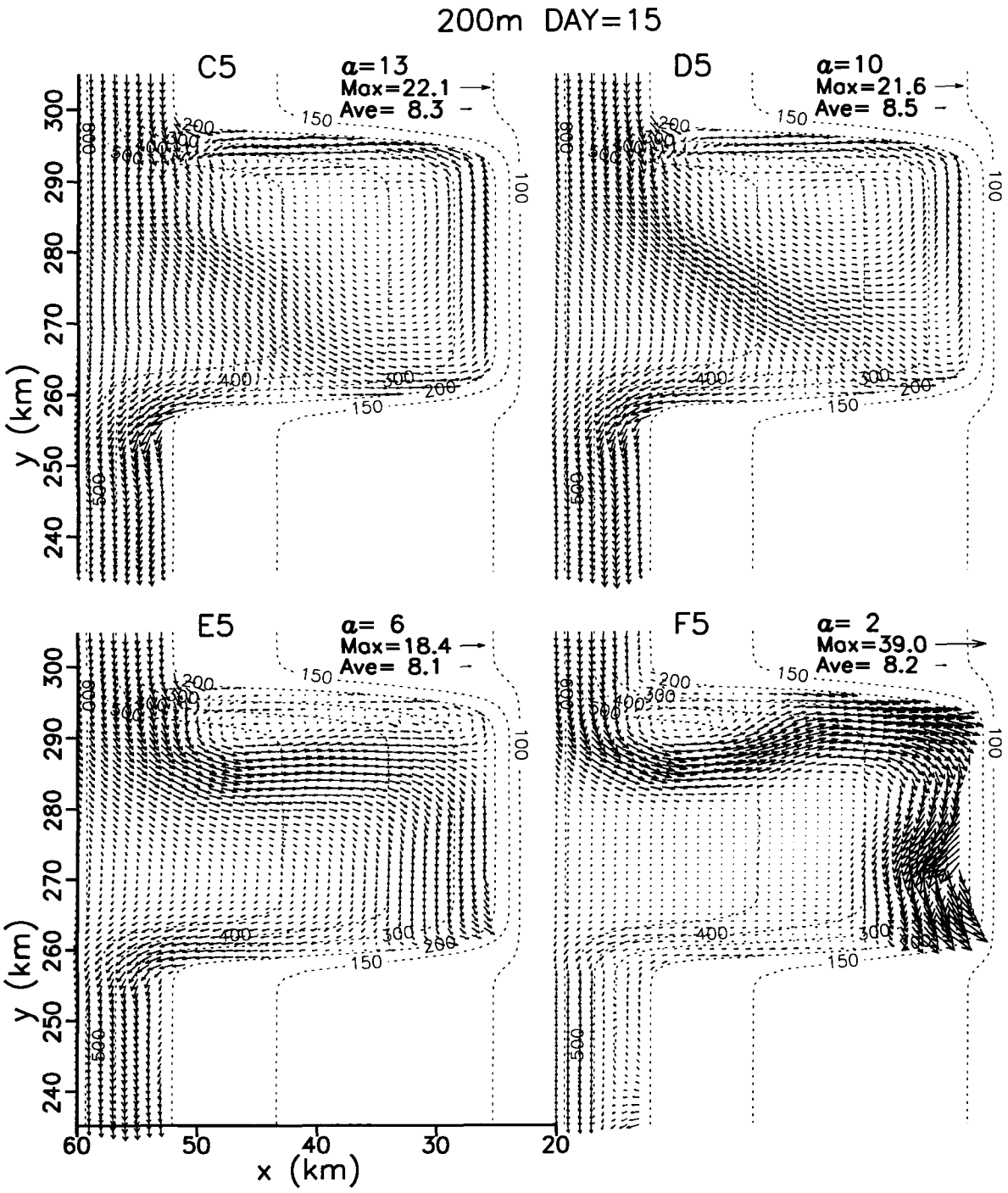

Figure 23. (continued)

flow along the upstream wall, which makes a cyclone. The other branch continues to flow downwind over the downstream slope as a slope jet. The width of cyclone becomes less than the width of canyon under weak stratifications a=6 and 2 km (E3, F3). This result supports that a canyon width of $2a$ is a separating case between narrow and wide canyons described in the previous chapter.

The 40-km canyon is wider than $2a$ of the strongest stratification (36 km). All 40-km cases (A5-F5) have a cyclone narrower than the canyon width and a stagnation point at the downstream wall, except the case with a=18 km (A5) in which the cyclone is almost fitted to the canyon and the stagnation point exist near the offshore corner of the downstream wall. The size of cyclone decreases as stratification is reduced.

The cyclone occupies the whole canyon as it should for these narrow canyon cases. The width of the cyclone is the same as the canyon width. The center of the cyclone is located at the center of the canyon. Onshore flows occurs at the downstream wall and offshore at the upstream wall. Onshore and offshore flow is symmetrical at both walls. The offshore flow at the upstream wall is strong under strong stratifications and reduces as the stratification is reduced. This result represents that the net onshore flow within the canyon becomes smaller as the stratification increases. Upwind flows occurs along the head of canyon. The slope jet and the cyclone are stronger as stratification decreases. The stratification number for these cases is greater than 0.5, which means that the width is less than 2 internal deformation radii ($2a$). These cases can be classified as narrow canyons. The separating cases between narrow and wide are D3 and A5 for the canyon widths, respectively. D3 and A5 have quite similar horizontal circulation pattern despite A5 is twice as wide as D3 as their stratification numbers are very close (S=0.5 and 0.45).

Weak stratification for the 20 km canyon (E3) has a cyclone narrower than the canyon. Onshore flow is stronger and is distributed at the downstream half of the canyon. The core of the onshore flow occurs parallel to the downstream wall. It

occurred on the downstream wall for stronger stratifications. Offshore flow is very weak and confined to the upstream wall. The 40 km case (E5) has a cyclone much narrower than the width. The incoming onshore flow detached from the upstream slope is separated into downwind and upwind flow at the canyon head. The downwind flow also is separated into onshore and offshore flow at the downstream wall. So two stagnation points exists at the canyon head and the downstream wall. The offshore flow in the cyclone located near the upstream wall is very weak.

The nearly homogeneous case (F3 and F5) show the circulation quite different from other cases. They have a small and circular cyclone at the offshore corner of the upstream wall. The cyclone looks like a simple overshooting due to the inertia of the upstream slope jet. An anti-cyclonic circulation occurs in the inner canyon which follows isobaths until it reaches the nearshore corner of the downstream wall. Onshore flow and downwind flow is very strong along the canyon head while offshore flow is very weak along both walls.

Alongshore sectional views of across shelf current for four stratifications are compared (Figure 24) to see the effect of stratification on across shelf flow within the canyon. Surface current above 100 m goes downwind without the influence of the canyon topography (figure not shown). Weak stratification shows onshore flows between the depth of 30-100 m over the canyon. This result indicates that stratification reduces canyon geometric effect which shows the maximum onshore flow for the nearly homogeneous case. Similarly as in the horizontal view, the first two stratifications show the similar current pattern despite the different strength of flow. Onshore flow mainly occurs at the downstream wall within the canyon. At the top of the upstream wall, a small amount of onshore flow occurs. Below the top of the upstream wall, offshore flow (dotted line) occurs, which makes a canyon cyclone along with the onshore flow at the downstream wall.

Weak stratification (E3, F3) show different patterns. Onshore flow is separated

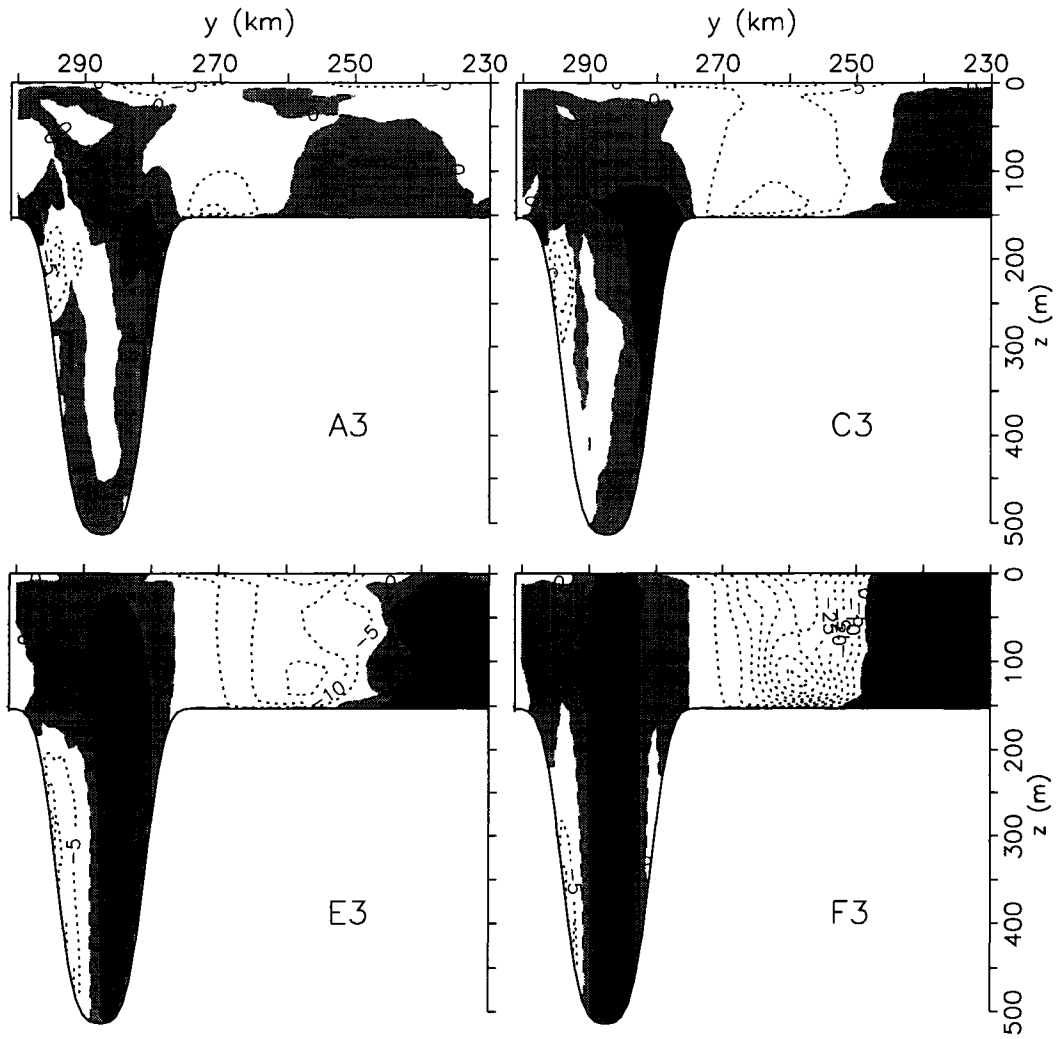

Figure 24. Across shelf flow speed at day 15 for Section K for four stratification cases of the 20 km canyon. The first internal Rossby radii are 18, 13, 6 and 2 km, respectively. Solid and dotted contours are onshore and offshore, respectively. Shaded area indicates onshore speed greater than 5 cm s^{-1}. The zero contour is dashed. The view is from offshore looking towards the coast.

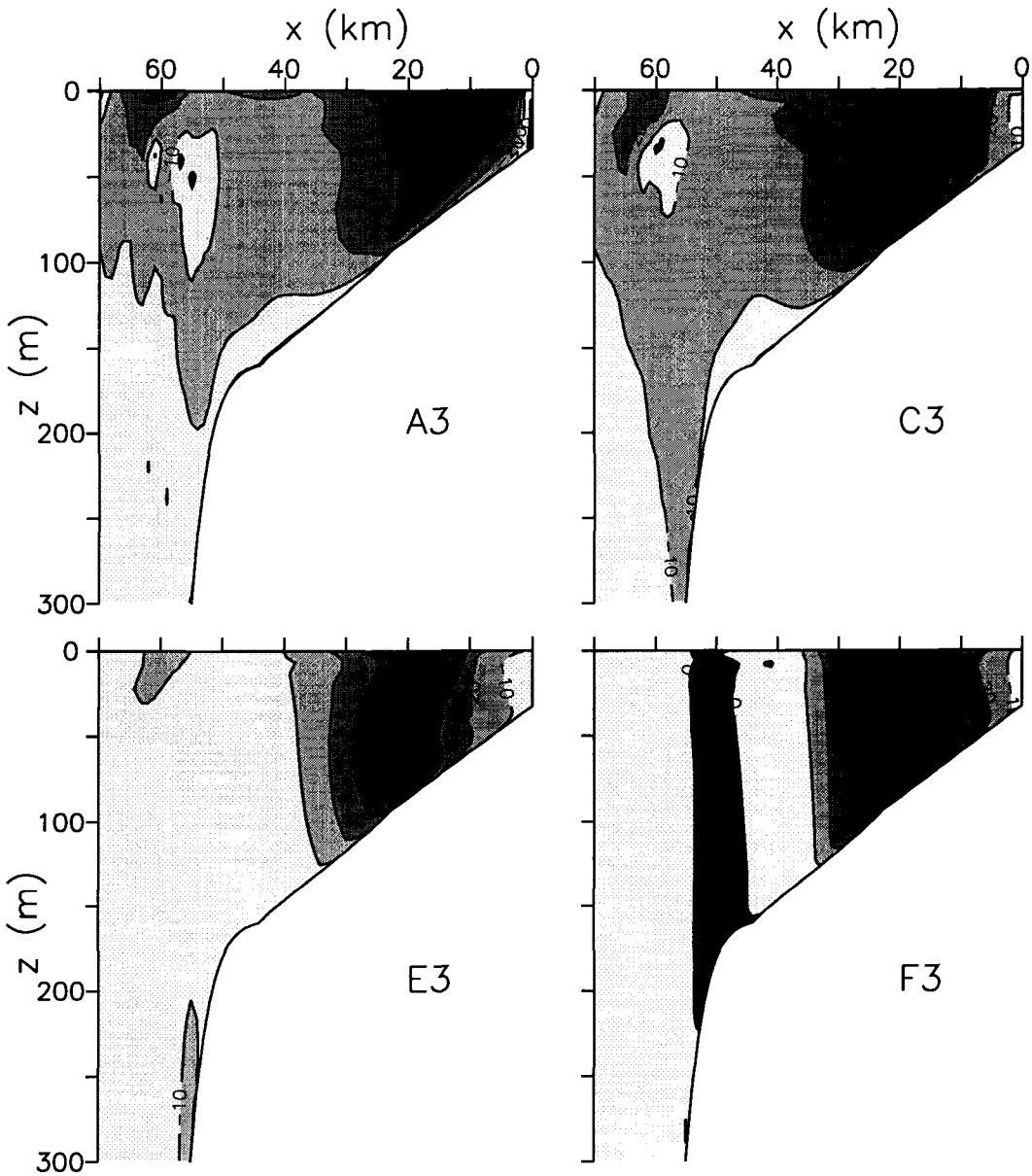

Figure 25. Across sectional view of alongshore flow (v, cm s^{-1}) at Section SC at 15 d for Cases A3, C3, E3 and F3. The first internal Rossby radii are 18, 13, 6 and 2 km, respectively. Contour interval is 10 cm s^{-1}.

from the downstream edge. Onshore flow is distributed from the surface to the bottom of the water column. Onshore flow does not occur at the top of the upstream wall. Downstream of canyon the disturbance of offshore and onshore flows occurs and becomes stronger as the stratification is reduced. The location where offshore flow occurs downstream moves far apart from the downstream wall as the stratification is reduced. This result indicates that onshore-offshore disturbance downstream of canyon reflect the onshore flow within the canyon. If the onshore flow is strong under weak stratification, the disturbance downstream of canyon is strong. If the onshore flow reduces as the stratification increases, the downstream disturbance reduces.

Alongshore flow at the downstream edge (Figure 25) shows the geometric effect of the canyon under various stratifications. Under strong stratification (A3), the upwelling jet is as strong as 70 cm s^{-1} and is limited to the surface layer. The upwelling jet in the surface layer becomes weaker as the stratification decreases. Instead the lower layer jet occurs and becomes stronger, which indicates the strong canyon effect under weak stratification. The maximum speed in the lower layer jet is as strong as 60 cm s^{-1} under nearly homogeneous case (F3), which indicates strong across shelf exchange through the downstream edge of canyon.

In summary, strong stratification greater than S=0.5 shows a cyclone occupying the whole canyon and symmetric onshore and offshore flows at the downstream and upstream walls, respectively. These can be classified as narrow canyons. Weak stratification less than S=0.5 shows a cyclone smaller than the canyon which has stronger onshore flows at the downstream half of canyon and weaker offshore flows at the upstream wall. The nearly homogeneous case shows a very small and circular cyclone which stick to the outer corner of the upstream slope. In the inner canyon, a very strong onshore flow occurs through the canyon head.

IV.3 ISOPYCNAL MOTION

Chapter 3 showed that the upwelling is stronger within the canyon than outside and is stronger within narrow canyons than wide canyons for a fixed stratification and that vortex compression occurs in the upper layer below the canyon rim and vortex stretching in the lower layer. In general, stratification inhibits the vertical movement of particles by increasing the stability of the water column (increasing the Brunt-Väisälä frequency). Thus canyon upwelling can be increased by the geometric effect and reduced by stratification. This section describes the upwelling within the canyon focusing the effect of stratification by looking at the temporal variation of isopycnal displacement (Figure 26).

Vertical displacement is smaller under strong stratification than weak stratification. The isopycnal initially at 300 m shows the biggest difference of vertical displacement with stratification. Each case shows the vertical displacement of 50 m, 120 m, 200 m and 230 m, respectively, from strong to weak stratifications. The corresponding upwelling speeds are 2.5, 6.0, 10.0, 11.5 m day^{-1}. The weak stratification case (E3) shows very strong upwelling over the whole canyon. This result indicates that strong upwelling occurs under weak stratification. The isopycnal rise is strong near the coast and the bottom rather than the offshore and the interior. The nearly homogeneous case (F3) shows the largest isopycnal rise in the bottom Ekman layer. The rise occurs at the mouth of canyon and the head of canyon but the isopycnal falls in the middle of the canyon. Isopycnals at the bottom of the canyon shows a very large vertical displacement (500 m for ρ=27.355 at 600 m).

Alongshore sections show that the rising speed of isopycnals is different at upstream and downstream walls within the canyon. For strong stratification (A3), the canyon upwelling lifts each layer within the canyon about 30 m for 20 days. Each layer does not show layer compression or stretching. C3 shows layer compression at the top of the canyon and layer stretching in the lower layer as described in Chapter

3. A strong anti-cyclonic stretching vorticity of about -0.5f is generated in the upper layer for E3. There is a bias of stretching vorticity at the upstream and downstream walls, which is one of the characteristics for wide canyons as described in Chapter 3. This result indicates that the 20 km canyon responds as a wide canyon under a stratification with a=6 km, which supports the canyon size classification in Chapter 3.

IV.4 TRACER TRAJECTORY

Horizontal behavior of tracers released at 250 m at the upstream slope at 2 d is displayed in Figure 28. In all cases, tracers travel downwind due to the wind driven flow on the upper continental slope. Tracers released on the outer slope follow isobaths. Tracers released near the shelf break turn into the canyon and join the cyclonic circulation for strong stratification (A3, C3) but anti-cyclonic circulation occurs for weak stratification and the nearly homogeneous case (E3, F3). Most tracers exit the canyon through the nearshore corner of the downstream wall except strongest stratification case in which few tracers exit the canyon. The source region of tracers which exit the canyon onto the downstream shelf is three release locations near the shelf break. As stratification increases, the source region becomes confined to one or two offshore lines close to the shelf break.

The strength of canyon upwelling can be measured by the number shown in Figure 28 which indicates the number of tracers which exit the canyon onto the downstream shelf and its averaged duration period. Strong canyon upwelling is expected to have more tracers exit the canyon in a shorter period. This number was displayed at every 50 m depths as a function of the internal deformation radius (Figure 29). This number increases as the stratification is reduced for the tracers released above 350 m, indicating that the strength of canyon upwelling decreases linearly with stratification.

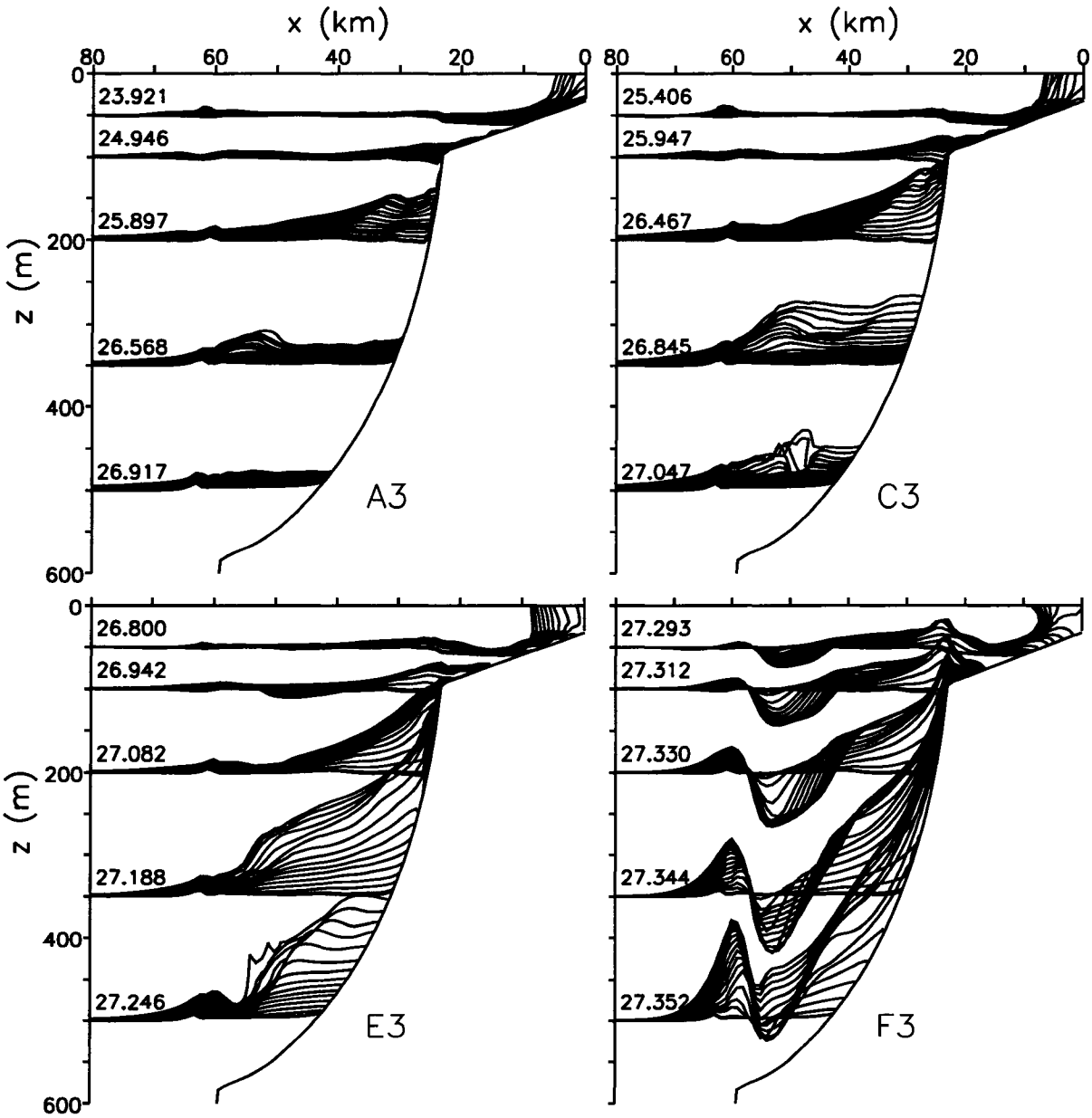

Figure 26. Location of isopycnals initially at 50, 100, 200, 350 and 500 m at daily intervals for four stratification cases along the canyon axis (Section CX) for the period of 0-15 d. Initial isopycnals are level. The first internal Rossby radii are 18, 13, 6 and 2 km, respectively.

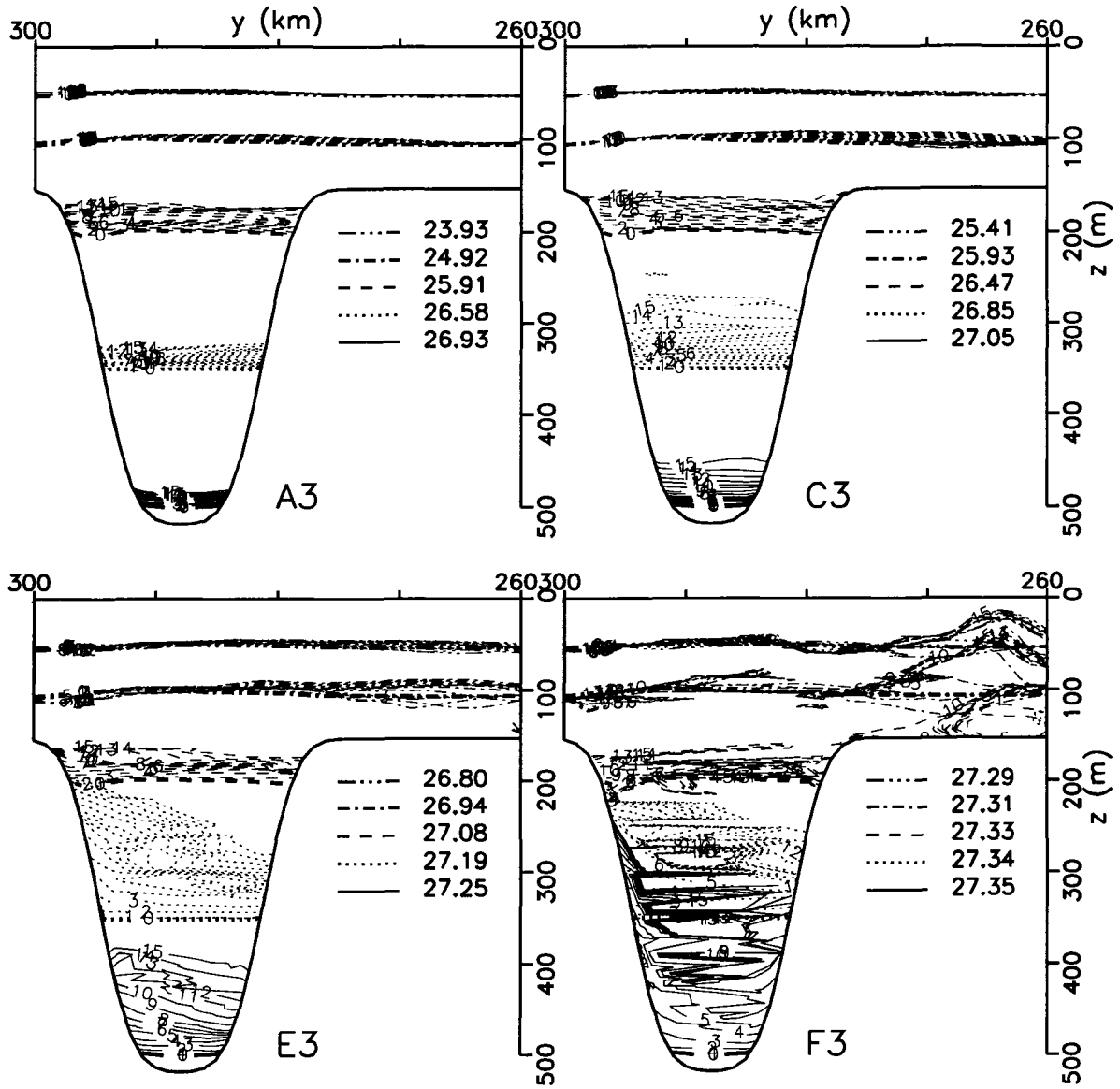

Figure 27. Location of isopycnals initially at 50, 100, 200, 350 and 500 m at daily intervals for four stratification cases A3, C3, E3 and F3 along Section K for the period of 0-15 d. Initial isopycnals are level. The first internal Rossby radii are 18, 13, 6 and 2 km, respectively.

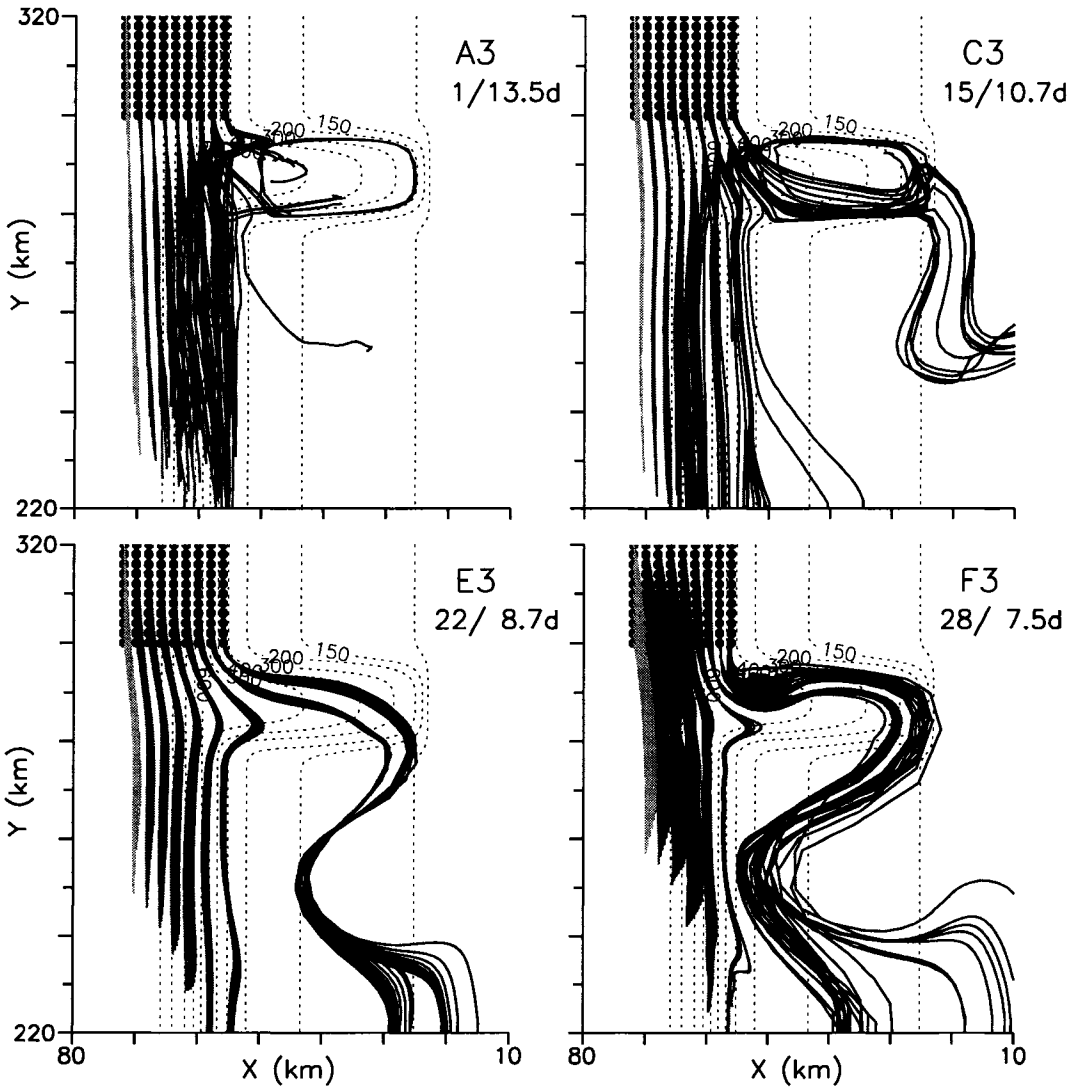

Figure 28. Tracer trajectories for the 20 km canyon cases under four stratifications (A3, C3, E3 and F3). Ninety nine (9×11 strings) tracers are released in a rectangular pattern spaced every two grid points at 250 m on day 2. The gray scale of each trajectory shows the released locations offshore. The numbers on the upper right of each panel are the number of tracers that upwell onto the shelf break depth (150 m) and the average time taken until they reach the shelf break depth.

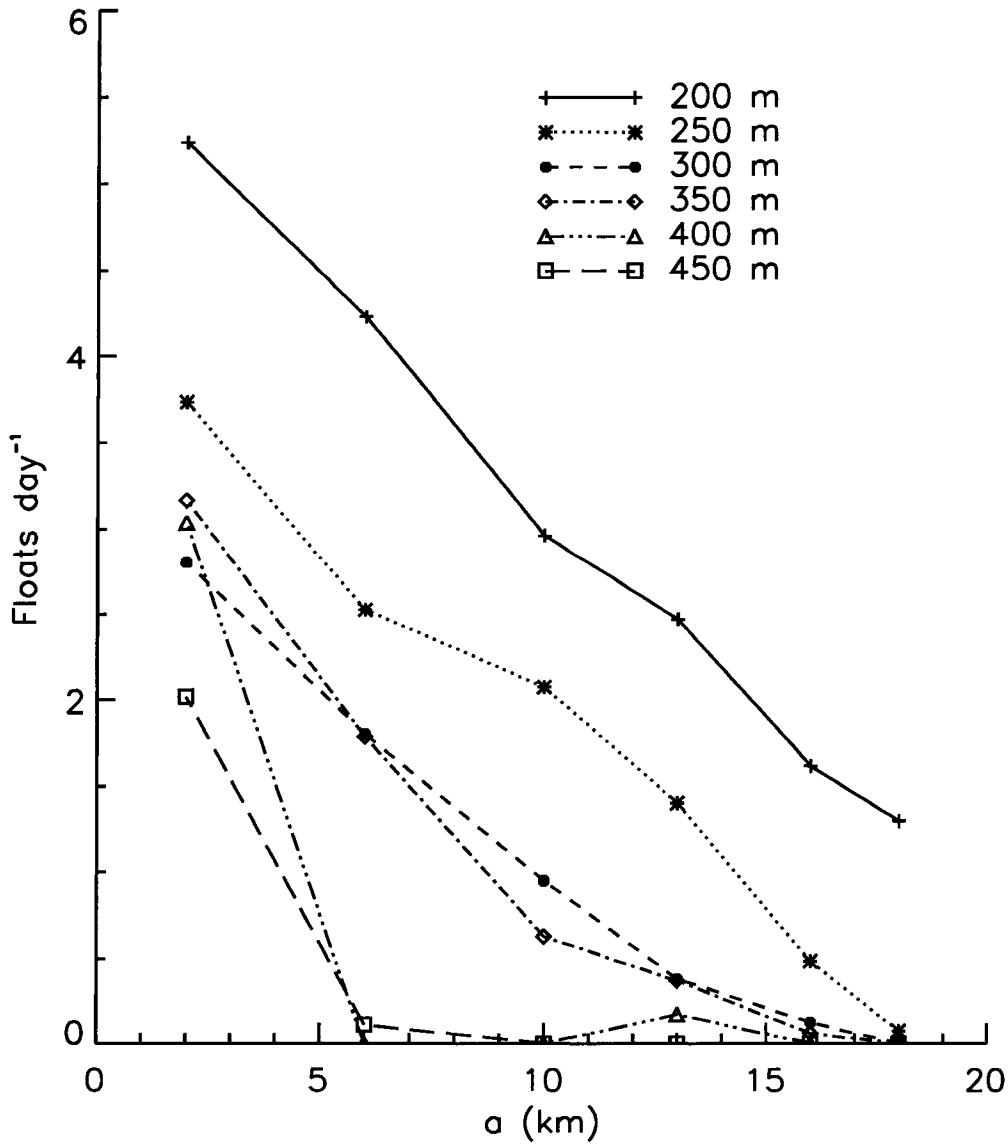

Figure 29. The relationship between the number of tracers per day which exit the canyon onto the downstream shelf and the internal deformation radius (a). Different line style indicates released depths.

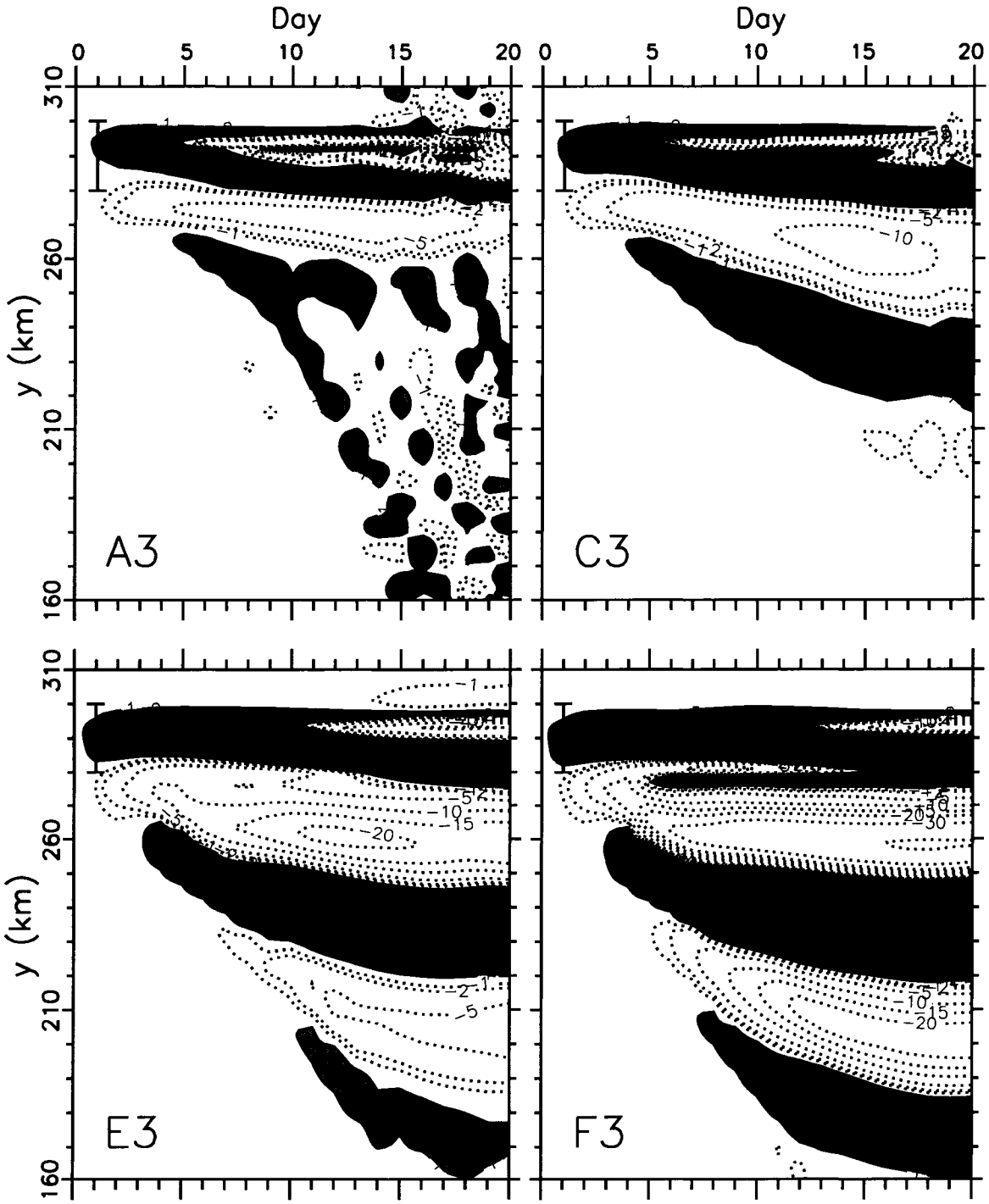

Figure 30. Temporal variation of across shelf transport (mSv) across section K at alongshore locations y=160-310 km. Solid line indicates onshore transport and dotted line does offshore transport. Contours are -50, -30, -20, -15, -10, -5, -2, -1, 1, 2, 5, 10, 15, 20, 30 mSv. Canyon widths are marked by the bar on the figure.

IV.5 ACROSS SHELF EXCHANGE

The across shelf volume transport across Section K versus alongshore locations shows the effect of stratification on across shelf exchange over a 20 km canyon (Figure 30). For all stratifications, initial flow follows isobaths, entering the canyon on the upstream half. For all stratifications, onshore transport increases within the whole canyon until offshore transport occurs at the upstream half at 5 d for stronger stratifications (A3-C3) or at 10-12 d for weaker stratifications (E3-F3). For the nearly homogeneous case (F3), offshore transport within the canyon is very small compared to the onshore transport. Occurrence of onshore and offshore transports within the canyon indicates adjustment of flow within the canyon, developing a cyclonic circulation. Adjustment occurs earlier for stronger stratifications compared to weaker ones.

Larger onshore transport within the canyon is reflected by a larger offshore transport south of downstream edge of canyon. Onshore-offshore fluctuation continues further downstream of canyon for all stratifications. The fluctuation is the largest for nearly homogeneous case indicating the largest geometric effect of canyon (F3). Small disturbances occurs further downstream of the canyon due to the baroclinic instability under strong stratification.

A power function was related between alongshore transport and onshore transport in the canyon by Equation 13, where it was shown that the onshore transport per alongshore width declines sharply at a canyon width above 2 internal radii ($2a$). All stratifications show a good fit of a power function between alongshore transport and onshore transport in the canyon ($U=mV^n$, Figure 31). Both alongshore (V) and onshore transports (U) increase with time until they reach an approximate steady state at 15 d (Figure 31). Afterwards they gather around the value at 15 d as shown by grouping of points at the end of each line. Alongshore transport has a value of about 1.0 Sv under strong stratification (A3-C3 in Figures 31 and 32) but decreases

to about 0.8, 0.6 and 0.5 Sv as the stratification is reduced. The alongshore transport has the lowest value (about 0.5 Sv) at quasi-steady state for the nearly homogeneous case. This result indicates that it is difficult to compare onshore transport at the same quasi-steady alongshore transports. The decrease of the slope of the curve as the stratification increases indicates that onshore transport within the canyon is not influenced much by the upstream alongshore transport under strong stratification. The straightening of the curve as the stratification increases indicates that the U-V relationship becomes linear as the stratification increases. These two results indicates that the topographic effect of canyon is reduced as the stratification increased.

The growth in time in alongshore transport is high under strong stratification. As the stratification is reduced, alongshore transport increases very slowly. This result indicates that stratification enhances alongshore transport.

On the other hand, onshore transport at quasi-steady state decreases linearly from 0.46 to 0.03 Sv from weak to strong stratifications. Onshore transport increases very slowly with time under strong stratification. The growth rate in onshore transport (slope of the curve) increases as the stratification is reduced. Weak stratification cases have larger onshore transport than strong stratification for a given alongshore transport. This result indicates that the effect of canyon geometry is strong under weak stratification because onshore transport in the canyon increases rapidly even if alongshore transport is not strong compared to strong stratification. This means that stratification reduces the canyon effects.

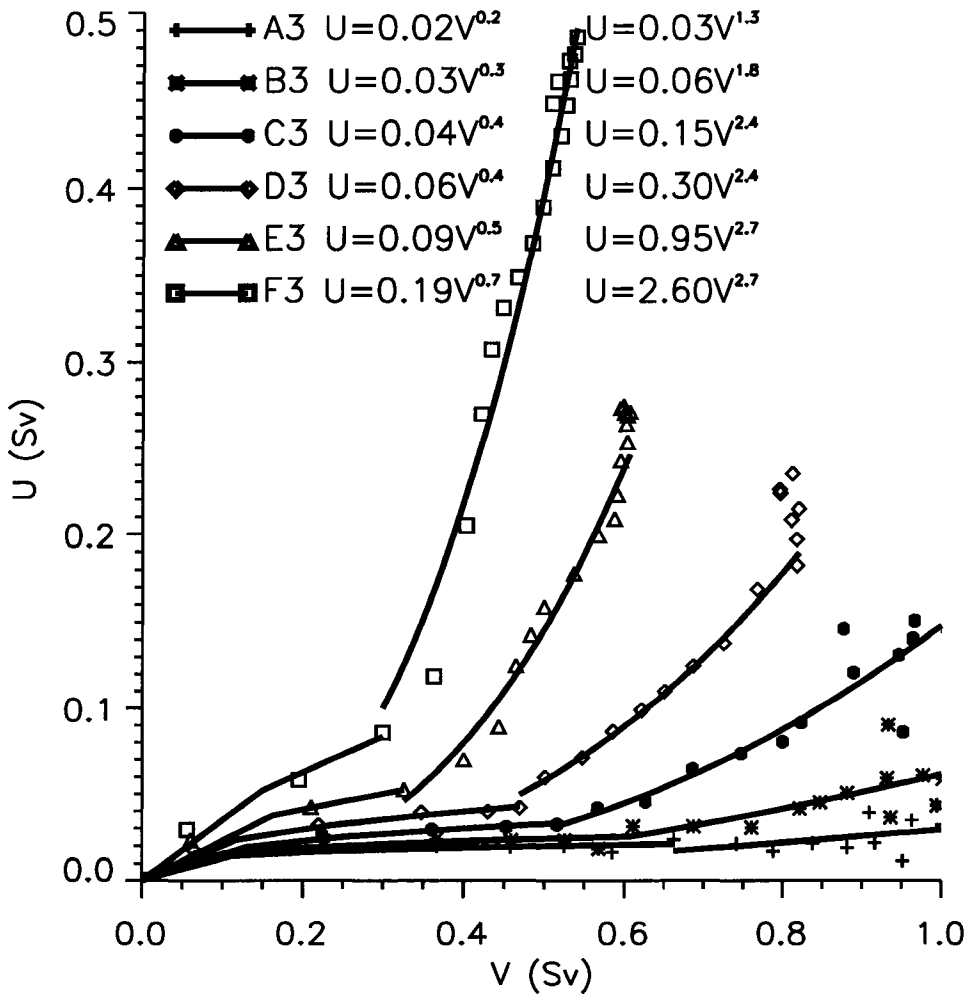

Figure 31. Relationship between across shelf transport (U) and alongshore transport (V) for six stratification cases over the 20 km canyon for each day over 20 d. Across shelf transport is integrated within the canyon along Section K. Alongshore transport is integrated from Section K to the coast at Section NC. The lines with different symbols are a power function ($U = mV^n$) fit to each case. The parameters of each functional fit are included in the figure or Table 7.

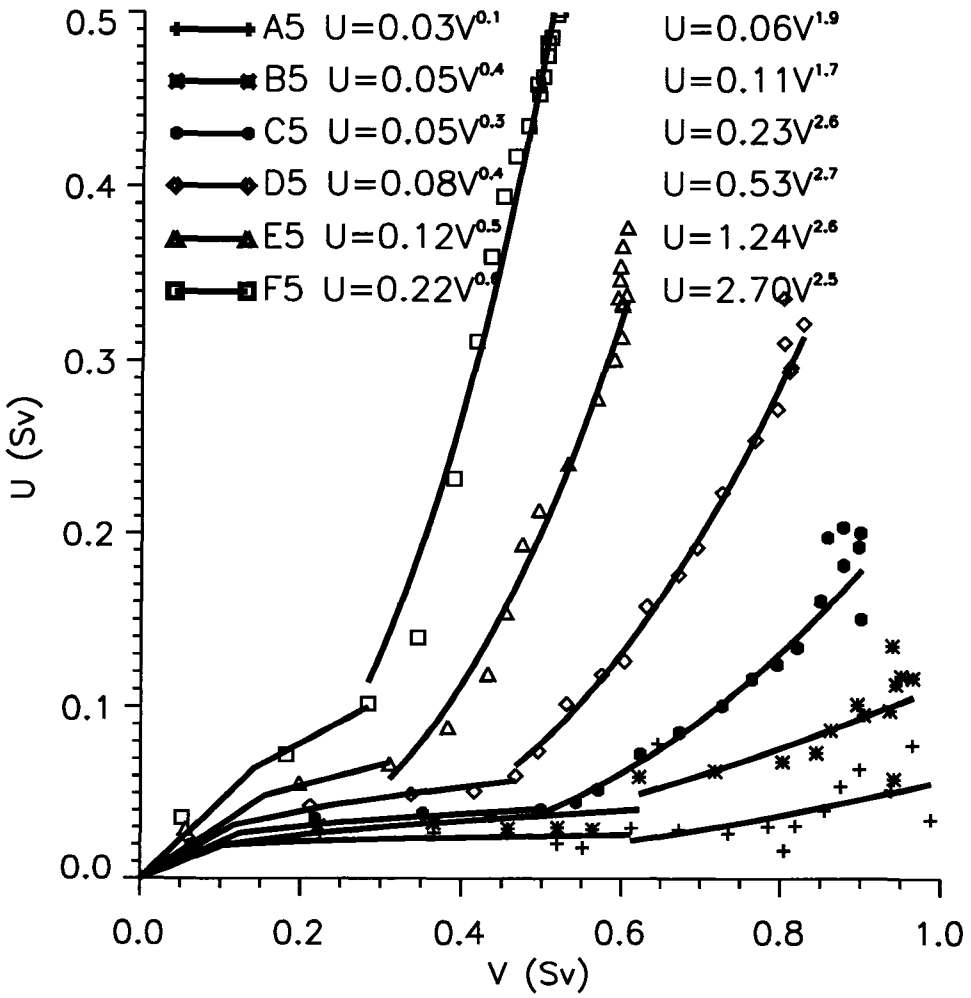

Figure 32. Same as Figure 31 except the canyon width (W=40 km).

CHAPTER V

DISCUSSION

V.1 EFFECT OF LENGTH AND DEPTH

A submarine canyon is defined by upstream and downstream walls. The distance between upstream and downstream walls of a canyon, which is the width of canyon, characterizes the fluid dynamics within the canyon. The distinct canyon dynamics is caused by a mixture of the effects of two walls. Both canyon depth and length also play a role in the canyon dynamics. Allen (2000) reported that strong seasonal scale upwelling is observed over a very long and deep canyon (Juan de Fuca) whereas it is episodic over a shorter and shallower canyon (Astoria). Juan de Fuca Canyon has a very specific topography which cuts the whole continental shelf from the slope into the Strait of Juan de Fuca. The dynamics over this canyon are the result of three parameters (length, depth and cutting through the whole shelf) acting together. Some simulations for the canyons with varying lengths but the same depth and width have been run (figure not shown). The canyon cyclone is longer and the flow is a bit stronger within longer canyons. As the canyon becomes shorter, the geometric effect of the canyon decreases. However canyon dynamics basically do not change unless it is very long or short. Thus the effects of length and depth are assumed here to be less than that of width and stratification and so their variation is not considered in this study.

V.2 CANYON CYCLONE

The upstream escarpment generates a cyclone formed by the upstream wall due to inertia (C7 in Figure 8). A simulation without inertial terms had flow that followed isobaths and no cyclone was generated (figure not shown). Thus, flow inertia is critical for creating a cyclone within a canyon. As the width narrows, the cyclone

is squeezed due to the reduced space between two walls. Then the fluid dynamics does not follow the general along-shelf dynamics within narrow canyons which is a geostrophic balance. The width of cyclone depends, generally, on the stratification and forcing. Simulations with two different forcing show different width of cyclone at a given time (figure not shown). Also model simulations show that the cyclone is not developed or small at the early spinup. The width of the cyclone reaches the maximum size when the adjustment occurs within the canyon after about two weeks of forcing. Under the same forcing and stratification, the cyclone width does not change with canyon widths, beyond a certain minimum width. For the cases considered here, 30 km and wider canyons have the same width cyclone for a fixed stratification (a=13 km). A 20 km wide canyon (C3 in Figure 8) has a slightly thinner cyclone with a=13 km and the similar size of cyclone with the canyon width for a=10 km, while narrower canyons are too small for a full cyclone to appear. Wider canyons (C6-C7 in Figure 8) show clearly that the cyclone width is around $2a$ for the given first internal deformation radius. The size of cyclone increases with stratification.

V.3 POTENTIAL VORTICITY

The potential vorticity budget was investigated using the Rossby-Ertel potential vorticity equation (Gill 1982, p238) for a stratified fluid,

$$\frac{DQ}{Dt} = (Q \cdot \nabla)\vec{u} - \frac{1}{\rho}\nabla \times (\nabla \frac{P}{\rho}), \tag{15}$$

where Q=$(\zeta + f)/\rho$ which is the potential vorticity for a stratified parcel of water and ζ is the relative vorticity. The vertical component of Equation (15) can be expressed as

$$Q_t + (uQ_x + vQ_y + wQ_z) - Qw_z - \frac{1}{\rho^3}(\rho_x P_y - \rho_y P_x) = 0, \tag{16}$$

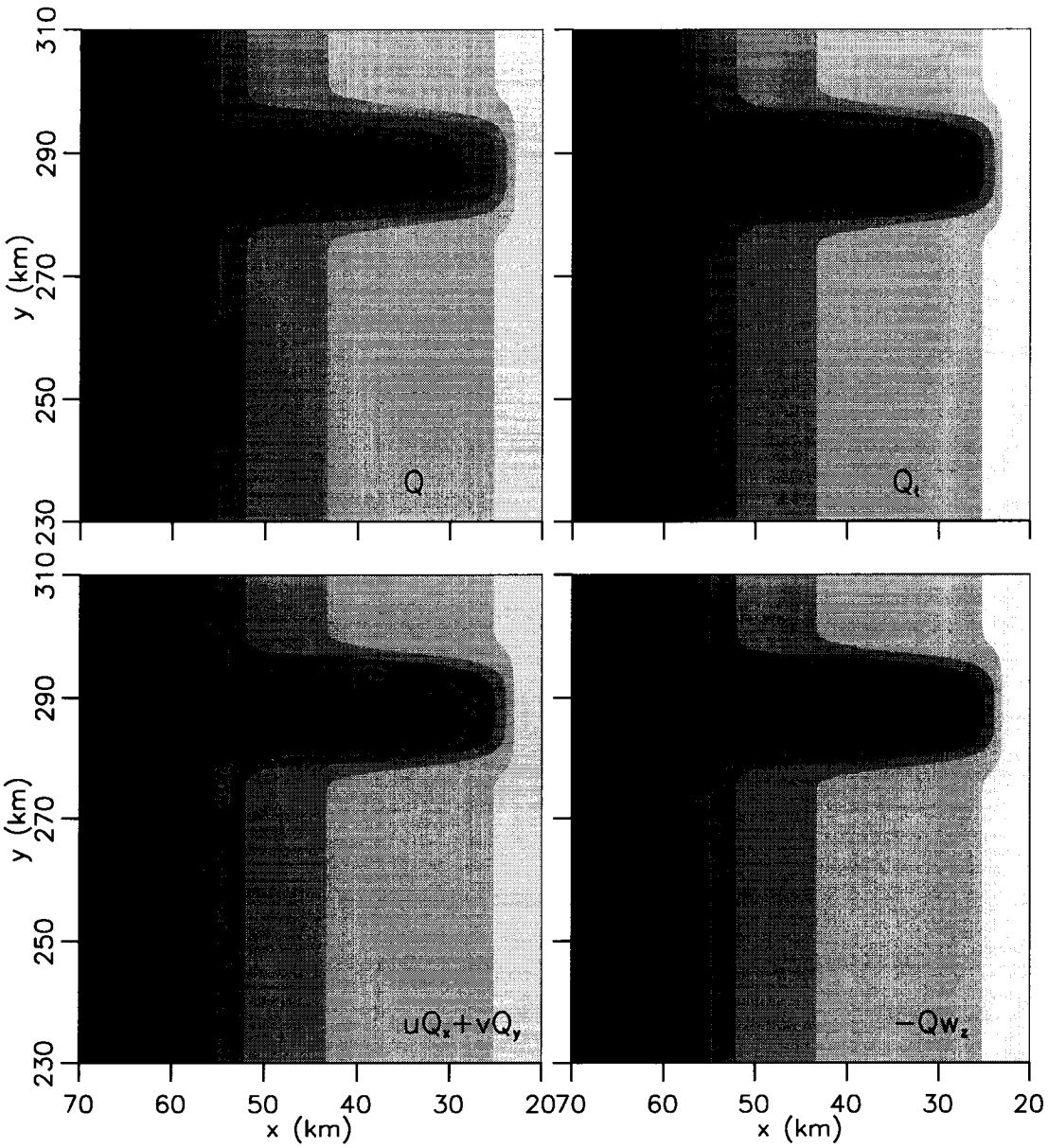

Figure 33. Potential vorticity (Q=(ζ+f)/ρ, upper left) at 250 m at 15 d for Case C3 with the contour interval of 0.5 $\times 10^{-7}$ m ^{3}kg^{-1}s^{-1}. Contour line less than or greater than 1.0 is dotted or solid, respectively, with dashed line for 1.0. Three terms in Equation 34 are depicted: Q_t, $(uQ_x + vQ_y)$ and $-Qw_z$ on the upper right, lower left and lower right, respectively. The contour intervals are -5, -1, -0.2, 0.2, 1, 5, 10, 20 $\times 10^{-12}$ m^{3}kg^{-1}s^{-2}. Negative values are dotted. Bathymetry is contoured with the interval of 100 m including 150 m.

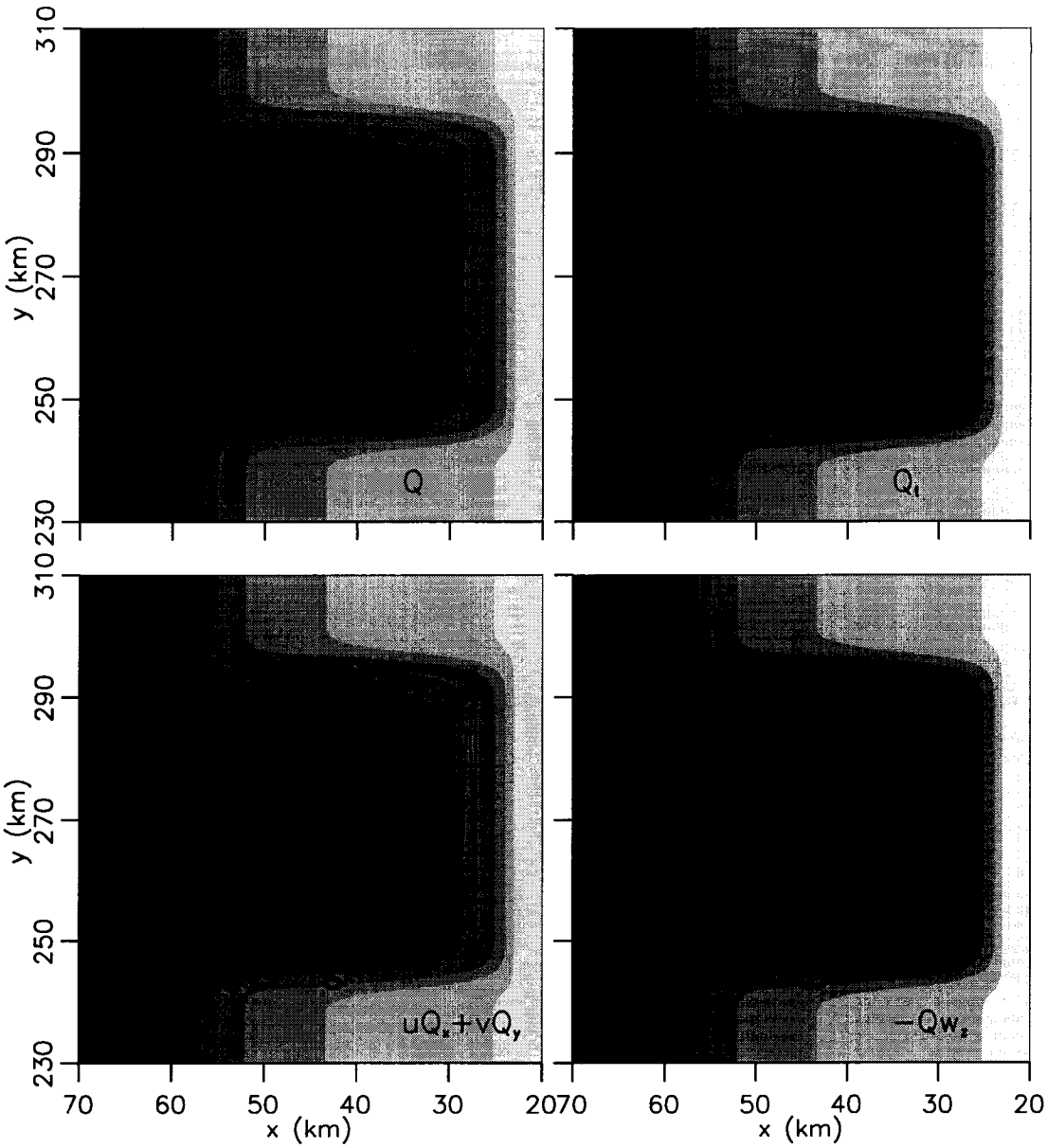

Figure 34. Potential vorticity (Q=(ζ+f)/ρ, upper left) at 250 m at 15 d for Case C6 with the contour interval of 0.5 $\times 10^{-7}$ m ^{3}kg^{-1}s^{-1}. Contour line less than or greater than 1.0 is dotted or solid, respectively, with dashed line for 1.0. Three terms in Equation 34 are depicted: Q_t, $(uQ_x + vQ_y)$ and $-Qw_z$ on the upper right, lower left and lower right, respectively. The contour intervals are -5, -1, -0.2, 0.2, 1, 5, 10, 20 $\times 10^{-12}$ m^{3}kg^{-1}s^{-2}. Negative values are dotted. Bathymetry is contoured with the interval of 100 m including 150 m.

where subscripts denotes partial differentiation. This equation says that potential vorticity for a stratified fluid is conserved by balancing between potential vorticity advection (second term) and the vorticity by vertical velocity change (third term) and vorticity production due to baroclinicity (**B**, fourth term). The vertical velocity change generates vorticity due to vortex stretching or compression. So does baroclinicity when the density surfaces are inclined to pressure surfaces. Potential vorticity Q and each term in Equation 16 was calculated (Figures 33 and 34).

Potential vorticity Q (upper left in Figure 33) is changing between 0.5-1.5, indicating that ζ changes between $\pm 0.5f$. The contour line of 1.0 represent almost zero relative vorticity. Negative relative vorticity (dotted line) follows the 250 isobath, indicating the bottom Ekman layer. It is contrasted to the positive vorticity generation along the 250 m isobath outside the canyon associated with the slope jet. The major positive vorticity generation occurs in the middle of canyon (solid line) producing the cyclonic circulation within the canyon. Advection of the upstream slope jet generates positive vorticity when it detaches the upstream offshore corner. For the rest of canyon, Q does not change substantially.

For a wider canyon (upper left in Figure 34), it is clear that negative relative vorticity (0.5 contour line) occurs following the 250 m isobath at the upstream and downstream walls. Near the upstream wall, strong positive vorticity is generated (1.5 contour line). The canyon is divided into two parts: positive vorticity generation region (greater than 1.0) and negative vorticity generation region (less than 1.0). This result matches that there are cyclonic and anti-cyclonic circulation region over wide canyon in the flow field analysis.

The other three panels in Figures 33 and 34 display the potential vorticity budget. Three terms in Equation 16 are depicted. Baroclinicity vector **B** and the vertical advection of potential vorticity wQ_z were very small (1% or less) compared to other terms, indicating that baroclinic torque does not generate vorticity. Time change

of potential vorticity (Q_t, upper right) occurs mainly within the canyon and south of the downstream offshore corner. Q_t shows increase in Q near the offshore corner of the upstream wall but decrease in the middle of canyon and increase near the downstream wall. The temporal increase and decrease of Q occurs south of offshore corner of the downstream wall. The vertical velocity change and potential vorticity advection (lower panel) are two dominant terms in this balance.

Advection reduces the potential vorticity but the vertical velocity change enhances it along the slope outside the canyon. This result indicates that the vortex stretching generates the cyclonic vorticity over the general slope, which balances anti-cyclonic vorticity generated by advection. But these two terms do not cancel, indicating that the cyclonic vorticity by the continuous vortex stretching in the bottom Ekman layer is largest. The opposite pattern occurs along the canyon head of wide canyon (Figure 34), i.e., advection enhances the potential vorticity but the vertical velocity compression reduces it along the canyon head (C6). These two terms almost cancel each other along the head of canyon of wide canyon. But in the upper layer (for example 200 m) of canyon, advection reduces potential vorticity (figure not shown) with the vertical velocity change, generating the anti-cyclonic circulation following the canyon rim. Recall that the upwind undercurrent is very strong along the canyon head which is negligible outside the canyon. Wave-like pattern of vorticity enhancement and reduction occurs near the canyon mouth, indicating major vorticity generation region. Vorticity generation by advection is stronger near the canyon mouth. Along the 250 m isobath within a narrow canyon (Figure 33), vorticity reduction occurs by both advection and vertical velocity change, indicating that strong canyon cyclone is retarded by anti-cyclonic vorticity in the bottom Ekman layer. Vorticity enhancement is dominant near the canyon mouth by both terms, which generates the canyon cyclone even though potential vorticity has complex changes within the canyon.

V.4 CANYON DRAG

Canyon drag is an important element of the topographic effect of canyons on coastal flow. Alongshore transport upstream of a canyon is different for canyons with different widths due to different canyon drag. The drag force is partitioned into skin friction (F_{skin}, due to dissipative losses in the bottom boundary layer) and form drag (F_{form} associated with the pressure difference across the canyon). We consider the drag force only in the alongshore direction to determine the effect of the canyon on the alongshore flow.

The form drag F_{form} is determined by integrating the horizontal component of the pressure force acting normal to the canyon surface,

$$F_{form} = \frac{1}{A}\int P_{form} dA = \frac{1}{A}\int P_b \sin\theta \; dA, \tag{17}$$

where P_{form} is the form pressure representing the bottom pressure normal to the bottom. P_b is the bottom pressure and θ represent the slope of the bottom in the alongshore direction at the point where the pressure is applied, and A is the area over which the integration is performed. The total integration area extends 60 km from the coast in offshore direction and 100 km plus the canyon width in the alongshore direction. The bottom pressure P_b changes with the free surface and density,

$$P_b = P_i + P_\rho + P_\eta, \tag{18}$$

where P_i is the initial bottom pressure at day 0, P_ρ is the pressure due to density redistribution and P_η is the pressure due to the free surface. F_{form} has two parts: F_ρ, due to baroclinic contribution to the pressure; F_η, due to the free surface slope.

Skin friction (F_{skin}) is generated by flow over the bottom, which was calculated as

$$F_{skin} = \frac{1}{A}\int D_{coef} v_0 \sqrt{u_0^2 + v_0^2} \; dA, \tag{19}$$

where the bottom drag coefficient D_{coef} is 3×10^{-3} and u_0, v_0 are flow speed in the deepest layer in the model.

With upwelling winds, the free surface falls near the coast but the density increases downstream of canyon with time due to upwelling of dense water through the canyon. The free surface change reduces bottom pressure but the increase of density enhances it. The pressure increase due to the density redistribution is strong in the middle of the canyon and near the coast. The total bottom pressure decreases because the free surface reduces the pressure more than density enhances it (figure not shown). The contribution to the pressure by the free surface is 4-5 times that of the density redistribution, indicating that the bottom pressure changes mainly due to the free surface. However, the form pressure (P_{form}) in the alongshore direction peaks at both steep slopes of canyon and is zero at the flat bottom by definition. It changes mainly by the density increase because the pressure changes due to the free surface is nearly parallel to the coast which does not generates the form pressure in the alongshore direction. Skin friction in the alongshore direction is very small within the canyon because the alongshore flow is so slow at the bottom within the canyon. It is very large near the nearshore corner of the downstream wall of canyon and downstream of canyon due to faster flow there. Thus the main drag force is the form drag within the canyon and skin friction outside the canyon. Nash and Moum (2001) reported that the form drag is much larger than the skin friction over a sea bank in the Oregon shelf. Similarly the canyon drag is mainly determined by the form drag.

The form drag increases with time and always positive which is opposite to the downwind flow (Figure 35). Wider canyons have larger form drag which retards the alongshore flow more than narrower canyons. Skin friction is similar to form drag over narrower canyons but the main skin friction comes not over the canyon but downstream of it. As the canyon widens total form drag is much larger than total skin friction. Form drag of canyons dominates the drag forces over wider canyons.

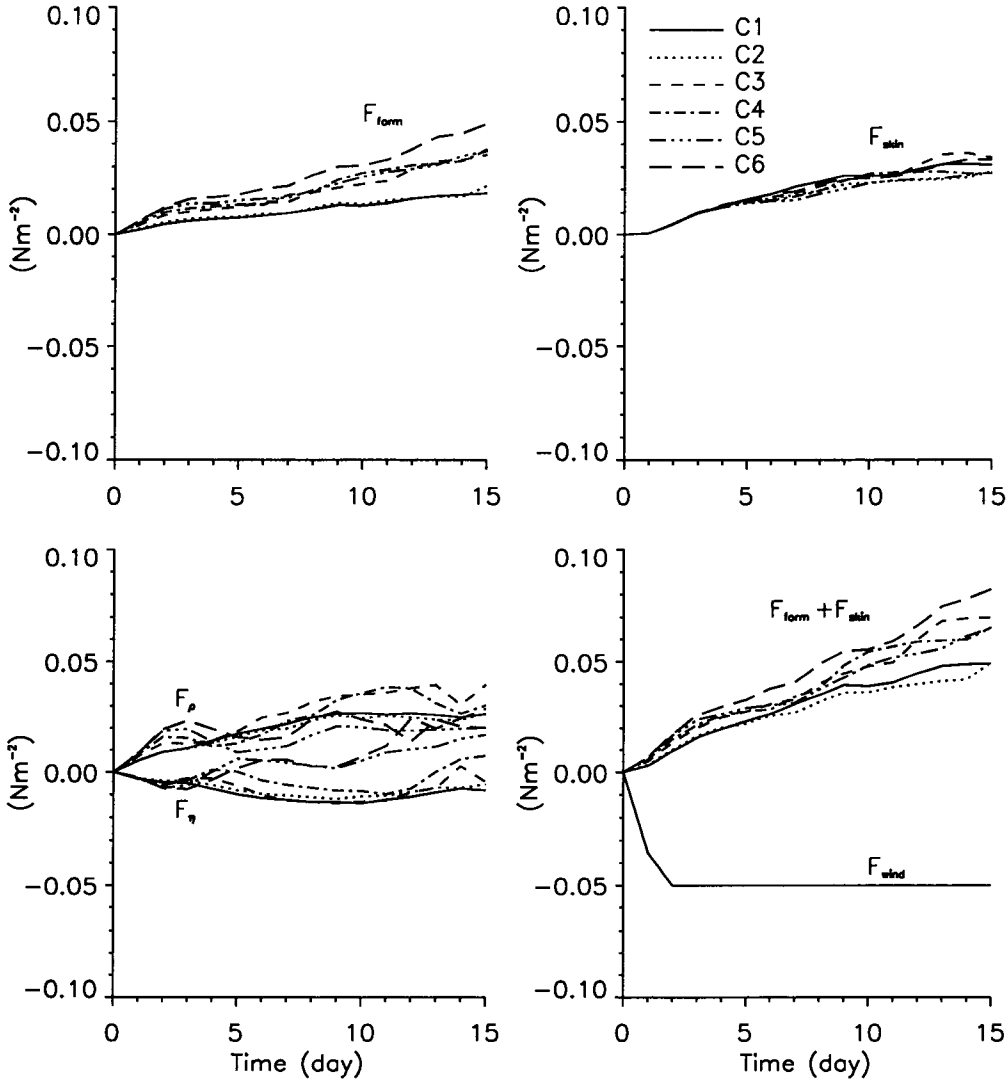

Figure 35. Temporal variation of form drag (F_{form}), skin friction (F_{skin}) and form drag due to the free surface and density (F_η and F_ρ) for cases C1-C6. Temporal variation of total bottom drag (sum of form drag and skin friction) and the surface wind stress (F_{wind}) are depicted on the lower right. Different line styles indicate different cases as shown on the upper right. The integration area is 60 km from the coast in x direction and 100 km plus canyon width in the alongshore direction.

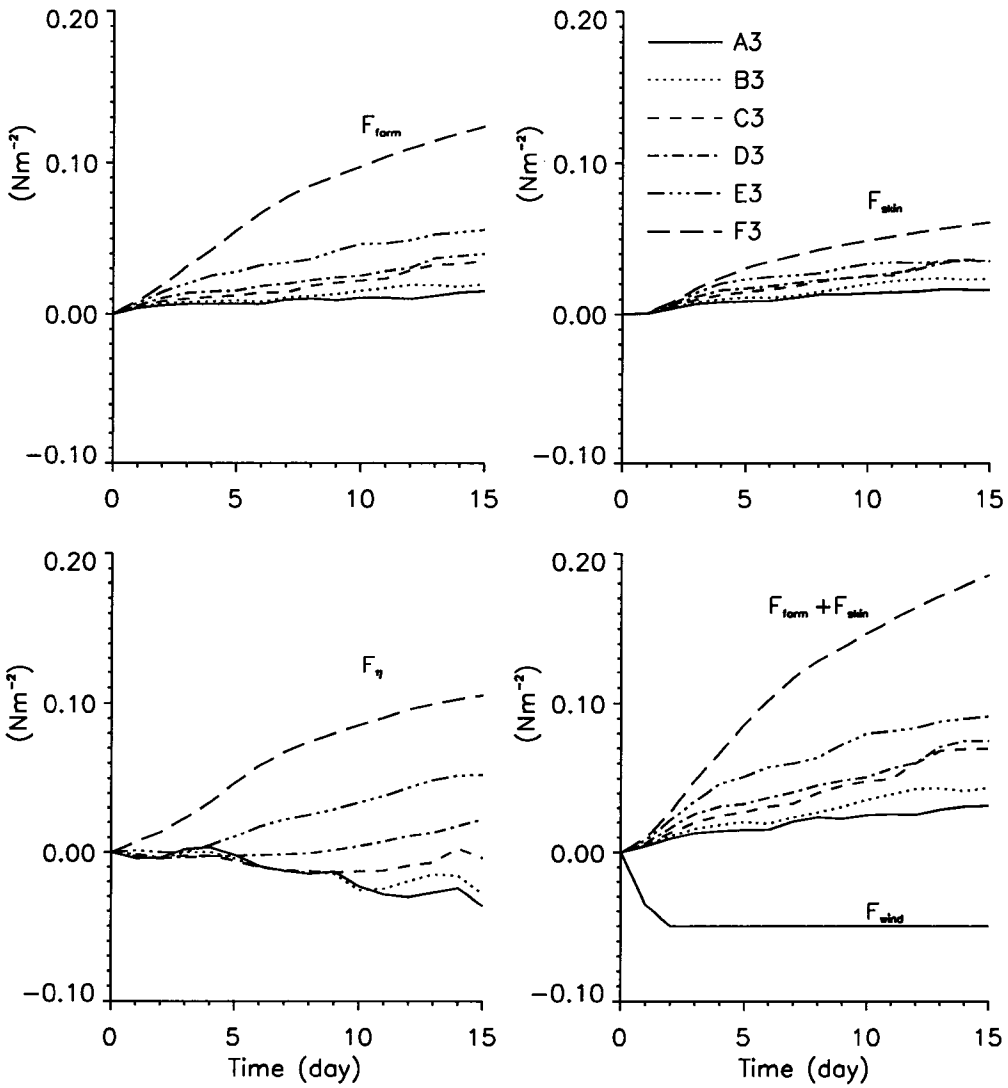

Figure 36. Temporal variation of form drag (F_{form}), skin friction (F_{skin}) and form drag due to the free surface (F_{η}) for stratification cases A3-E3 for the 20 km canyon. Temporal variation of total bottom drag (sum of form drag and skin friction) and the surface wind stress (F_{wind}) are depicted on the lower right. Different line styles indicate different cases as shown on the upper right. The integration area is 60 km from the coast in x direction and 100 km plus canyon width in the alongshore direction.

As described above, the form drag is divided into contributions by the free surface (F_η) and density (F_ρ) (lower left panel in Figure 35). The free surface contribution is negative over narrower canyons which drives the flow downwind. It is positive over wider canyons. This results matches the description of the free surface in Section III.1 and can be used for canyon size classification. Thus the baroclinic effect and the free surface slope compensate producing a small canyon drag over narrow canyons. But the free surface slope magnifies the baroclinic effect on canyon drag, resulting in large canyon drag over wider canyons. Reduced canyon drag enhances the alongshore flow upstream of canyon which passes over the canyon without feeling the presence of the canyon. The bottom drag force and the surface wind stress (Figure 35) are not balanced, indicating that a larger region may be involved in the steady balance or that the model is still adjusting. Note that wider cases include less of the downstream area with high skin friction. Bottom drag is slightly less than the surface force over narrow canyons (8 km and 12 km). But it is larger than the surface force over wider canyons.

Stratification has a strong effect on both the canyon drag and skin friction. Temporal variation of the form drag under various stratifications is shown in Figure 36. Skin friction and form drag increase with time and as stratification is reduced (upper panel in Figure 36). They are very strong for nearly homogeneous case (F3) and very weak for strong stratification (A3). The main source of form drag comes from the free surface slope within the canyon (lower left panel in Figure 36). The form drag due to the free surface (F_η) is always positive under weaker stratification which makes strong drag effect. But it is negative under strong stratifications, which means that the free surface slope drives the downwind flow. But the baroclinic effect exceeds the free surface slope, producing the total canyon drag opposite to the downwind flow under strong stratification. Under weak stratification, the form drag due to the free surface is very large and exceeds the baroclinic effect. The total drag is larger than

the surface wind stress in this region. Reduced skin friction and reduced canyon drag result in large alongshore transport under strong stratification over the shelf and the canyon. On the other hand, alongshore transport is very small under weak stratification due to large skin friction and form drag (Section IV.1). Enhanced canyon drag reduces alongshore transport but enhances onshore transport within the canyon. Finally, a slow alongshore flow by enhanced skin friction result in strong onshore flow by the enhanced form drag of canyon under weak stratification. It seems that two drag effects generates the strong onshore flow within the canyon under weak stratification.

V.5 NON-LINEAR EFFECT

It was shown that the canyon circulation is closely related with the stratification number which is the ratio of the internal radius to the canyon width. However alongshore transport (V) and onshore transport (U) within the canyon are not directly related to the stratification number. The U-V relationships for all cases are compared to examine the pattern between the stratification number and U-V curves (figure not shown). Cases with the similar stratification number have different curves. For example, a pair of S=0.15 and 0.17 shows different alongshore transport but a similar onshore transport. Another pair of S=0.80 and 0.83 show stronger onshore transport for S=0.83 but stronger alongshore transport for S=0.80. This means that the same stratification number does not show the same transport but there is a relationship between transport and parameters of canyon width and stratification. This result can be expected because the alongshore transport (V) upstream of canyon is not mainly influenced by the width of canyon but by the stratification. The fixed stratification cases show larger onshore transport over wider canyons for a given alongshore transport. There should be another factor that controls U-V relationship. One candidate is the Rossby number representing the advection of alongshore flow. Onshore transport (U) was contoured by the Rossby number and the stratification number in Figure

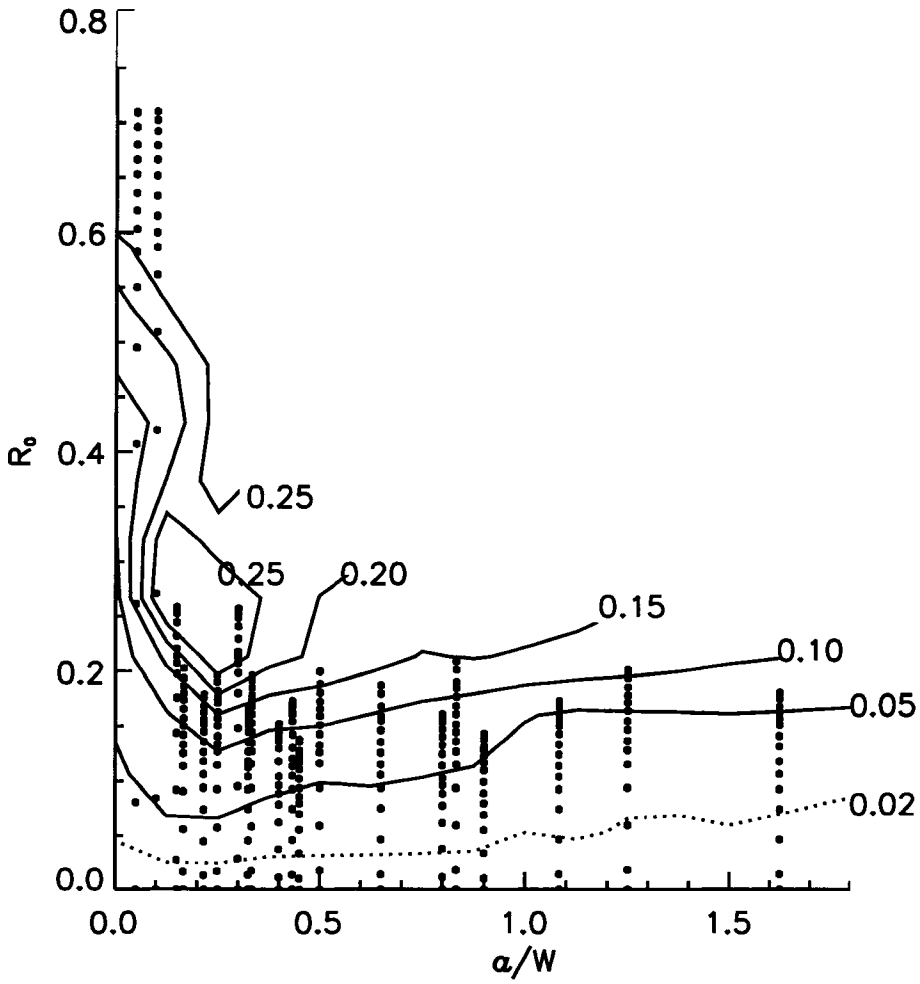

Figure 37. Across shelf transport (U, Sv) within the canyon by the Rossby number (R_0) and the stratification number (a/W). Daily values of transport for 0-15 d are plotted.

37. As the stratification number decreases and the Rossby number increases, onshore transport increases.

V.6 STAGNATION POINT

The downstream escarpment (C8 in Figure 8) exhibits a stagnation point on the canyon wall about 1/3 of the way offshore of the canyon head where the alongshore flow either turns offshore to follow the downstream shelf slope or turns onshore to flow upwind along the upstream shelf slope. As the width of the canyon narrows, the alongshore flow in the canyon meets the downstream wall farther offshore; thus, shifting the stagnation point offshore. For the narrowest canyon, the flow that detaches from the upstream corner of the canyon moves only a short distance onshore before it meets the downstream wall, so the stagnation point moves to the offshore corner of the downstream canyon wall.

Upwind flow along the canyon head is stronger over wide canyons (C5-C6) than over the escarpment case (C8). Thus, a very wide canyon still has the effect of the two walls even though they are far apart. However the general flow pattern is almost the same as the infinitely wide canyon without a canyon wall. Thus the canyon width classification still remains valid.

V.7 FLUSHING TIME

The model results show that across shelf exchange within the canyon increases with time over all canyons compared to that outside. Onshore transport occurs through all canyons. Total onshore transport integrated from the initial spinup to the quasi-steady state (15 d) through the canyon can be calculated using Equations (11) and (13) for a given stratification and canyon width. First alongshore transport upstream of canyon can be obtained from Equation (11). Parameters V_m and K_d are determined for a given stratification and canyon width (Tables 5, 6 and 8). Total onshore volume

can be obtained from the time integration of onshore transport

$$\begin{aligned} U_{tot} &= \int_0^{t_a} U dt + \int_{t_a}^{t_w} U dt \\ &= \int_0^{t_a} m_1 V^{n_1} dt + \int_{t_a}^{t_w} m_2 V^{n_2} dt \\ &= \int_0^{t_a} m_1 [\frac{V_m t}{K_d + t}]^{n_1} dt + \int_{t_a}^{t_w} m_2 [\frac{V_m t}{K_d + t}]^{n_2} dt, \end{aligned}$$

where t_a is the adjustment time (3 d, 5 d, 7 d) and t_w is wind duration (7 days here). The time scale of winds over the western shelf of North America is typically less than a week (Hickey 1998). The steady state which appears in the model simulations is hardly to be reached in the real ocean. Onshore volume transport was integrated for a week to estimate the flushing time. Total onshore volumes are calculated as 8.4, 11.2, 13.8, 21.0, 32.9 and 63.8 km^3 for six stratifications over the 20 km canyon for the period of 0-7 days by the numerical integration. Assuming that another canyon exists 100 km downstream, the flushing time can be obtained from the volume calculation. The volume of the downstream shelf (45 km by 100 km) is about 415 km^3 for a given shelf depth (30-150 m).

Thus the number of upwelling events (N_up, Table 10) which persist for a week to refresh the whole downstream is 49, 37, 30, 20, 13, 7 from strong to weak stratifications for 20 km canyon (A3-E3). In other words, total 30 times of continuous upwelling favorable winds can refresh the whole shelf area by driving the upwelling of dense water from a 20 km canyon for a basic stratification (a=13 km). This calculation is comparable to the result of She and Klinck (2000), who calculated that the steady upwelling would flush the shelf (100 m deep and 100 km wide) in about 2 years.

Table 10. Onshore volume (U_{tot}, km^3, upper panel) integrated for 7 days and number of upwelling events (N_{up}) which is consistent for a week which can flush the whole downstream shelf (415 km^3).

		a=18	16	13	10	6	2
	W=8			10.3	15.5		
	12			9.2	15.1		
U_{tot}	20	8.4	11.2	13.8	21.0	32.9	63.8
	30			16.8	22.7		
	40	13.9	17.1	18.3	27.6	43.6	77.9
	60			24.7	29.4		
	W=8			40	27		
	12			45	27		
N_{up}	20	49	37	30	20	13	7
	30			25	18		
	40	30	24	23	15	10	5
	60			17	14		

CHAPTER VI

CONCLUSIONS

The effect of canyon width and stratification on circulation in a submarine canyon was investigated using a 3-d numerical model simulating wind driven coastal upwelling. Wind strength, along with canyon depth and length, are kept constant over all cases.

All simulations reach an approximate steady state after two weeks of wind forcing, although some oscillation continues in some cases. Alongshore transport (V) over the shelf increases with time having the form $V = V_m/(K_d + t)$. Cyclonic circulation, continuous onshore transport and upwelling occur within the canyon under all stratifications after the alongshore flow into the canyon is adjusted to the canyon topography (about 5 d). The adjustment occurs earlier under weaker stratification. The strength and the shape of canyon circulation and across shelf transport varies with width and stratification. The effect of stratification is stronger than the geometric effect of canyon width based on the onshore transport and upwelling within the canyon. All canyons can be classified as narrow, intermediate or wide by the ratio of the internal deformation radius to the canyon width, based on these patterns of flow, where a width of about 2 internal deformation radii ($2a$) is the separating case between wide and narrow canyons.

Wide canyons show the effect of the two remotely separated walls of the canyon. A cyclone with a width of about $2a$ occurs near the upstream canyon wall. The alongshore jet on the upper continental slope, driven by the winds, separates from the upstream corner of the canyon and turns into the canyon. This jet impacts the downstream canyon wall separating into two parts: one that turns offshore, exits the canyon and continues along the slope; the other turns toward the head of the canyon and flows upwind along the head of the canyon.

For narrow canyons, the size of the cyclone, which occupies the whole canyon, is

the width of canyon which is much less than $2a$. The impact point of the detached jet moves toward the downstream, offshore corner of the canyon. Onshore and offshore flows occurs at both downstream and upstream walls, respectively but onshore flow is stronger. The geometric effect of a narrow canyon is very strong based on the onshore transport per unit width and tracer moving speed within the canyon. Intermediate canyons (W$\sim 2a$) shows the flow characteristics between narrow and wide canyons.

The retarding force over the canyon is mainly the form drag while the skin friction is dominant over the shelf. Canyon drag decreases as the canyon narrows and stratification increases. It is mainly determined by the baroclinic part not by the free surface slope. Reduced canyon drag enhances the alongshore flow upstream of canyon which passes over the canyon undisturbed without feeling the presence of narrow canyons. Skin friction over the shelf increases as stratification decreases. Reduced skin friction and canyon drag result in large alongshore transport under strong stratification. Alongshore transport is very small under weaker stratification due to large skin friction and canyon drag. Canyon drag reduces alongshore transport but enhances across shelf transport within the canyon. A slow alongshore flow by enhanced skin friction result in strong onshore flow by the enhanced canyon drag under weak stratification. Two drag effects generates the strong onshore flow within the canyon under weak stratification.

Alongshore transport (V) upstream of canyon and onshore transport (U) within the canyon has a relationship of power function $U=mV^n$ but the coefficient is different before and after the adjustment. Net onshore volume transport occurs within the canyon for all stratifications. Onshore transport increases rapidly as stratification is reduced. More onshore transport occurs for a given alongshore transport over wide canyon due to the effect of downstream wall. Weaker stratification shows more onshore transport for a given alongshore transport indicating that the geometric effect of canyon increases as the stratification is reduced. But onshore transport per unit

alongshore distance (km) is stronger over narrow canyons under a fixed stratification, indicating a strong narrow canyon effect. The onshore transport per width declines sharply at a canyon width of about $2a$, which supports the canyon classification.

Onshore-offshore flow is adjusted within the canyon earlier for strong stratification. A second onshore exchange occurs about a canyon width downstream of the canyon created by the canyon wake. In all cases, the influence of the canyon extends less than 100 km downstream. The offshore-onshore fluctuation downstream of canyon becomes stronger as the canyon widens and stratification is reduced. Strong onshore transport through the downstream edge generates an alongshore jet in the lower downstream shelf differing from the upwelling jet in the surface. As the canyon widens or stratification is reduced, the jet becomes stronger.

Vortex compression occurs at the top of the canyon below the canyon rim, which generates an anti-cyclonic circulation following the rim. Canyon cyclone is mainly generated by vortex stretching of the water column. Vortex compression and stretching occurs simultaneously at both walls of a narrow canyon. Over wide canyons, vortex compression and stretching occurs strongly at the upstream wall. Vortex compression or stretching is much reduced with stratification. Isopycnal displacement shows that upwelling speeds are 2-12 m day^{-1} below the canyon rim from strong to weak stratifications. The isopycnal rise is strong near the coast and the bottom Ekman layer rather than the offshore and the interior.

Canyon upwelling is strong over narrow canyons and downstream nearshore corner of a wide canyon based on the number of tracers which exit the canyon. As stratification is reduced canyon upwelling becomes stronger and has a linear relationship with stratification. Canyon upwelling is strongly influenced by the stratification not by the canyon width.

Nearly homogeneous case has quite different dynamics from others. It has a small

cyclone which is located at the offshore corner of the upstream slope. Strong anti-cyclonic circulation occurs near the canyon head. Onshore flow occurs from the top to the bottom within the canyon. Isopycnal initially at 500 m moves up to the shelf break for 20 days (18 m day^{-1}).

Tracer trajectories show that water flowing into the canyon from offshore upwells onto the shelf near the canyon head. Narrow canyons have onshore flow throughout the canyon width while wide canyons have upwelling mainly along the downstream nearshore corner of the canyon. Tracer trajectories show that downstream corner of the canyon head is a preferred place for deep water upwelling. Deep water for across shelf exchange mainly comes from the upstream slope just below the shelf edge. The range of depth and width of the source region for across shelf exchange varies with stratification.

REFERENCES

Aagaard, K and A.T. Roach, Arctic ocean-shelf exchange: Measurements in Barrow Canyon, *J. Geophys. Res., 95,* 18163-18175, 1990.

Allen, S.E., Topographically generated, sub-initial flows within a finite length canyon, *J. Phys. Oceanogr., 26,* 1608-1632, 1996.

Allen, S.E., On subinertial flow in submarine canyons: Effect of geometry, *J. Geophys. Res., 105 (C1),* 1285-1297, 2000.

Allen, S.E., M.S. Dinniman, J.M. Klinck, D.D Gorby, A.J. Hewett and B.M. Hickey, On vertical advection truncation errors in terrain-following numerical models: Comparison to a laboratory model for upwelling over submarine canyons, *J. Geophys. Res., 108 (C1),* 1-16, 2003.

Alvarez, A., J. Tintoré and A. Sabatés, Flow modification and shelf-slope exchange induced by a submarine canyon off the northern Spanish coast, *J. Geophys. Res., 101 (C5),* 12043-12055, 1996.

Arakawa, A. and V.R. Lamb, *Methods of Computational Physics*, pp. 174-265, Academic Press, 1977.

Ardhuin, F., J.-M. Pinot and J. Tintore, Numerical study of the circulation in a steep canyon off the Catalan Coast (western Mediterranean), *J. Geophys. Res., 104 (C5),* 11115-11135, 1999.

Barton, E.D., A. Huyer and R.L. Smith, Temporal variation observed in the hydrographic régime near Cabo Corveiro in the northwest African region, February to April, *Deep Sea Res., 24,* 7-23, 1977.

Burrows, M., S.A. Thorpe and D.T. Meldrum, Dispersion over the Hebridean and Shetland shelves and slopes, *Cont. Shelf. Res., 19,* 49-55, 1999.

Chapman, D.C. and G. Gawarkiewicz, Offshore transport of dense shelf water in the presence of a submarine canyon, *J. Geophys. Res., 100 (C7),* 13373-13387, 1995.

Charney, J.G., The generation of ocean currents by wind, *J. Mar. Res., 14,* 477-498, 1955.

Chen, X. and S.E. Allen, The influence of canyons on shelf currents: A theoretical study, *J. Geophys. Res., 101 (C8),* 18043-18059, 1996.

Church, T.M., C.N.K. Mooers, and A.D. Voorhis, Exchange processes over a middle Atlantic bight shelfbreak canyon, *Estuarine Coastal Shelf Sci., 19,* 393-411, 1984.

Dinniman, M.S. and J.M. Klinck, The influence of open versus periodic alongshore boundaries on circulation near submarine canyons, *J. Atm. Ocean. Tech., 19,* 1722-1737, 2002.

Durrieu de Madron, X., P. Castaing, F. Nyffeler and T. Courp, Slope transport of suspended particulate matter on the Aquitanian margin of the Bay of Biscay, *Deep-Sea Res. II, 46,* 2003-2027, 1999a.

Durrieu de Madron, X., O. Radakovitch, S. Heussner, M.D. Loye-Pilot and A. Monaco, Role of the climatological and current variability on shelf-slope exchange of particulate matter: Evidence from the Rhône continental margin (NW Mediterranean), *Deep-Sea Res. I, 46,* 1513-1538, 1999b.

Ezer, T., H. Arango and A.F. Shchepetkin, Developments in terrain-following ocean models: intercomparisons of numerical aspects, *Ocean Modelling, 4,* 249-267, 2002.

Flather, R.A., A tidal model of the northward European continental shelf, *Mem. Soc. R. Sci. Liege, Ser. 6, 10,* 141-164, 1976.

Freeland, H.J. and and K.L. Denman, A topographically controlled upwelling center off southern Vancouver Island, *J. Mar. Res., 40,* 1069-1093, 1982.

Gill, A.E., *Atmosphere-Ocean Dynamics,* 662 pp, Academic Press, San Diego, Calif., 1982.

Gill, A.E. and A.J. Clarke, Wind-induced upwelling, coastal currents and sea-level changes, *Deep-Sea Res., 21,* 325-345, 1974.

Granata, T.C., B. Vidondo, C.M. Duarte, M.P. Satta and M. Garcia, Hydrodynamics and particle transport associated with a submarine canyon off Blanes (Spain), NW Mediterranean Sea, *Continental Shelf Res., 19 (10),* 1249-1263, 1999.

Haidvogel, D.B. and A. Beckmann, Numerical models of the coastal ocean, in *The Sea,* edited by K.H. Brink and A.R. Robinson, Vol. 10, pp 457-482, John Wiley and Sons, New York, 1998.

Haney, R.L., On the pressure gradient force over steep topography in sigma coordinate ocean models, *J. Phys. Oceanogr., 21,* 610-619, 1991.

Hedström, K.S., (Draft) User's Manual for an S-coordinate Primitive Equation Ocean Circulation Model (SCRUM) Version 3.0, *Institute of Marine and Coastal Sciences, Rutgers University Contribution # 97-10,* 116pp, 1997.

Hickey, B.M., E. Baker and N. Kachel, Suspended particle movement in and around Quinault Submarine Canyons, *Mar. Geol., 17,* 35-83, 1986

Hickey, B.M., Patterns and processes of circulation over the Washington continental shelf and slope, in *Coastal Oceanography of Washington and Oregon,* M. Landry and B. Hickey (eds.), *Elsevier Science, Amsterdam,* pp 41-116, 1989.

Hickey, B.M., Coastal Submarine canyons. *Proc. 'Aha Huliko'a Workshop on Flow Topography Interactions,* Honolulu, HI, Office of Naval Research, 95-110, 1995.

Hickey, B.M., The response of a steep-sided, narrow canyon to time variable wind forcing. *J. Phys. Oceanogr., 27,* 697-726, 1997.

Hickey, B.M., Coastal oceanography of western North America from the tip of Baja

California to Vancouver Island, in *The Sea, Vol. 11*, A.R. Robinson and K.H. Brink (eds.), *John Wiley, New York*, pp. 345-393, 1998.

Hotchkiss, F.S. and C. Wunsch, Internal waves in Hudson Canyon with possible geological implications, *Deep Sea Res., 29 (4A),* 415-442, 1982.

Hsueh, Y., On the theory of deep flow in the Hudson Shelf Valley, *J. Geophys. Res., 85,* 4913-4918, 1980.

Hunkins, K., Mean and tidal currents in Baltimore Canyon, *J. Geophys. Res., 93 (C6),* 6917-6929, 1988.

Huthnance, J.M., Circulation, exchange and water masses at the ocean margin: the role of physical processes at the shelf edge, *Progress in Oceanography, 35,* 1021-1033, 1995.

Hydes, D.J., A.C. Le Gall, A.E.J. Miller, U. Brockmann, T. Raabe, S. Holley, X. Alvarez-Salgado, A. Antia, W. Balzer, L. Chou, M. Elskens, W. Helder, I. Joint, M. Orren, Supply and demand of nutrients and dissolved organic matter at and across the NW European shelf break in relation to hydrography and biological activity, *Deep-Sea Res. II, 48,* 3023-3047, 2001.

Jiang, L. and R.W. Garwood Jr., Effects of topographic steering and ambient stratification on overflows on the continental slopes: A model study, *J. Geophys. Res., 103 (C3),* 5459-5476, 1998.

Kinsella, E.D., A.E. Hay and W.W. Denner, Wind and topographic effects on the Labrador Current at Carson Canyon, *J. Geophys. Res., 92,* 10853-10869, 1987.

Klinck, J.M., The influence of a narrow transverse canyon on initially geostrophic flow, *J. Geophys. Res., 93*, 509-515, 1988.

Klinck, J.M., Geostrophic adjustment over submarine canyon, *J. Geophys. Res.,94*, 6133-6144, 1989.

Klinck, J.M., Circulation near submarine canyons : A modeling study, *J. Geophys. Res.,101 (C1),* 1211-1223, 1996.

Large, W.G., J.C. McWilliams and S.C. Doney, Oceanic vertical mixing: A review and a model with a nonlocal boundary layer parameterization, *Rev. Geophys., 32,* 363-403, 1994.

Nash, J.D. and J.N. Moum, Internal hydraulic flows on the continental shelf: High drag states over a small bank, *J. Geophys. Res., 106(C3),* 4593-4612, 2001.

Noble, M. and B. Butman, The structure of subtidal currents within and around Lydonia Canyon: Evidence for enhanced cross-shelf fluctuation over the mouth of the canyon, *J. Geophys. Res., 94 (C6),* 8091-8110, 1989.

Peffley, M.B. and J.J. O'Brien, A three-dimensional simulation of coastal upwelling off Oregon, *J.Phys. Oceanogr. 6,* 164-180, 1976.

Puig, P., A. Palanques, J. G. and E. García-Ladona, Deep slope currents and suspended particle fluxes in and around the Foix submarine canyon (NW Mediterranean), *Deep Sea Res. I: Oceanographic Res. Papers, 47(3),* 343-366, 2000.

Røed, L.P. and O.M. Smedstad, Open boundary conditions for forced waves in a rotating fluid, *SIAM J. Sci. Stat. Comput., 5,* 414-426, 1984.

Shchepetkin, A.F. and J.C. McWilliams, The regional ocean modeling system: a split-explicit, free surface, topography-following coordinate ocean model. *Geophysics and Planetary Physics, UCLA, Los Angeles, CA,* 31 pp., 2000.

She, J. and J.M. Klinck, Flow near submarine canyons driven by constant upwelling winds, *J. Geophys. Res.,105, C12,* 28671-28694, 2000.

Shepard, F.P. and K.O. Emery, Submarine topography off the California coast: Canyons and Tectonic Interaction, *Geol. Soc. of Amer., # 31,* 171 pp, 1941.

Shepard, F.P. and N.F. Marshall, P.A. McLoughlin, and G.G. Sullivan, Currents in Submarine Canyons and Other Seavalleys, *Amer.Assoc. Petroleum Geologists, AAPG Studies in Geol. # 8,* 173pp, 1979.

Signorini, S.R., A. Münchow, and D. Haidvogel, Flow dynamics of a wide canyon, *J. Geophys. Res., 102 (C8),* 18661-18680, 1997.

Sobarzo, M.F. and L. Djurfeldt, Upwelling of subsurface water into the rim of the Biobío submarine canyon as a response to surface winds, *Continental Shelf Res., 21 (3),* 279-299, 2001.

Stetson, H.C., Geology and paleontology of the Georges Bank Canyons, *Geology, 47,* 339-366, 1936.

Wåhlin, A.K., Topographic steering of dense currents with application to submarine canyons, *Deep Sea Res.I: Oceanographic Res. Papers,* 2001.

Yuan, D., A numerical study of barotropicly forced intrusion in DeSoto Canyon, *J. Geophys. Res., 107(C2),1-15,* 2002.

Kyung Hoon Hyun

ADDRESS

Dept. of Ocean, Earth and Atmospheric Sciences

Old Dominion University

Norfolk, VA 23529, USA

EDUCATION

- M.S., Oceanography, 1997, Cheju National University, Korea

  Thesis - "Seasonal Variation of Warm Waters in Eastern Yellow Sea and Yellow Sea Warm Current in Summer."

- B.S., Oceanography, 1991, Cheju National University, Korea

PUBLICATIONS

- Hyun, K.H. and J.M. Klinck, The effect of submarine canyon width on coastal circulation forced by upwelling winds. *J. Geophys. Res.*, (submitted)

- Hyun, K.H., I-C Pang, J.M. Klinck, K-S Choi, J.-B. Lee, E.N. Powell, E.E. Hofmann and E.A. Bochenek, The effect of food composition on Pacific Oyster *Crossostrea Gigas* (Thunberg) growth in Korea: A Modeling study. 2001, *Aquaculture,* 199, 41-62.

- Pang, I.C. and K.H. Hyun, 1997, Seasonal Variation of Water Mass Distributions in the Eastern Yellow Sea and Yellow Sea Warm Current, *J. Kor. Soc. Oceanogr.*, 33(3), 41-52.

MEMBERSHIPS

- American Geophysical Union

- Korean Society of Oceanography